EXTRACTION OF IRON OXIDE FROM STEEL ROLLING INDUSTRY SLAG AND DOPING COPPER CHROMATE: A COMPARATIVE STUDY

By: ZEKARIAS GEBREYES ETICHA

NOVEMBER 2022

JIMMA UNIVERSITY INSTITUTE OF TECHNOLOGY

NOVEMBER 2022

JIMMA UNIVERSITY

JIMMA UNIVERSITY INSTITUTE OF TECHNOLOGY

SCHOOL OF GRADUATE STUDIES

FACULTY OF MATERIALS SCIENCE AND ENGINEERING

EXTRACTION OF IRON OXIDE FROM STEEL ROLLING INDUSTRY SLAG AND DOPING COPPER CHROMATE: A COMPARATIVE STUDY

A PHD. DISSERTATION SUBMITTED TO THE SCHOOL OF GRADUATE STUDIES OF JIMMA UNIVERSITY IN PARTIAL FULFILMENT OF THE REQUIREMENTS FOR THE DEGREE OF DOCTOR OF PHILOSOPHY (PHD) IN MATERIALS SCIENCE (METALLURGICAL ENGINEERING)

BY

ZEKARIAS GEBREYES ETICHA

SUPERVISOR: ESAYAS ALEMAYEHU (PROF. DR. ING., JIT)

COSUPERVISORS:

OLU EMMANUEL FEMI (DR. ASSOCIATE PROF., JIT) AND

ABUBEKER YIMAM (DR. ASSOCIATE PROF., AAIT)

NOVEMBER 2022

JIMMA, ETHIOPIA

DEDICATION

This Dissertation is dedicated

TO

My aunt, Commander **Birhane Aweke H/Giorgis**, died of breast cancer while I was a PhD student

and to

My Mother “Ahungena Aweke H/Giorgis”

My Beloved Wife "Birhane Getachew Asfaw" and

My Little Angel “Yohannes Zekarias Gebreyes”

DECLARATION

I hereby declare the thesis entitled " **Extraction of iron oxide from steel rolling industry slag and Doping copper chromate: A comparative study.**" Embodies the results of investigations carried out by me for the specialization of metallurgical engineering in the faculty of Materials Science and Engineering, Jimma Institute of Technology, Jimma University as a full-time PhD student under the supervision of ***Professor Dr-Ing Esayas Alemayehu,*** Co-Supervisors ***Dr Femi Emmanuel Olu*** and ***Dr Abubaker Yimam*** and the same has not been submitted elsewhere for any other degree.

In keeping with the general practice of reporting scientific observations, acknowledgement has been made wherever the work described is based on the findings of other investigators.

Name: **Zekarias Gebreyes Eticha**

Signature:_____

Date: _____

Place: _____

Date of submission: _____

This dissertation has been submitted for examination with my approval as The **Candidate's first Promoter (supervisor).**

Name: (Professor Dr-Ing Esayas Alemayehu (Full Professor, JIT.)

Signature: _____ _____

Date: _____

Candidate's second Promoter (co-supervisor).

Name: Dr Femi Emmanuel Olu (Associate Professor, PhD. JIT)

Signature: _____

Date: _____

Candidate's third Promoter (co-supervisor).

Name: Dr Abubeker Yimam (Associate Professor, PhD, AAiT)

Signature: _____

Date: _____

ACKNOWLEDGEMENTS

This dissertation is the result of several years of hard work, during which I received a great deal of assistance and encouragement from many people. Looking back on the road and remembering everyone who has helped and encouraged me along this long but rewarding journey is one of the pleasures of accomplishment. First and foremost, I want to express my gratitude to the almighty God and his mother, St. Merry, for blessing me throughout my studies, enabling me to persevere in adversity, and providing me with health, strength, and safety. Apart from God, completing this PhD dissertation would not have been possible without the help of many people. I want to express my heartfelt gratitude to every one of them.

My supervisor, Professor Dr-Ing Esayas Alemayehu, deserves special acknowledgement for his unwavering support throughout the research phase and his vital encouragement and achievements. This success would not have been possible without his assistance. Despite his hectic schedule, Professor Dr-Ing Esayas Alemayehu, a cheerful and enthusiastic individual, has always made himself available to answer my questions. I consider it a tremendous honour to complete my PhD under his supervision and benefit from his research expertise.

Dr Femi Emmanuel Olu and Dr Abubeker Yimam deserve recognition for their academic support in carrying out the study; especially Dr Femi has been very encouraging and compassionate, and I am grateful to him. I want to acknowledge Dr Rocio Estefania Rojas Hernandez and Prof. Irina Hussianova (DSc) for their invaluable assistance and encouragement during my visit to their Lab at Tallinn University of Technology in Estonia. I want to thank Dr Thomas C Alex and Dr Sanjaye Kumar for their assistance at the National Metallurgical Laboratory in Jamshedpur, India. Furthermore, Mr Durgesh, Ms Tanusheere, Mr Abyshake, Mr Suhanto, Ms Reshmi, and Mr Rameya support me in the synthesis and characterization work at NML Jamshedpur, as well as Dr Mayuri Ghandi at IIT, Mumbai, and Ms Dharita Chandravanshi at IIS Bangalore.

I owe my tremendous and profound thanks to my wife, Birhane Getachew Asfaw, who has always supported and listened to me and whose smile has always lifted me throughout my work. I thank all the Bio and Emerging Technology Institute researchers and administrative staff, particularly Mr Abiy Lolasa, Ms Hana Asrat, Dr Wondimagegn Mamo, Mr Megos Reda, and Ms Nuhamin Kassu, for their assistance. I want to express my appreciation to Dr Hailu Dadi, Deputy General Director of the Biotechnology Center, Mr Tewodros Bekele, Former emerging centre Deputy General director, and Dr Kassahun Tesfaye, General Director of the Bio and Emerging Technology

Institute, for their assistance in research activities. I'd also like to thank all of my colleagues with whom I've shared good and bad times; the good times will be remembered, and the bad times will strengthen me.

A special thanks to the Bio and Emerging Technology Institute for financial and Lab facility support, Jimma Institute of Technology, the European Regional Development Fund's Doctoral Studies and Internationalization Program Dora Plus and Tallinn University of Technology, the Indian National Science Academy- Junior Research Development (INSA-JRD) TATA Fellowship Program, and the National Metallurgical Laboratory (NML), Jamshedpur, India for lab facility and financial support. Addis Ababa University (AAU), Faculty of Natural Science, Department of Chemistry for XRD and FTIR characterization and Centre for Research in Nanotechnology and Science (CRNTS), Sophisticated Analytical Instrument Facility (SAIF), Indian Institute of Technology (IIT Mumbai) for SEM with EDS and UV-VIS service.

Zekarias. G. Eticha

LIST OF ABBREVIATIONS

ADCMA- American Dry Color Manufacturer Association

BC- Before the Birth of Christ

BET – Brunauer Emmett- Teller

CARG – Compound Annual Growth Rate

CICP – Complex Inorganic Coloring Pigment

CIE – International Commision on Illumination (Commision Intrnationale de I'Eclairge)

DIN – German Institute for Standardization (Deutsches Institut fur Norming)

DLS – Dynamic Light Scattering

EDS – Energy Dispersive Spectroscopy

eV- Electro-Volt

FEGSEM- Field Emission Gun Scanning Electron Microscopy

FTIR- Fourier Transform Infra-Red

FWHM – Full Wave Half Maximum

GDP – Growth Domestic Product

ICP-MS - Inductively Coupled Plasma- Mass Spectroscopy

ISO – International Standard Organization (International Organization for Standardization)

JCPDS-PDF - Joint Committee on Powder Diffraction Spectroscopy- Powder Diffraction File

KOAFEC – Korea-African Economic Cooperation

NML-National Metallurgical Laboratory

O/F - Oxidant to Fuel ratio

O/M – Oxygen to a Metal ratio

rpm – revolution per minute

SDG – Sustainable Development Goal

Steely RMI- Steely Rolling Mill Industry

Ss- Steel slag

TG-DTA - Termogravimetric- Differential Thermal Analyzer

UV-VIS-NIR – Ultra Violet- Visible- Near Infrared

XRD- X-ray Diffraction

XRF – X-ray Flourescence

Contents

LIST OF TABLES

LIST OF FIGURE

ABSTRACT

Increasing efforts to address environmental issues related to industrial waste and the consumption of natural resources by industrial activities have become a global issue. Development in all direction includes significant reductions in waste generation through waste prevention, reduction, recycling, and reuse strategies. At the same time, the expansion of industries worldwide requires a considerable amount of pigment for the industries as an input. The project's main activities were two broad classes; extracting and processing steel slag from steel rolling waste for pigment application. Then, synthetic and extracted iron was doping in the copper chromate pigment to study its colouring properties. In the first part, the iron content of the steel slag was investigated using X-Ray Fluorescence (XRF); then, iron was extracted using sulphuric acid as a leaching agent, the Inductively Coupled Plasma Mass Spectroscopy (ICPMS) were used to investigate the chemicals leached in the liquid solution. Next, the annealing temperature was determined from the thermographic-Differential Thermal analyzer (TG-DTA), and based on the result extracted sample was annealed at 700˚C, 800˚C, 900˚C and 1000˚C. After annealing the extracted sample, the crystalline property, crystallite and particle size, morphology, optical and colouring properties were investigated using X-Ray Diffraction (XRD), Dynamic Light Scattering (DLS), Field Emission Gun-Scanning Electron Microscopy (FEG-SEM), Ultraviolet-Visible Spectroscopy Near Infrared (UV-VIS NIR) and Commission Internationale de I'Echlarge (CIEL*a*b*). The characterization results indicated that the sample has good crystallinity, and the formation of hematite(α-Fe_2O_3) crystalline begins at 700˚C. However, a new crystalline structure with a chemical formula of ($Al_3Fe_{15}O_{12}$) was observed beyond 800˚C that overlapped with (α-Fe_2O_3). The overlapping was observed at around 33.3˚ and 35.8˚ 2 theta on the XRD peak. Moreover, the range of the extracted sample was from nano to micro with some agglomeration. The optical properties indicated a metal-to-ligand charge transfer at 250 nm while metal-to-ligand charge transfer was between 300 and 550nm. In the end, the colouring result becomes in good agreement with brown red and dark red pigment with good agreement with commercial hematite at 800˚C, with L* = 30.77, a* = 15.46 and b* = 29.76. In the second part of the study, the synthetic and extracted iron oxide were doped in the copper chromate pigment using a solid-state mechanism. In the process, mixing was done using an agate mortar and pestle; then, an attrition mill was used with 1000 rpm was used for 1:30 h. The sample was dried and ground for 30 min and pressed using

1 ton (9964.016 N) into a pellet of 25 mm diameter. The pelleted one was then calcined at 1350°C for 3 h to foster the reaction. After calcination, the calcined pellet was ground and sieved in 100 sieve size mesh (#100). In the end, the sample's crystalline structure, crystallite size, microstrain, morphology, structural, optical, Refractive index, and colouring properties were examined using XRD, SEM with EDS, FTIR, and UV-VIS NIR. The XRD result indicated that a successful spinel pigment was produced in both synthetic and extracted iron-doped copper chromate pigment. At the same time, the particle size distribution becomes reasonably good with spherical particulate formation. In addition, the FTIR confirmed the spinel structure formation, and UV-VIS NIR showed the absorption of all spectra, a confirmation of perfect black. The CIEL*a*b* confirms the achievement of the best pigment with an optimized result at 0.5 weight percentage iron is doped. In the end, all the parameters that contribute to tuning the colour of the pigment and its colouring axis are comparable with the commercial one and have a promising result.

Key Words:- Steel slag, doping, Composite pigment, Hydrothermal method, Solid-state method, synthetic pigment,

CHAPTER-ONE

1. INTRODUCTION

1.1 BACKGROUND

Almost every object in our environment is coloured in a variety of hues. Colour gives objects an aesthetic appearance and plays a role in visually communicating information, such as safety and warning colours. Pigments are an important class of additives, and they can provide colour to the object and improve the appellative qualities of the materials to which they are applied [1, 2]. They are coloured powders that are insoluble or poorly soluble in water and organic solvents. Therefore, they selectively absorb a part of visible light and display the complementary colours of the light absorbed. Colourings are compounds that, combined with other substances, impart or change a product's colour. Human eyes can distinguish red, yellow, blue, green, black, and different hues directly from visible light absorption or reflection caused by the product's wavelength-selective absorption [3].

Pigments have been used worldwide for centuries [4-6]. Naturally occurring pigments have been identified since the prehistoric era; the preparation and application of this pigment can be traced back over a million years [7]. The research output indicated that most of the pigments and dyes employed throughout the prehistoric period were markers of the era's technological advancement [8-10]. The red ochre paints applied to the bodies of North American Red Indians to defend themselves from evil, the paints used by Indian ladies to depict the married woman was also the colour of richness and grace, and their goddess Lakshmi are some of the historic testimonies on pigment and dyes. On the other hand, drawings at the Pech-Merle caves in Southern France and the image of Egyptian pharaohs were produced using paint in 4000 BC, utilizing synthetic blue dye made of calcium copper silicate ($CaCuSiO_4$), shown in **Figure 1.1 [**11-14]. The Chinese people have also used pigments to detect material deterioration [15, 16].

Pigments that were commonly used throughout the prehistoric period contained combustion components or elements and manufactured chemicals produced from suitable raw materials and hybrid pigments [17].

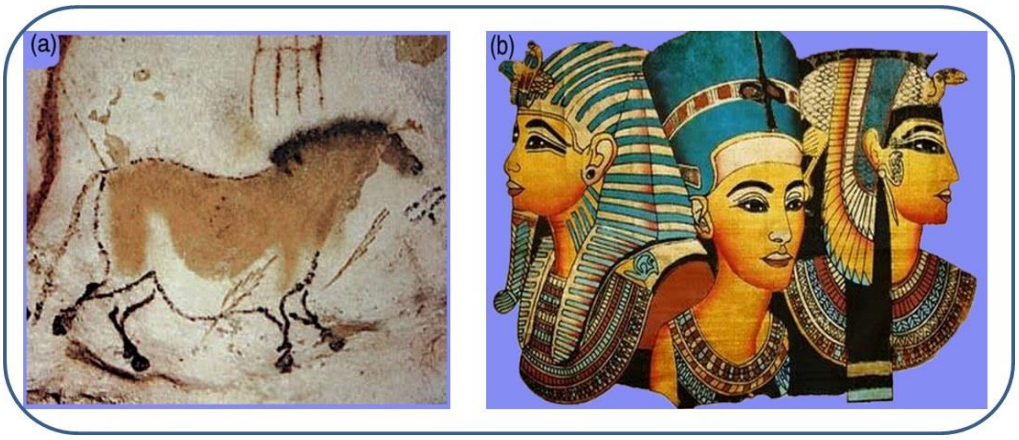

Figure 1. 1 (a) Patterned hose in the Pech Merle cave. (b) Ancient Egyptian Pharaohs [14].

Cahputal and Devy were the first scientists to use XRD to explore the qualitative analysis of pigments, most notably the chemical composition of naturally occurring Cuprorivite blue Egyptian pigment [18]. **Table 1.1** depicts the early historical age of pigment examination and their chemical names and formulas.

However, current research focuses on developing long-lasting pigments with powerful tones that can be changed to meet technological and environmental requirements [19]. In 2020, Prepared Pigments were the world's 529th most traded product, with a total trade of $4.27B; worldwide, the demand for pigments is predicted to rise to about 13.4 million tons in 2030 [20]. According to the American Dry Color Manufacturers Association (ADCMA), these heterogeneous chemical compounds contribute a wide range of colours to the pigment industry [21].

Table 1. 1 Common Chemical Substances Originally Named for Their Colour [4]

Ancient Name	Pigment colour type	Chemical Identity
Hematite	Blood like stone	Ion(III) oxide (Fe_2O_3)
Magnesia alba	White substance from Magnesia	Magnesium carbonate ($MgCO_3$)
Magnesia nigra	Black substance from Magnesia	Manganese dioxide (MnO_2)
Orpiment	Gold pigment	Arsenic (III) sulfide (As_2S_3)
Plimbum Cendidum	White lead	Tin(Sn)
Plumbum nigrum	Black lead	Lead (Pb)
Plumbum cinereum	Ash-coloured lead	Bismuth (Bi)
Verdigris	Green of Greece	Dibasic copper (II) acetate ($Cu(C_2H_3O_2)_2$ $2Cu(OH)_2$)
Vermilion	Worm-coloured	Red mercury(II) sulfide (HgS)

According to [21], the heterogeneous pigment synthesis of the 21st century focuses on the production of a wide range of cooling, the application of heat absorbers, the substitution of toxic pigments, and the formation of tunable colour properties from composite pigments [22-25]. In general, contemporary research and development in the field of transition metals pigments have mainly concentrated on "pigment sustainability," "eco-friendly pigments," "compatibility," and "circular economy"[26-28].

1.1.1 Definition and Classification of Terms in Pigment

1.1.1.1 Pigment, Colorant, and Dye

The pigment is the Latin word "pigmentum," which means "colouring matter" [29].

- It's the term for a chemical that provides colour in the form of insoluble particulates that are immobilized inside a binder.

The colourant is a general term describing any substance used to modify the colour of an object by changing its spectral transmittance or its reflectance.

- Colourants can be classified as pigments or dyes, as shown in **Figure 1.2**. The solubility properties of dyes in solvents distinguish them from pigment [30]**.** In general, the primary difference between dyes and pigments are listed **Table 1.2,** as shown below

Table 1. 2 Basic Differences in Dyes and Pigments [29]

No	Dyes	Pigments
1	Soluble in the host materials, like water	Dispersed in the solvents
2	Do not scatter light and looks transparent	Do not scatter light; hence looks opaque
3	Absorbed by coloured substances	It needs a binding agent to adhere to the surface
4	Quickly fade with light or rain	Can withstand environmental conditions and last for a long time

Unfortunately, the differences between a dye and a pigment are not considered, which frequently makes it confusing. The definitions in the dictionaries or some industries do not necessarily coincide with the technical terminology. Thus, dyes are distinguished from pigments primarily by their physical characteristics and their chemical characteristics [29].

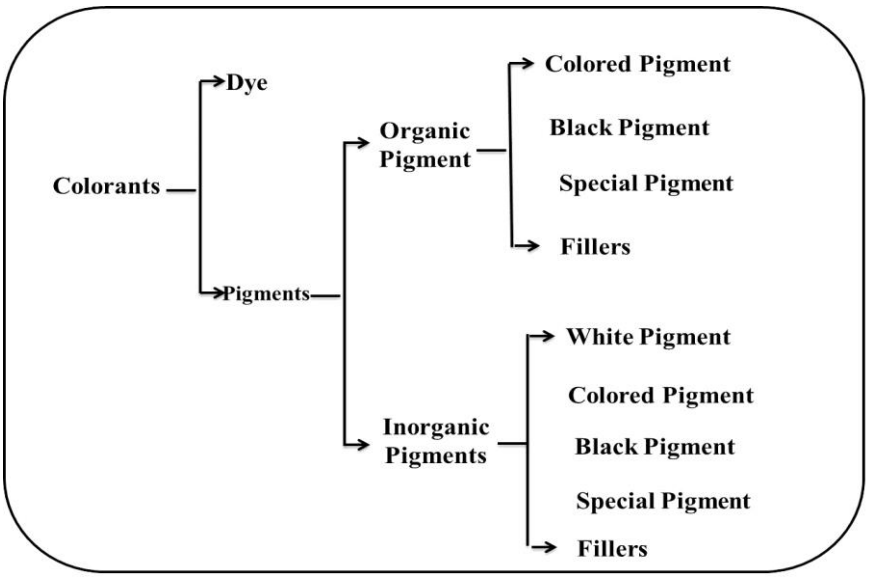

Figure 1. 2 Classifications of Colorants [29]

The solubility of pigment and dye is a significant characteristic that distinguishes them. Dyes are coloured substances soluble in water and used in textile production. Pigments, conversely, are colourants composed of insoluble particles in the mediums in which they are utilized [31]. Dyes have a higher affinity for the media to which they are applied, causing a temporary disruption in the crystal structure during the application process via absorption, solution, and mechanical retention via ionic or covalent chemical bonding [32,33]. In general, the following properties are essential for pigment synthesis [34];

General chemical and physical properties*:* including the chemical composition, moisture and salt content, content of water-soluble and acid-soluble matter, particle size, density, and hardness.

Stability properties*:* refers to resistance toward the light, weather, heat, and chemicals, anti-corrosive properties, and gloss retention.

Behaviour in binders*:* means interaction with the binder properties, dispensability, unique properties in specific binders, compatibility, and solidifying effect.

1.1.1.2 Organic and Inorganic Pigments

Pigments are classified based on their chemical composition (organic or inorganic) [35]. Unlike organic, inorganic pigments are not based on carbon chains and rings. Instead, they are made of dry minerals, metals and metallic salts. Because of their composition, inorganic pigments are

typically more opaque and insoluble than organic pigments. In general, inorganic pigments are the most commonly used in the industry owing to their lightfastness and low cost.

Inorganic pigments are a popular choice in the industry for various reasons, but they have some drawbacks. Some of the most important positive and negative properties of inorganic pigments are:

- **Excellent fading resistance:** One advantage of inorganic pigments is their excellent fading resistance when exposed to light. They are also more resistant to fading when exposed to sunlight and heat.
- **Cost-effective:** Inorganic pigments are typically less expensive, especially in large quantities required for industrial applications. This is due to the simple chemical reactions needed to make inorganic pigments.
- **Poor tonality:** While inorganic pigments have a high colour retention rate, the colour they produce on their own is frequently dull. Improving tonality and brightness is often possible by combining inorganic pigments with organic or dye pigments.
- **Toxicity** Because of lead salts in their composition, inorganic pigments are more harmful to the environment. Some are even poisonous, such as lead-based pigments.

Unlike inorganic pigments, organic ones are limited to short-term applications and become incompatible with high-temperature ceramic and polymer manufacturing due to their thermal, chemical, and solar instability [36].

Inorganic pigments have been greatly admired throughout the history of humankind owing to their potential usage in paints, inks, glazes, etc., for colourants. Different inorganic pigment chemical compositions are required for various applications. They are widely utilized in multiple applications, including paint, glazing, and ceramics [37]. Inorganic pigments are generally stronger than organic pigments in three primary characteristics: thermal stability, chemical resistance, and high tinting power, and they are obtained by using transition and heavy metals as colour activators as opposed to organic pigments [38-42]. It includes one or more transition metals, which typically contain partially filled orbitals, occur in various oxidation states, and are embedded in places with different geometrical configurations of anions or ligands. Generally, they are distinguished by their crystalline lattice structures [26]. Crystal defects and alteration of the crystal lattice affect the pigment characteristic.

Inorganic pigments are basically classified based on their chemical compounds, colouristic, light interaction, and composition. **Table 1.3** indicates that the developments of inorganic pigments are classified based on colouristic and chemical considerations, as recommended by ISO and DIN [29].

Table 1. 3 Classes of Inorganic Pigment [29]

Term	Definition
White Pigments	It is due to nonselective light scattering (TiO_2 and ZnS pigment
Coloured Pigments	Caused by selective light absorption and selective light scattering (Fe_2O_3, Chromium pigment, Cobalt pigment)
Black Pigment	By nonselective light absorption (Carbon black pigment and Iron oxide black)
Effect Pigment	The Optical effect is due to regular reflection or interference
Metal effect pigment	Mainly on flat and parallel metallic pigment particles (Aluminum flakes)
Pearl lustre pigments	Regular reflection on highly refractive parallel pigment platelets (Titanium dioxide on mica)
Interference Pigments	Coloured lustre is wholly or mainly by the phenomenon of interference (Iron oxide on mica)
Luminescent pigments	By the capacity to absorb radiation and emit it as light of a longer wavelength
Fluorescent Pigments	Light of longer wavelength is emitted after excitation without delay (Silver doped zinc sulfide)
Phosphorescent Pigments	Light of longer wavelength is emitted within several hours after excitation (Cu doped ZnS)

Due to their adjustable and enhanced properties relative to their parent source pigments, complex inorganic colouring pigments have become the most commonly used pigment types for use in conventional to advanced applications such as solar heat energy absorbers, engineering plastics, highly resistant roofing panel coatings, automotive finishes, light-reflecting sing, ceramic decorations, cosmetics, and space equipment [43,44].

The production of these pigments necessitates the control of several parameters, such as chemical composition, optical property, crystallography, colour characterization, and bandgap management. As a result, "doping" transition metal oxide powder on metal species has become one of the most often used ways of adjusting the substance's bulk properties, surface structure, and reactivity [45]. Because of the high cost of synthetic raw materials with industrial chemical purity, there has been a trend toward using less expensive natural materials and other alternatives [46]. In this sense, mixing waste from manufacturing facilities, such as steel rolling mills, with pure synthetic compounds reduces potential environmental pollution threats and conserves natural resources. Using industrial waste as a raw material for pigment manufacturing saves money while providing a home for many hazardous residues to human health and the environment or promoting the circular economy policy [47, 48]. As a result, the development of science and technology in recycling wastes as input raw materials for various industrial uses was the primary focus of the twenty-first century.

Steel slag (Ss) is one of the world's most debated solid wastes due to its high iron content [49]. Iron oxide is the second most commonly used pigment after TiO_2, combined with others as a composite form [50]. As a result, meeting all or part of the synthesis criteria is an effective strategy for lowering the cost of expensive pigments without sacrificing their properties [23, 51].

Even though some studies have been done previously to examine the effect of mixing the synthetic and extracted pigments in obtaining a colour chart while also meeting the aims of the circular economy, there are still few studies published in the literature.

1.1.2 Principles in colour in transition metal containing pigment

The colour produced by inorganic pigments is a sensory impression elicited by light rays entering the eye. If the light source is standardized, the optical properties of a pigmented layer of paint are determined by the optical properties of the pigment particles, their size, shape, and volume concentration, as well as the optical properties of the (usually colourless) dispersion medium [23]. It was stated that shading is determined by the ability of the pigment to confer colour on light-scattering materials by absorption properties [52].

The interaction between the coating material and visible light is the source of all colour phenomena observed in coatings. When a photon passes through a pigmented film, one of three things can happen:

1. The photon collides with a pigment particle and is absorbed.
2. The photon collides with a pigment particle and is scattered.
3. The photon passes through the coating without collision and is scattered or absorbed by the substrate [53].

Smaller particle size pigments have a greater absorbing region per colourant mass, and the tinting intensity usually increases as the particle size decreases. However, smaller particles create stronger agglomerates, making them more difficult to spread and disperse. This occurrence can lead to a smaller-than-expected increase in the tinting strength of the fine pigment [54, 55].

The pigment's hue is thought to be affected by the solar range of radiation energy, namely UV (200nm-400nm), visible area (400 nm -700 nm), and near-infrared (700 nm -2500 nm), which account for 5%, 43%, and 52% of total irradiation, respectively [22]. As a result, the pigment's optical and colouring qualities are based on the absorption of a single or a range of light frequencies, as shown in **Figure 1.3.** The pure pigment can only absorb a single frequency of light that is complementary to the frequency or colour reflected by the pigment. The frequency of absorbed light is thus related to the electronic interband transition, which might result in a thin absorption edge in the visible spectrum region [53].

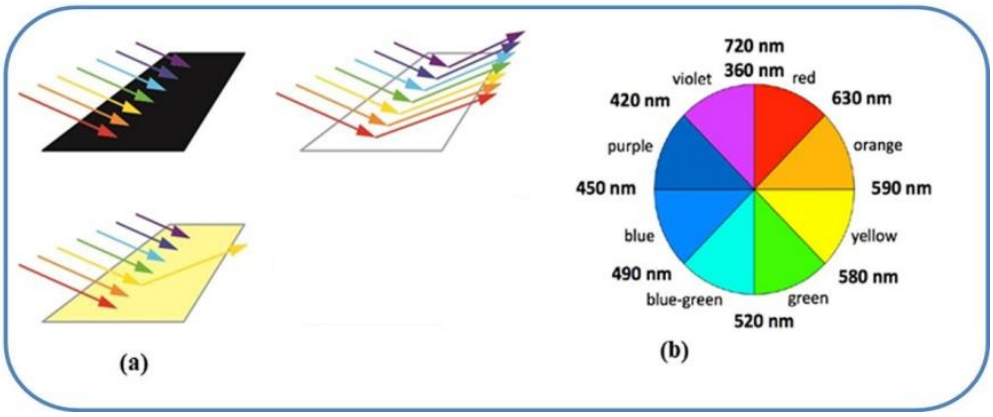

Figure 1. 3 (a) Principle of colour appearance (b) Observed colour with the corresponding wavelength

When atoms or molecules absorb light at the appropriate frequency, electrons are excited to higher-energy orbitals. The absorbed photons of many main group atoms and molecules are in the ultraviolet range of the electromagnetic spectrum, which cannot be seen with the naked eye. Because the energy difference between the d orbitals in coordination compounds frequently allows

photons in the visible range to be absorbed, transition metals are considered the best for inorganic pigment synthesis [56].

Most transition metal oxides have a wide range of band gaps, allowing the electromagnetic spectrum to be absorbed in the visible region. This band gap can be altered by sufficiently replacing chromophore metal ions and utilizing various synthetic processes to produce variable colour characteristics. The mixing ratio, particle size, shape, and concentration volume are all factors that influence the qualities of paint pigment [57, 58]. Apart from the metal cation employed, the ligands, coordination number, distance between metal ligands, and geometrical structure of the ligands all have an impact because these inorganic pigments depend on the metal oxide transition properties [59, 60].

1.1.3 Structural property of inorganic pigments

Inorganic metal oxides are often used as pigments and fillers in painting colours. Inorganic pigments differ in chemical structure and are found in oxides, sulfides, sulfates, carbonates, or oxy-hydroxides of transition metals, where the effect of colouring depends on the structure of the pigment [61]. Inorganic pigments with different colour ranges are usually a complex mixture of oxides. They are produced from calcination at high temperatures of metal oxides, minerals, or metal salts, with thermal stability being one of their most important properties [62].

The property of thermal stability at glaze firing temperature, minimal reaction with molten glaze, and good colour performance are required from pigments in the industries. The colouring property of the pigment depends on the particle size; as the size decreases from micro to nano-size, it will possess a high surface area and endure better coverage of pigment and homogeneous mixing of the pigment into paint and glazes [63].

Beyond the particle size, outstanding colour stability is made by synthetic crystalline metal oxide from Complex Inorganic Color Pigments (CICPs). The Oxygen / Metal (O/M) is the most significant factor determining the colourants' structure. As long as the metal ions are of comparable size, the O/M ratio largely determines the structure, as indicated in Table 1.8. Hematite, rutile, and spinel are the three crystal structures that dominate the class of CICPs [64].

CICPs are typically produced through high-temperature (700–1400°C) solid-state reactions in which metal oxide, hydroxide, carbonate, or other raw materials capable of yielding oxides upon calcination are intimately mixed and calcined in continuous or batch-style kilns. During calcination, metal oxide species inter-diffuse and create a final, stable, crystalline structure. In

CICPs, various metal cations are incorporated into a stable host lattice [65], and they will not exist alone as individual chemicals. However, it forms new chemical compounds with properties determined mainly by the host lattice.

Table 1. 4 Structures and Formulas of Common CICPs [64].

Crustal type	*Basic Formula*	*O/M ratio*
Rutile	MO_2	2
Hematite or Corundum	M_2O_3	1.5
Spinel	M_3O_4	1.33

Prof. S. G. Tumanov was the first to synthesize spinel-based pigments [66]. He created high-thermal-resistance ceramic pigments based on cobalt and nickel spinels. The suitability of a spinel structure $A^{II}B^{III}{}_2O_4$, and its chemical stability in a wide range of applications like magnetic materials, ceramics, and catalysis, is because of the two different cations of comparable ionic size. In the spinel structure, the oxygen ions form a cubic close-packed structure, whilst the two cations (A and B) occupy two unique crystallographic positions, tetrahedral and octahedral [67]. The combination between the size, coordination number, electronegativity and nature of the two cations, crystal field effect, and the condition of the preparation method determine the distribution of the two cations in the crystal lattice of spinel [68]. Based on the cations distribution in the crystal lattice, the structure can be normal spinel with AB_2O_4 or inverse spinel with $B(AB)O_4$ [69, 70]. As a result of the correlation between structure and properties like diffusivity, magnetic behaviour, catalytic activity, optical properties, and solar reflectance, the cation distribution structures in spinel structure become a focusing area.

1.1.4 Measuring the colouring property of the pigment

Most transition metals appear to be coloured due to a coordination complex. That means when this cation (cations containing the d-electron) are surrounded by other ions or polar molecules, either a complex in solution or solid form, a splitting of energy levels of the five d-orbitals, all having the same energy, occurs. At this moment, when light falls on such a system, electrons can move between those split levels. The energy absorbed in this process corresponds to the absorption of the light at a specific wavelength, usually in the visible light spectrum region; hence the colour is observed [71].

Generally, when the light absorption is significantly smaller than its reflection, in this case, the pigment appears to be white; the reverse is valid for a black one. But in coloured pigment, when the absorption and scattering are selective, the pigments are characterized by their spectral reflective curve [72].

The visible light regions of the electromagnetic spectrum ranging from 400nm to 700nm (3.10-1.77ev) [73, 74] are responsible for colours to make selective absorption and scattering phenomena. Absorption and scattering of light outside the visible region can also be important and valuable properties of a given Pigment [75, 76]. The colouring properties result from light absorption and light scattering power. Pigments with stronger light absorption than light scattering have a greater depth of colour [77]. Light will be scattered when pigment particles possess an index of refraction more significant than the materials in which they are dispersed. The scattering power of a pigment is influenced by the material's refractive index and pigment, the pigment particle size distribution, and the degree of dispersion [78].

The International Commission on Illumination, an international body concerned with lighting and colour concerns, created mathematical equations to get variables representing colour(colour axis); the (CIE) techniques. The L* a* b* colour space (also known as CIELAB) [79] is one of the most well-known of these systems. The CIE1976 L*a*b* colourimetric method works after calibrating with a standard white light using D65 illumination, and according to the (CIE), it works in the range of 200-800nm. L* denotes lightness in this space, as shown in Fig. 1.12(b), with a value ranging from 0 (black) to 100. (White), whereas the chromaticity coordinates are a* and b*. The axis a* and b* denote colour directions: +a* indicates red, -a* indicates green, +b* indicates yellow, and -b* indicates blue.

The colour saturation increases as a* and b* values increase and the point away from the centre. The colour is represented as a point in this area, allowing for a precise description. The tristimulus values XYZ [79] and Xn, Yn, and Zn, which are the tristimulus values XYZ of a perfect reflecting diffuser defined by the CIE in 1931, are proportional to the values of L*, a*, and b*, as seen in the transfer **Equations (1–3)**

$$L^* = \left(\frac{Y}{Y_n}\right)^{1/3} - 16 \quad (1)$$

$$a^* = 500\left[\left(\frac{X}{X_n}\right)^{\frac{1}{3}} - \left(\frac{Y}{Y_n}\right)^{\frac{1}{3}}\right] \quad (2)$$

$$b^* = 200\left[\left(\frac{Y}{Y_n}\right)^{\frac{1}{3}} - \left(\frac{Z}{Z_n}\right)^{\frac{1}{3}}\right] \quad (3)$$

The Chroma can be given by **equation 4 [43, 80, 81]**.

$$C^* = \sqrt{(a^*)^2 + (b^*)^2} \quad (4)$$

Where C* is the Chroma of the colour

The colour describing the degree of purity relative to natural grey refers to saturation and determines the colour intensity directly. Chroma then stood for colour saturation. Therefore saturation and Chroma determine a hue's "colourfulness" or purity [82]. Hues are the outer rim of the three-dimensional solid, lightness increases or decreases along the vertical axis, and saturation varies depending on the central point. To specify these criteria, value scales were devised, and several methods were developed to quantify colour and allow it to be expressed more quickly and precisely. For example, the hue angle, H*, measured in degrees, can be calculated using the range of 0^0 to 360^0 by **equation (5)** [43, 76].

$$H^* = \tan^{-1} (b^*/a^*) \quad (5)$$

At the same time, hue variation, which means the colour changes between samples of mixtures containing various quantities of pigments, is then evaluated by chromaticity differences. For example, suppose the differences between two colours in L*, a*, and b* are denoted by ΔL*, Δa*, and Δb*, respectively; the colour difference can be evaluated by the formula shown in **equation (6)** [74, 83].

$$\Delta E = \sqrt{(\Delta L^*)^2 + (\Delta a^*)^2 + (\Delta b^*)^2} \quad (6)$$

The value of delta refers to the difference between the standard and samples. The maximum difference implies the sample is out of tolerance and the sample needs correction, which means that if Δa^* is out of tolerance, the redness/greenness needs to be adjusted. Moreover the positive Δa^* indicates that the sample is redder than the standard. The overall colouring hue and Chroma with each axis are shown in **Figure 1.4 a and b** [84].

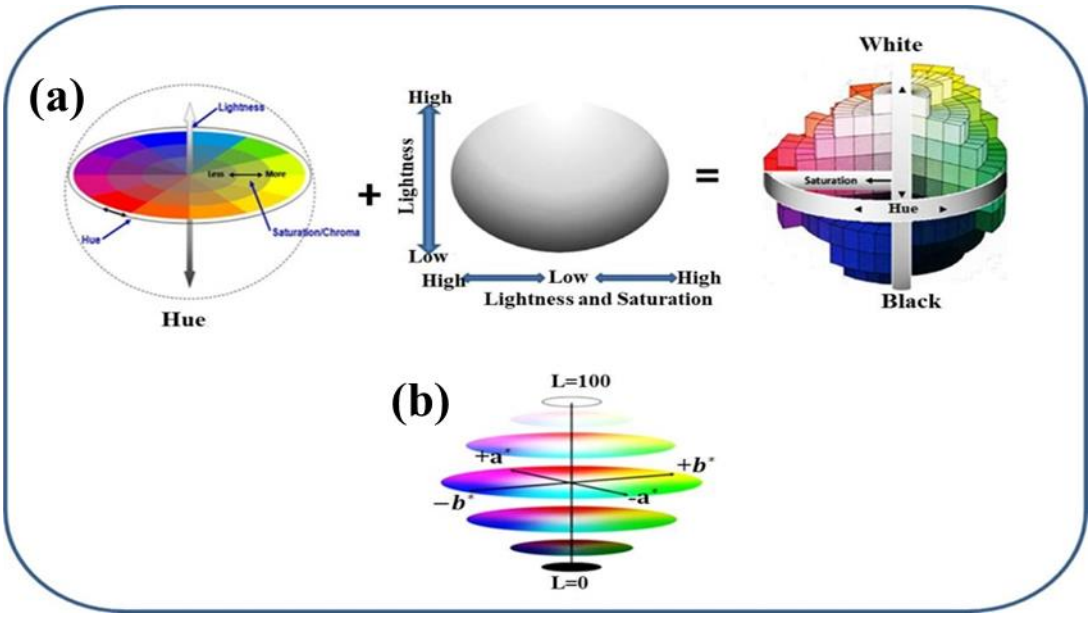

Figure 1. 4 (a.) The three tristimulus components of colour, (b.) The CIELAB colour model [79, 82].

Similarly, the optical property of the pigment can be determined from the Kubelka Munk function. It converts the diffuse reflectance spectroscopy data of powder generated from UV-Vis spectroscopy into equivalent absorption coefficients (α) [85]. It is mainly used to calculate the band gap of the synthesized pigment [43], which is used to measure absorption by the powder. The function K–M is given by [76].

$$K - M = \alpha = \frac{(1-R)^2}{2R} \qquad (7)$$

Where R is the reflectance of samples, a plot of K–M and wavelength can be used to determine the absorption edge from the plot. Similarly, the bandgap of the pigment can also be calculated using the equation [86]

$$(F(R)h\upsilon) = (\alpha h\upsilon) = A(h\upsilon - E_g)^Z \qquad (8)$$

Where h and υ are constants, F(R) is the Kubelka-Munk function, F(hυ) is the energy function, R is the reflectance of the sample, α is the absorption coefficient, and Z is the value between 1/2,

3/2, 2 and 3 depending on the direct allowed, direct forbidden, indirect allowed and indirect forbidden electronic transitions, respectively [86, 79].

1.1.5 Methods of Synthesis of Inorganic Pigment

Various synthesis methods are used to produce inorganic pigment based on the fundamental idea of crystal chemistry [42]. As a result, many inorganic pigments have been developed, ranging from simple oxides to complex oxide crystals and heterogeneous nano-size and inorganic matrices [26]. Even though several methods of synthesis of inorganic pigments from synthetic and recycled precursors have been recorded in the literature, the most commonly used methods are: hydrothermal [52, 87], sol-gel [50, 88-90], solid-state [91-94], and precipitation and combustion synthesis [35, 95, 96]. Each synthesis process has advantages and disadvantages, and researchers select synthesis mechanisms that are most suited to achieving their goal.

1.1.5.1 Hydrothermal Methods

In the hydrothermal mechanism, the products are achieved by mixing metal salts in an aqueous solution and heating them at the right temperature. The hydrothermal synthesis method develops the use of metal salts as a starting material [86, 97]. This technique is suited for manufacturing highly crystalline inorganic nanoparticles [98]. The metal oxide Nanopowder synthesis utilizing metal nitrate as a precursor involves two phases: precipitation of metal hydroxide and dehydration to produce the metal oxide, as listed in equations (9) and (10) [99].

$$M(NO_3)_x + XH_2O = M(OH)_x + XHNO_3 \quad (9)$$

$$M(OH_3)_x = MO_{x/2} + X/2\ H_2O \quad (10)$$

The results in **Figure 1.5,** as well as different researchers, indicated that the product size and shape were controlled using controlling parameters like temperature, pressure, time, and pH; those parameters played essential roles in determining the pigment characteristics during the process [100-102].

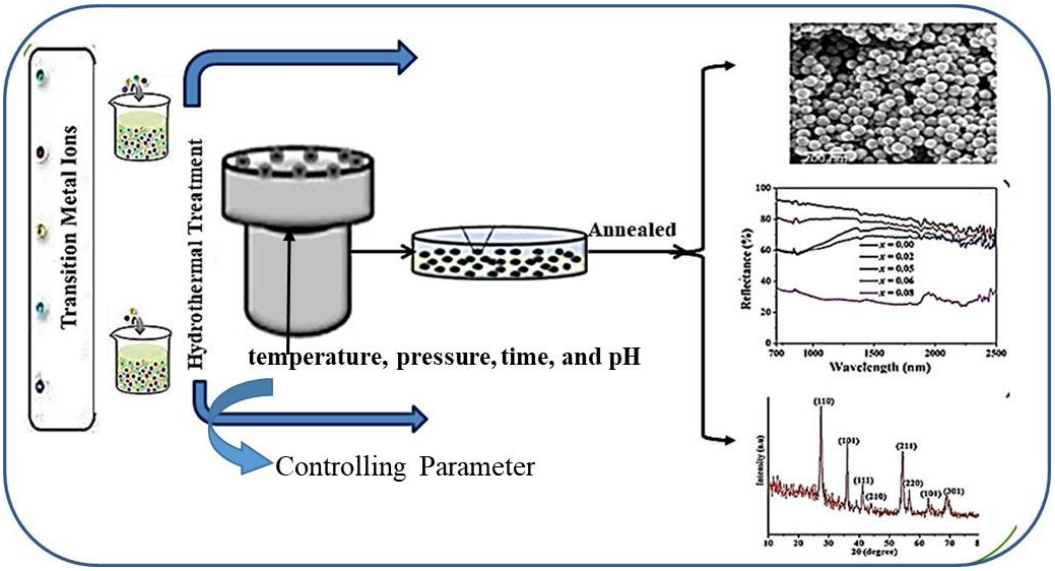

Figure 1. 5 Hydrothermal synthesis mechanism of nanoparticles and characterization results

The outcomes of these parameters are shown in a study on the synthesis of goethite utilizing synthetic starting material in a hydrothermal process [103]. **Figure 1.6 (a and b)** shows the selected area electron diffraction pattern of goethite (α-FeOOH) exhibiting a difference in form due to annealing time. The XRD result of the goethite pigment particle after annealing at 140^0C for 4 h is poorly crystallized, but the sample gets its crystalline structure (rod-shape) when the annealing time increase to 8 h, as indicated in **Figure 1.6b**. Furthermore, as the annealing period increases to 12 h, the goethite is partially transformed into hematite, as shown in **Figure 1.6 C**. All the mentioned behaviour of the pigment indicated that the heat treatment for a longer time allows the water to remove and the particles to be arranged adequately and form a crystalline structure. But the extended time heat treatment made the materials transform into hematite.

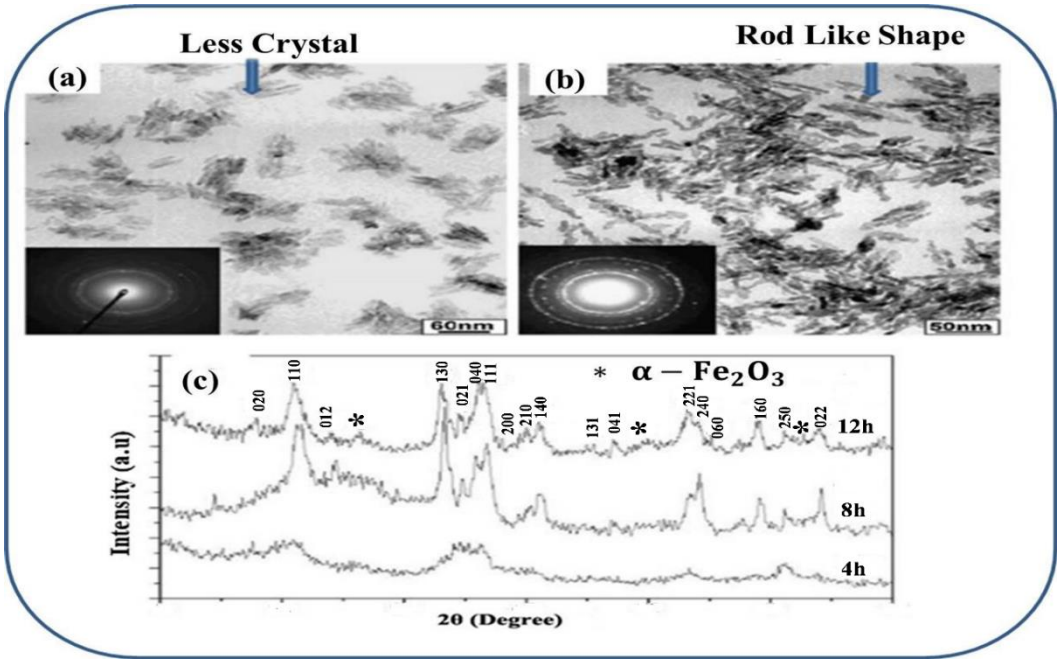

Figure 1. 6 (a) TEM image of the sample produced at 140˚C for 4 h. (b) TEM image of the sample produced at 140˚C for 8 h. (c) XRD pattern of the sample annelid at 4hr, 8hr, and 12 h [103]

Similarly, Dailong Chen et al. 1999, showed that a change in temperature and time causes a variation in the size and morphology of the particle product generated by the hydrothermal process, as shown in **Table 1.5** [104].

Table 1. 5 Reaction conditions and particle properties of zinc oxide powder compound without additives

No	*Reaction Conditions*		*Particles Property*	
	Temperature (ºC)	**Time (h)**	**Morphology**	**Size (nm)**
1	100	10	Bullet-like	100-200
2	160	6	Rod-like	100-200
3	180	6	Sheet	50-200
4	200	6	Polyhedron	200-400
5	220	5	Crushed stone-like	50-200

On the other hand, Hiromichi and Hayashi can change the temperature, time, pH, and reaction pressure to change the particle size and morphology of synthetic metal oxide preparation using a

hydrothermal method, which influences the colouring properties [54, 98, 99]. In the $BiVO_4$ synthesis experiment using the hydrothermal method, the annealing temperature was the controlling parameter; it attained a tetragonal structure as it was annealed at 110˚C for 24 h. In contracts, the shape becomes monoclinic due to the annealing temperature change to 240˚C [27]. In conclusion, even though the method is better at controlling the shape and size of the product, it needs a better understanding of the solubility of the mixed starting materials and compounds formed throughout the process, and the mechanism is expensive [97].

1.1.5.2 Combustion Method

It is a mechanism for synthesizing metal oxide using low temperatures [105, 106]. Researchers have recently become more interested in this strategy due to its time-efficient and cost-effective use of soft chemical approaches that rely on quick and sustainable redox reactions [23, 51, 107]. According to Arvind Varma,2016, the solution combustion synthesis approach is one of the most extensively utilized procedures for synthesizing nanoscale products [108].

The fuel, the oxidizer, and the temperature required to generate the combustion process are all considered [109]. The ratio of the reducer to the oxidizing agent, temperature, and reaction time during the synthesis process all influence the particle's conversion degree, composition, agglomeration, and shape [110-112]. **Figure 1.7** depicts a schematic picture of the combustion process, which illustrates that the process is divided into three primary components: the mixture's composition, the gel's formation, and the combustion process.

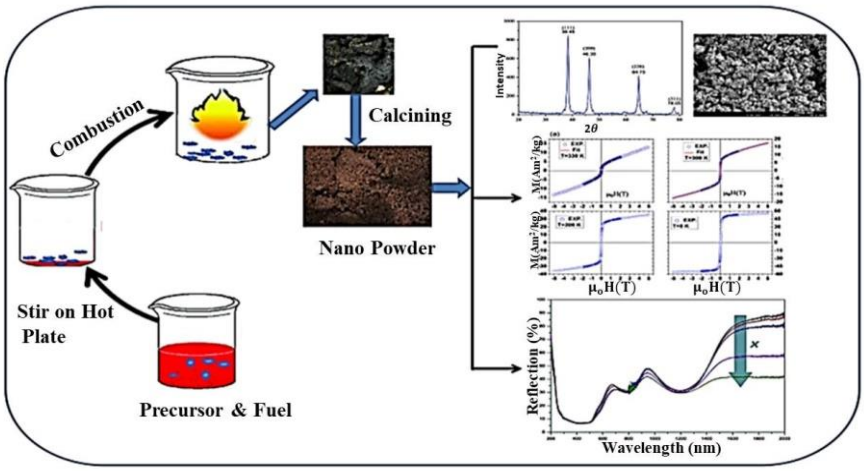

Figure 1. 7 Synthetic particle production procedure using solution combustion method

The exothermic redox chemical reaction is the immediate chemical interaction between the oxidizer and the fuel needed to produce light, ash, and heat. Next, dehydration of the mixture generates the gel during the process, and lastly, combustion occurs between the fuel and the oxidant. The above argument implies that organic ligand-group fuel plays a crucial role in creating different phases and the shape of various metal cations. Furthermore, the chemical energy produced by the exothermic reaction between various metal nitrates and fuel varies [113]. According to Mahdi Shafiei Chafi et al., 2017, the crystal structure of the particles generated by the solution combustion process is determined by the oxidizer-to-fuel (O/F) ratio [114, 115].

The XRD peak in **Figure 1.8** shows the link between the total O/F ratio and the particle production process. In comparison, the XRD peak indicates that iron-oxide formation increases as the ratio of O/F increases.

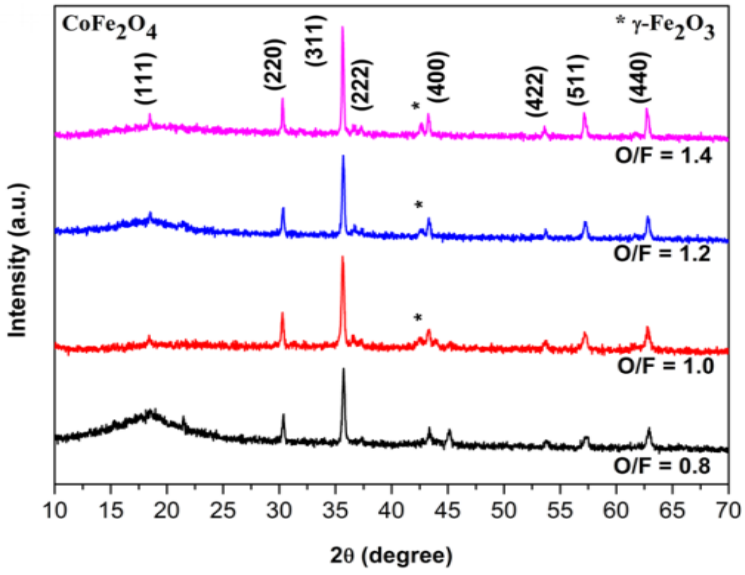

Figure 1. 8 XRD patterns of Cobalt iron oxide pigments prepared [116].

According to the report by S. Rasuli et al.,2014, the structure and particle size improvements in the O/F ratio of the synthesized samples using urea and glycine as heat, in addition to the temperature of the furnace that controls the process, is a determining factor for the ignition that occurs in the combustion synthesis [115, 116]. The reaction furnace temperature must be measured depending on the intended product, and the combustion temperature is determined by the type of fuel used [118]. Urea, glycine, citric acid, ethanol, oxalyldihydrazide, and alanine are the most often employed fuels in combustion processes [119-121]**.**

1.1.5.3 Sol-gel Method

This technique employs a chemical solution or a colloidal gel [122], which is regarded as one of the strategies for manipulating the chemical and physical properties associated with the desired sample properties [123, 124]. Sol-gel chemistry was found in the nineteenth century when $SiCl_4$-prepared alkoxide began to form a gel when exposed to oxygen [125].

This technique comprises the generation of metal oxide in contrast to the traditional mixed powder. At room temperature, salts, metal alkoxide, or hazardous waste are used as a precursor to the solution in sol-gel chemistry [126, 127]. The technique involves two chemical reactions: hydroxylation of the precursor by altering the pH of the salts or hydrolysis of the metal alkoxide in the organic solvent and condensation of the hydroxyl group.

It is an energy-intensive method because it operates at a relatively lower temperature than the solid-state synthesis method. According to Xiaojun Zhang, 2019, the exothermic peak of the TGA result was caused by the synthesis of $BiCl_3$ produced at 349°C using the sol-gel technique. In contrast, the identical solid-state synthesis procedure resulted in the same peak at a significantly higher temperature, 650°C [28]. However, this approach's challenge is controlling stoichiometry and precipitation homogeneity [128, 129]. Furthermore, the hydrolysis and condensation method is used to synthesize gelatin in sol-gel. [130].

The reactivity of the organic component or the chemistry of the oxygen-carbon bond in the reaction mixture influences the structural, morphological, and compositional behaviour of the final product of metal oxide and inorganic oxide-based monohydrate [131].

Figure 1.9 shows that the particle size distribution is dependent on the pH Value of sol-gel synthesized $LaPO_4$. In the research output, the particle size distribution of the samples produced by the sol-gel method depended on the pH of the solution; in addition, the varied reagent concentrations create products of various shapes [132].

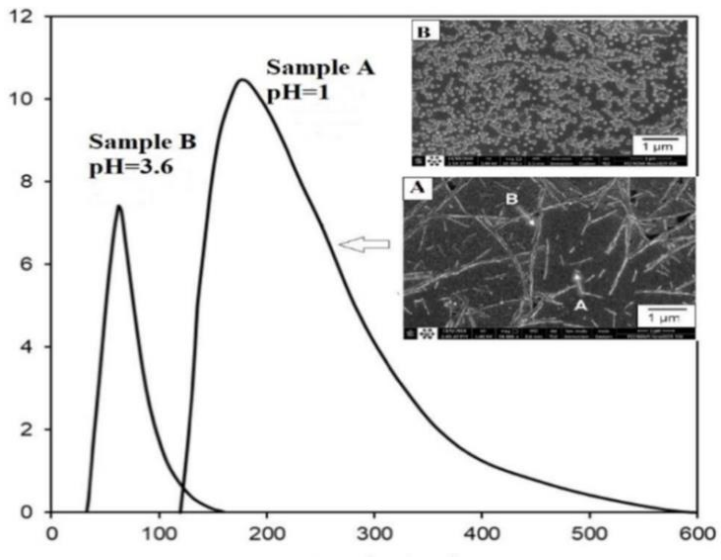

Figure 1. 9 Size distribution and SEM microstructure of synthesized $LaPO_4$ at different pH.

The initial reaction conditions influence the particle size, textural and structural aspects of materials created via the sol-gel technique. In addition, those particles' physical properties affect the colouring property of the product [133-109].

1.1.5.4 Solid State Method

This mechanism primarily results in the combining of polycrystalline non-volatile solids, which react to form the desired final product with the help of heating or calcination and mechanical or hand grinding to be mixed [136, 137]. The technique is high-energy synthesis, and the needed temperature ranges are primarily between 900 and 1600˚C [138]. Materials such as mixed metal oxides, sulfides, nitrides, and aluminosilicates can be employed [92, 139]. Unlike previous approaches, the solid-state process does not introduce impurities into the synthesis pigment and is simple, making it appropriate for creating a diverse range of complex inorganic compounds [91]. These chemical elements must meet the purity and grain dispersion requirements specified in the application.

These solid-state processes employ an agate mortar and pestle, allowing them to require a more extended calcination period and more energy at high temperatures [140-142]. **Figure 1.10** depicts the pelletizing procedure after the complete grinding of the mixed starting ingredients.

.

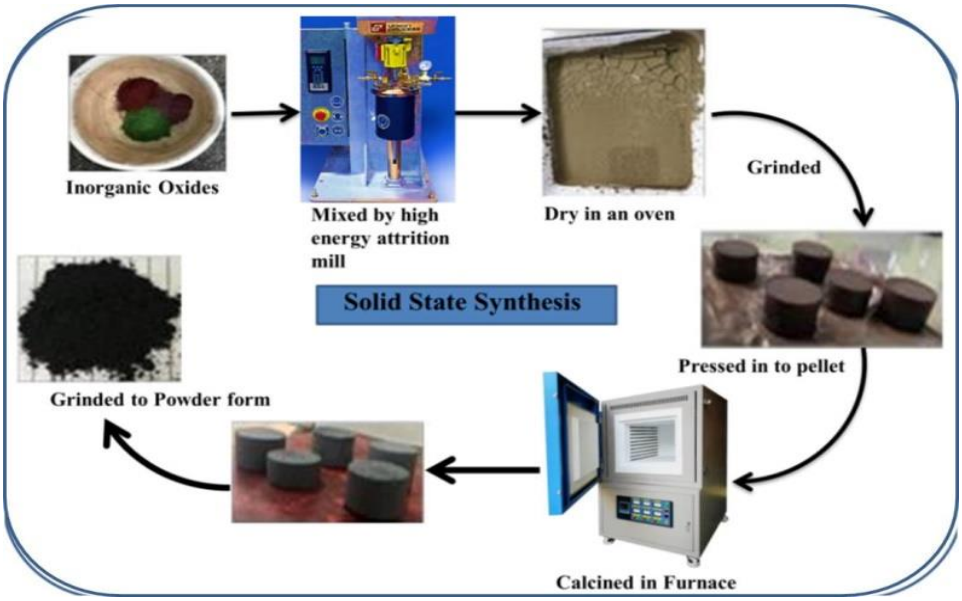

Figure 1. 10 Schematic processes of solid-state synthesis method of synthetic powder

Depending on the type of reaction, this technique would allow the chemical reaction to take place effectively, enhance the particle's surface area, and homogenize the manufactured particles [143-145]. Additionally, planetary milling, ultrafine grinding, and pulverization are effective methods for reducing the size [146]. As a result, the size of the reactive particles reduces, and the surface area increases as the grinding time increases, as shown in **Table 1.6** [147].

Table 1. 6 Specific surface areas and grain sizes of $CoFe_2O_4$ obtained by BET for different milling hours using pulverize.

	Attrition Milling (Time in h)			
	1	**2**	**3**	**4**
Bet Surface Area(m^2/g)	2.00	2.23	2.37	2.43
Bet Particle Size (nm)	560	507	477	465

The solid-state method is considered more energy-intensive, requiring higher energy calcination. To facilitate the reaction to happen, researchers use pressing into the pellet before calcining [147]. A pigment with chemical formula of $Ca(Co_xMg_{1-x})Si_2O_6$ was synthesized by researcher by solid-state method using agate mortar and pestle to combine the starting metal oxides and investigate its

effects; in the process, the researcher used a pressing machine to form a pellet during the experiment before calcining the grounded powder.

The research on Nd_2O_3 and SiO_2 showed how calcining temperature affects the mixing process to form a pigment [139]. On the other hand, $Zn_{1-x}Co_xO$ green pigment with a near-infrared reflectance property was synthesized by (Zhou et al.,2017) using the solid state method; in the process, the effect of high-energy ball milling has been investigated. In addition to those mentioned parameters, doping (adding) inorganic metal oxide on the parent pigment and wetting medium during the ground also affects the pigments' colouring properties, as shown in **Table 1.7.** The colouring indicated that the colouring property of the same chemical compositions and calcined at the same temperature, as shown in **Table 1.7,** were affected due to the wetting differences (Ethyl glycol and NaOH).

Table 1. 7 The colour axis of $YIn_{1-x}Mn_xO_3$ prepared with Ethylene Glycol and NaOH [139].

Compounds/condition	**CIEL*a*b***		
Condition 1 [using Ethylene Glycol]	L*	a*	b*
$YIn_{0.92}Mn_{0.08}O_3$–1000 °C	35.07	−1.26	−26.43
$YIn_{0.92}Mn_{0.08}O_3$–1100 °C	39.55	4.1	−40.61
$YIn_{0.92}Mn_{0.08}O_3$–1200 °C	34.96	10.73	−45.26
$YIn_{0.92}Mn_{0.08}O_3$–1300 °C	28.75	14.97	−42.66
Condition 2 [using NaOH]			
$YIn_{0.92}Mn_{0.08}O_3$–1000 °C	47.24	−4.58	−30.25
$YIn_{0.92}Mn_{0.08}O_3$–1100 °C	45.92	0.84	−38.54
$YIn_{0.92}Mn_{0.08}O_3$–1200 °C	42.43	5.87	−45.54
$YIn_{0.92}Mn_{0.08}O_3$–1300 °C	38.56	9.41	−48.07

While numerous pigment synthesis processes have been reported utilizing synthetic inorganic metal oxide as a starting material, most of them are not a cost-effective method as the precursors are costly and not recommended for mass production. On the other hand, using industrial waste for pigment synthesis has been recorded as having relatively low pigmentation strength, chemical stability, and treatment cost. Hence considering the mixing of recycled wastes with synthetic ones to bring the desired property is still a challenge for researchers [148-151], but it will have a good result if recycled industrial wastes are considered as secondary raw material combined with

synthetic ones to achieve a good result, for eco-purposes, and to balance the circular economy [152].

1.1.6 Effects of doping on colouring properties of inorganic pigment

Although several chemical compounds have been used as inputs in the pigment industry for decades, new mixtures that combine colour quality, minimize or remove the toxicity of these elements, and lower costs are now needed [149, 153, 154]. In addition, focusing on sustainability is a critical consideration for the industry in today's manufacturing context. As a result, pigment manufacturers are actively adjusting to the evolving regulatory climate and exploring and producing new and renewable pigments that consumers need [155].

In contrast, these pigments, which have remarkable properties, are considered to have poisonous effects. As a result, recent studies concentrate on the development of environmentally safe pigments with extraordinary properties in a wide variety of colours, replacing these dangerous pigments with a doping mechanism [156-161].

Most inorganic metals, especially the d-orbitals, have symmetrical/regular ligands, such as tetrahedral and octahedral structures. However, a recent study focuses on irregular/less symmetrical ligand fields, which have important properties for producing new inorganic colour pigments. Furthermore, these recently discovered pigments exhibit optical absorption properties in the visible range (380-740 nm) and the IR field. This optical property is due to the ligand field effect of this doped transition metal and the change in the load period between the two atoms. In this regard, the inorganic metals are suitable in the formation of irregular/less symmetrical ligand regions consisting of a compound with remarkable colouring properties of inorganic pigments [162, 163].

1.1.7 Crystallographic, Bandgap, and colouring property

1.1.7.1 Effects of crystallographic and colouring Property

Structural considerations, such as chemical composition, crystal structure, and phase composition, have been used to evaluate the properties of the materials and are based on the process of preparation, the starting materials used, and the criteria for predicting the mode of application and the properties of the substance [42]. In addition, the structural properties of these pigments are crucial in determining the physicochemical reactions undergoing and influencing the longevity and optical properties of the pigment [164]. The experimental result reported by Jian Zou et

al.;2020 suggested that the addition of the metal ion indicates a slight shift in the XRD peak angle [165-168].

Doping activity allows the doped radicals to join the lattice structure and substitute one or more radicals in the structure of the initial powder pigment. The overall effect causes the XRD peak to shift to a lower or higher Bragg angle as a function of the amount of doped radicals in the crystal lattice structure and can influence the pigment's colour [169-171]. On the other hand, doping of Vanadium on $LnPO_4$ showed a shift in the diffractogram peak towards the lower angle [172].

1.1.7.2 Effects of doping on bandgap and colouring property of the materials

The study result shown in **Figure 1.11** concluded that the small amount of Ni doping allows it to be diffused through the $BaTi_5O_{11}$ lattice to form a stable solution and decreases the energy bandage from 3.08eV, 2.51eV to 2.44eV as the Ni content rises to 10%. This band gap affects the colouring properties, as seen in **Figure 1.11 C [165]**. On the other hand, in doping of Ba^{2+} and Sm^{3+} on Ce_2S_3 in the formation of red γ-(Ba, Sm)Ce_2S_3, the energy band gap varies with the amount of doped radicals; this causes a change in the tone of colour. [173].

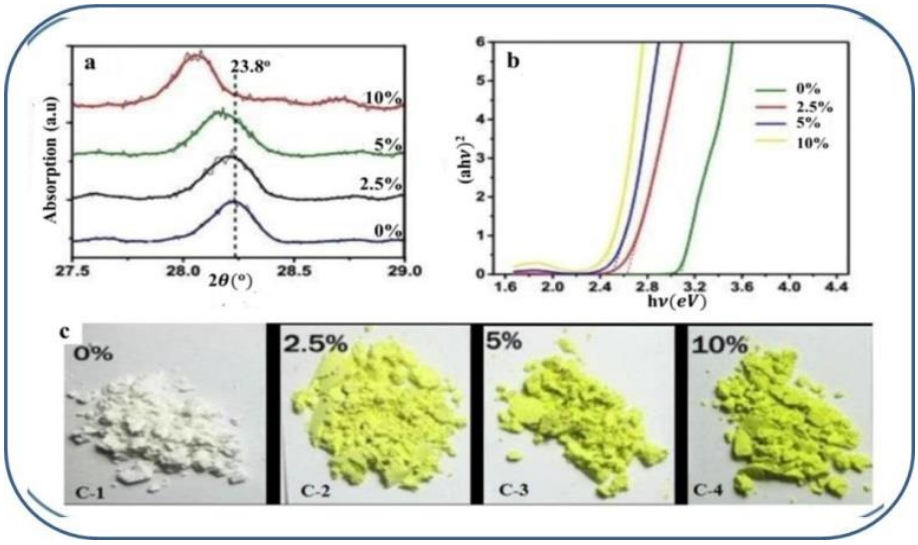

Figure 1. 11 (a) Slight shift in peak (b) Energy bandgap shift (c) Color shifting from white to green due to Ni doping in different percentages [165].

Although pigment production using doping transition metal oxide shows a remarkable change, replacing primary/pure starting materials by recycling waste can help reduce the final product's price. Besides, the presence of an impurity in a controlled quantity can serve as a mineralizing/fluxing agent and help to reduce sintering temperature [149]. The experiment on the

synthesis of Mg (FeAl)O_4 shown in **Figure 1.12** reveals the pigment derived from chromium sludge and Cobalt doped [172]; the result showed that the extracted chromium added Mg, Al, and Fe, seen on the XRD peak in **Figure 1.12.** Moreover, cobalt doping does not influence the location of the XRD peak. Finally, the researcher used pure chromium (S6) to compare and separate the structure of Co_2O_3, and the result reveals that S3, which has 1.99wt % of Co_2O_3, has a similar colour to industrial Cr_2O_3.

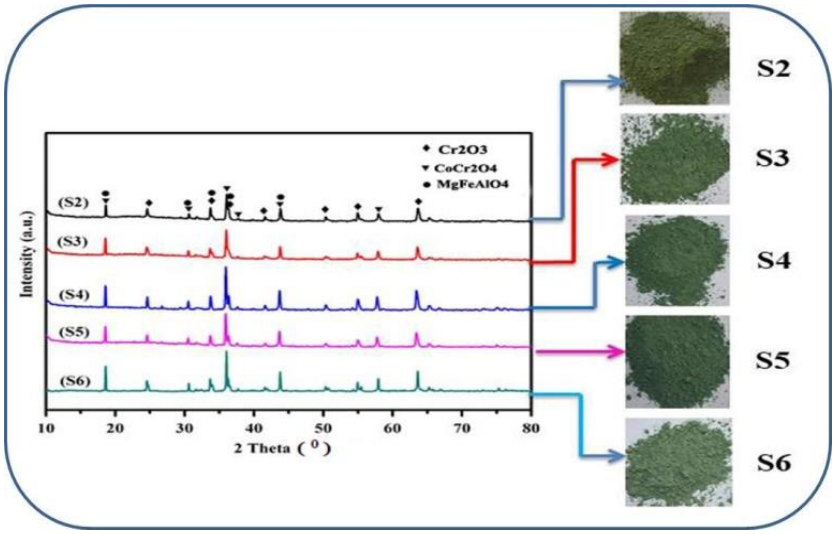

Figure 1. 12 XRD peak and colour of extracted chromium oxide with Co_2O_3 Doped in 1.02 wt%,

In addition, Table 1.8 summarizes that partial substitution of pure metal ion on a composite pigment shows distortion in the crystal lattice; as a result, the XRD peak shifts in angle either to the right or to the left based on the substituted/doped metal ion. This doping also influences the lattice volume and the absorption peak of the sample pigment, independent of the synthesis mechanism. On the other hand, Xiaolong Qing stated in his experiment that the amount of Mo^{6+} doped in the TiO_2 pigment induces neutralization and affects the NIR value due to a rise in the prohibited bandgap[174]. Moreover, a flexible synthesis mechanism has been implemented as the starting material is a relatively pure and controlled chemical composition. Even though most researchers have used a single mechanism of synthesis when the starting material is recycled, it has many impurities that can act as a mineralizer and display a comprehensive chart of colour in the pigment industry.

Table 1. 8 Synthesis mechanism and effects of doping on the colouring property of the pigment

Synthesis mechanism	**Doped metal ion and the composite**	**Effects of doping on the pigment and particle arrangement**	**References**
Sol-gel	Mn/N on $ZnAl_2O_4$	- XRD peak shifts towards the lower peak as doped Mn increases. - Lattice shift slightly increase from 8.0778 to 8.0891) - Bandgap varies from 3.64eV to 2.90eV - Changed from white to flesh colour	[175]
Solid-state method	Mn^{2+} on $CaCu_3Ti_4O_{12}$	- The lattice parameter changed - Bandgap increase from 2.04 to 2.11eV - Absorption peak shift from 603nm to 584nm - Brightness increased, and colour changed from orange to yellow - NIR percentage increase	[176]
Sol-gel process	Tb and Fe doped on $Y_2Zr_2O_7$	- XRD peak shift slightly - Tb facilitate the incorporation of iron ion in the lattice - Cell volume decreases - Tb allowed having a good absorption in the blue region, - Sample has good red colouration in combination with iron ions.	[177]
Hydrothermal	Cr and Sb added to TiO_2	-The XRD peak shift to the lower angle. - Increasing the broadness of the XRD peak. - Decreasing the crystallite size of the Nanopowder. - Lightness remains unchanged, but chromatic value decreases.	[178]

Solid-state	Nd-doped to holmium molybdate (Ho_2MoO_6)	- Shape change occurs due to ion radius mismatch of Ho^{3+} and Nd^{3+}. - Maximum addition of Nd^{3+} (x= 0.8) and maximum stirring rate cause the diffraction peak of the sample in XRD to change from monoclinic to tetragonal. - particle size increases as a function of Nd^{3+}, temperature, and stirring rate - The lightness decrease with an increase in Nd^3	[179]
Solid-state	Al_2O_3 doped in to Cr_2O_3 form $Cr_{2(1-x)}Al_{2x}O_3$	- Peak position remain unaffected due to similar ionic radius electronegativity and the chemical valance of Al_2O_3 and Cr_2O_3. - Forms hexagonal structure. Higher temperatures show a peak angle shift in the XRD, and some peaks disappear due to oxygen escape. - Agglomerates occur and form large particles, causing the sample to have more reflexive properties.	[180]

1.2 GAP ANALYSIS

Since the early 1800s, (CICPs) have been used. Their application in the ceramic and pottery industries is well-known for their overall inertness, which contributes to exceptional heat, chemical, and UV resistance. CICPs in industrial coatings, on the other hand, are less common and used for specialized purposes. Up to now, great interest has been shown in the pigment industries in developing ceramic pigments with intense tonalities which satisfy both technological and environmental requirements. Most of the time, adding chromophore ions and transition metals in an inert matrix (oxides) brings this pigment's colour [179].

Moreover, this pigment must fulfil criteria like thermal stability or maintaining its identity while temperature increases, chemical stability when firing with the matrix, and tinting strength during

dispersion and firing with ceramic matrix. Moreover, a high refractive index is the required property of ceramic pigments in ceramic industrial applications [80]. Although the chemical composition and crystal structures that arise from mineralogical composition determine the stability of the pigment, the composition of starting materials affects the whole system [180].

Out of various pigments, inorganic black is widely used as a colourant in today's ceramics industry, either for ceramic bodies or glazes [181]. Black paints are increasingly popular and considered high-grade jewels with their pure and dignified ornamental impact. The spinel structure accounts for over 25% of the total usage of commercial black pigment formulations [182, 183].

Different mechanisms have been used to obtain those black pigment colours, but the primary issue was getting the raw materials: metallic oxide or salts with industrial purity [184]. A pigment's ability to absorb visible light is determined by its chemical composition. All visible light wavelengths (380 – 750 nm) are absorbed by black. Only a small percentage of fine carbon black pigment is needed to achieve full opacity, but it can degrade at high temperatures [185].

Hence, copper chromate black pigment with metallic salts and metallic oxides used as a starting material has been employed for different applications, and selective solar absorption is one [186, 187]. Similarly, Aivaras Kareiva et al., 2019 synthesized ceramic glaze with carbon black pigment having Pb_3O_4 and SiO_2 were added with a molar ratio of 2.85:1.9 at 900°C [188]. The zircon-encapsulated ceramic black pigment with a carbon sphere as a carbon source was synthesized by precipitating Zr^{+4} and Sr^{+4} on the surface of the carbon sphere [189].

Even though synthetic raw materials bring a better property to the pigment, those starting materials, metallic oxides, and salts are expensive and depleted over time. As a result, different researchers tried to develop cost-effective ones with the required colouring parameters [184]. In line with the idea of producing highly stable pigments that show intense tonality to fulfil technological, economic, and environmental requirements, recycling industrial waste as an input in pigment synthesis has become a current scenario [190-192]. Among these is a study on black pigment made from two industrial wastes, iron-rich vanadium tillage waste and chromium from leather industry waste, with no pure chemicals added. Based on the report, the product looks suitable for commercial glazes. Whereas the research done by Lazhen Shen et al., 2010 witnessed the production of black iron oxide from the blast furnace fuel dust [193].

On the other hand, many inorganic pigment structures have symmetrical/regular ligands, such as tetrahedral and octahedral structures. A recent study focuses on irregular/less symmetrical ligand

fields, which have important properties for producing new inorganic colour pigments; this is due to the ligand field effect of this doped transition metal and the change in the load period between the two atoms. In this regard, rare earth metal ions have been used to doping inorganic compounds for this irregular/less symmetrical ligand region consisting of a compound with extraordinary properties [162. 163].

Even though a lot has been reported on doping inorganic metal oxide for enhancement of the property of the pigment [194, 195], only a few were reported on the study of recycled waste to enhance the property of black ceramic pigment with the corresponding crystal, morphology and optical properties. As a result, this research mainly focused on extracting iron oxide from steel slag and studying its colouring and purity level independently, then synthesizing the synthetic iron oxide doped copper chromate and comparing its property with the commercial one. Finally, the synthetic iron oxide was replaced by extracted one, and its properties were studied and compared with the one synthesized with the commercial iron oxide doped pigment.

1.3 STATEMENT OF THE PROBLEM

Wastes generated by the industrial manufacturing sector are a significant environmental concern of the region. Scrab is commonly used in the steel rolling industry; as a result, wastes contain some toxic components in trace concentrations, and these substances are dangerous to human health [27, 28]. Furthermore, the wastes cover enormous land areas for damping, posing a hazard to groundwater and covering the area's arable land. At the same time, natural resource scarcity threatens future generations. So transforming those wastes into valuable products can be viewed as a double opportunity for those firms to save money on waste treatment while reducing the utilization of natural resources. It can also reduce health risks and environmental pollution.

According to a Business Research Company study, the global synthetic pigments market is expected to rise at an 8.2 % compound annual growth rate (CAGR) from $37.03 billion in 2020 to $40.07 billion in 2021 [196, 197]. Similarly, the Ethiopian Chemical and Construction Inputs Industry Development Institute report indicated that the three-year average imported inorganic pigment was roughly 1,109,013kg per year (2017-2019), costing 8,083,047.90 Ethiopian Birr.

Furthermore, black pigments were employed in the pottery industries (both modern and traditional), and they can also be used as paint for solar energy collectors. As a result of these criteria, several studies should be needed to obtain high-quality and cost-effective black ceramic pigments. Because iron oxide is a widely used pigment, extracting iron oxide from steel slag of

industrial iron waste, studying its properties, and replacing part of the synthetic inorganic pigment in the ceramic paint industry with iron oxide extracted from mill-scale waste of steel rolling industry is an ideal approach to alleviating scarcity.

1.4 RESEARCH QUESTIONS

- Do recycled steel industry slag can have the required amount of iron in it and assure the sustainability of the resources?
- Does the solid-state doping of synthetic iron on copper chromate assure the quality of the pigment?
- Does the extracted iron viable in the processes of doping on copper chromate?
- Can we get a comparable colour when synthetic iron is replaced by extracted iron in doping on copper chromate?

1.5 RESEARCH OBJECTIVES

1.5.1 General Objectives

- To extract iron oxide from steel rolling industry slag and examine its property when doped on copper chromate relative to the synthetic iron doped pigment.

1.5.2 Specific Objectives

- To extract iron oxide powder from mill scale of steel rolling industry waste for pigment application.
- To examine the colouring property of synthetic iron-doped copper chromate pigment relative to the commercial one.
- To examine the colouring property of extracted iron-doped chopper chromate pigment.
- To make a comparative study on the colouring property of the two pigments.

1.6 SCOPE AND LIMITATION OF THE PROJECT

This project aimed to extract iron oxide as a pigment from discharged wastes of the iron/steel processing industry, create an inorganic pigment comprising synthetic copper, chromium, and iron oxide, replace the synthetic iron oxide with extracted iron oxide and compare the effects. Due to resource constraints and to keep the work manageable within the project duration, the scope of the research is limited to the following specific works. Industrial waste contains potential elements in magnetic, transistor, sensor, and other applications; however, this project primarily focuses on synthesising inorganic black pigments.

- Solid waste collection from the Iron /Steel industry (*Steely RMI*).
- Investigate the chemical composition of the waste and check its content feasibility for pigment synthesis.
- Production of quality iron oxide pigment from steel slag and
- Characterizing its particle size, product purity (chemical composition), crystalline structure, and colouring with pigment quality.
- Doping the synthetic iron oxide on the copper chromate pigment, studying its property, and comparing it with commercial copper chromate.
- Doping extracted iron oxide on copper chromate pigment and compared its effect to synthetic.

1.7 SIGNIFICANCE OF THE STUDY

The study's findings revealed a new insight into the pigment industry in doping extracted inorganic metal to already-known synthetic complex inorganic pigments. Furthermore, the work output demonstrated the efficacy of the solid-state synthesis method in producing complex inorganic pigments comparable to commercial ones. Moreover, recycling iron slag as the pigment that was extracted using the hydrothermal method showed the scientific world's approach to the circular economy and environmental remediation; this result provides researchers insight into other industrial wastes to recycle and use for different applications.

1.8 OUTLINE OF THE REMAINING CHAPTER

The current work was composed of two major sections; extracting iron oxide from steel industry slag (waste), then studying its property and doping synthetic and extracted iron oxide on synthesising copper chromate pigment and their properties. As a result, the following chapters deal with the subject.

Chapter 1 includes a literature review section which includes; the fundamental differences between pigments and dyes, the theoretical background of the colour formation, the synthesis mechanisms of those colouring pigments and their pros and cons, and the effects of doping on the colouring particles' morphology, crystal structure colouring, and energy band gap, the principle of colour measurement—finally, the complex inorganic black colouring pigment and the gap within the field done so far.

Materials and procedures used in all subsequent sections of the current study were extensively provided and described in **chapter 2** at this early stage. The materials used to extract the required powder pigments, extraction procedures, mixing of the pigment components to obtain a colouring combination, and operational factors are described.

In **Chapter 3**, we addressed the chemical components of iron slag, the extraction processes utilized to obtain iron oxides, the texture, purity of the extracted sample (uniformity), particle size, thermal stability, energy bandgap, and colouring property.

The synthesis techniques of synthetic pigments using CuO, Cr_2O_3, and Fe_2O_3 to generate a pigment with the structural formula $Fe_xCu_{1-x}Cr_2O_4$ were described in **Chapter 4**. The CuO, Cr_2O_3, and Fe_2O_3 were organized in varied weights based on the stoichiometric proportion in the process. Furthermore, the mechanism for mixing them, the calcination process, has been thoroughly described. Finally, based on scientific evidence, the characterization result containing synthesised spinel inorganic synthetic pigment's thermal, crystallinity, morphological, optical, and colouring property was studied and compared with the commercial pigment.

The effect of doping extracted iron oxide was discussed in detail in **Chapter 5**. The sample was synthesized the same way in **chapter 4,** except that synthetic Fe_2O_3 was replaced by extracted iron oxide. Finally, the sample's characterization result was compared to the results found in **Chapter 4.** In the end, the overall conclusions of the current study are presented in **Chapter 6**

CHAPTER-TWO

2. MATERIALS AND METHODS

2.1 EXPERIMENTAL SITE

The iron/steel slag sample was collected from Bishoftu, Ethiopia, 45km East of Addis Ababa, Ethiopia. Iron Oxides extraction from iron/steel was done in the former Ethiopian Biotechnology (the current Emerging Technology institute) laboratory, Addis Ababa, Ethiopia, and characterization of the extracted samples and part of extraction were done in National Metallurgical Laboratory in Jamshedpur, India, and Tallinn University of Technology in the department of mechanical and environmental engineering, Tallinn, Estonia.

.

2.2 CHEMICAL AND MATERIALS

The chemicals used to synthesize the required pigments are chromium oxide (99%), copper oxide (95%), iron oxide (99.7%), sulfuric acid (98%), hydrogen peroxide (30%), ammonium hydroxide (25%), acetone, potassium di-chromate, and ethanol were purchased from Loba Chme, India, which are all analytical reagent grade and used without further purification. Steel slag was also brought from Steely RMI in Bishoftu, Ethiopia.

2.3 METHODOLOGY

2.3.1 Extraction of iron oxide from still slag

The iron powder was extracted from Iron/Steel slag collected from the Steely RMI iron rolling industry, Bishoftu town, using the wet chemical method, with sulphuric acid as a leaching agent [198]. Then the leached iron oxide was precipitated using ammonium hydroxide. After the extracting process, the powder undergoes a thermal test using TGA to determine the calcination temperature, and then based on the TGA result, the sample was calcined at 700°C, 800°C, 900°C, and 1000°C to examine the temperature effect of extracted pigment. The overall extraction process is shown in **Figure 2.1,** and details are presented in chapter 3**.**

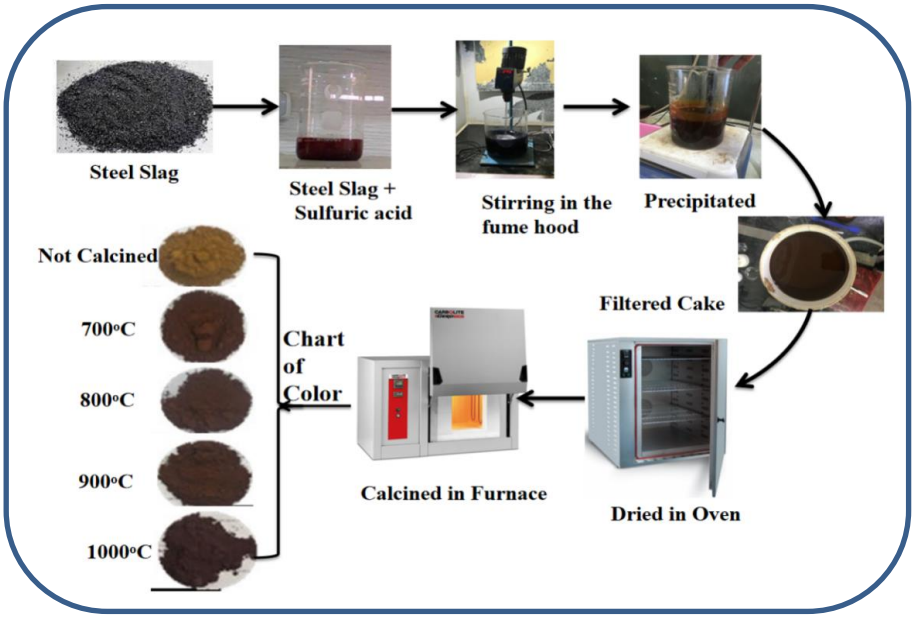

Figure 2. 1 Extraction process of iron oxide from steel slag (Steel processing industry waste)

2.3.2 Preparation of $Fe_xCu_{1-x}Cr_2O_4$ pigment and doping iron oxides

Inorganic oxides containing iron oxide, copper oxide, and chromium oxide of industrial chemical purity were mixed without further purification in different weight percentage ratios. It was synthesized using a solid-state mechanism by attrition mill using acetone as a wetting medium, which was adapted from [199, 200].

The three synthetic inorganic metals were selected based on their size and respective oxidation degree. The uniformity of those oxides was attained using an attrition mill shown in Figure 2.2 for 1:30h at 1000 revolutions per minute (rpm). It was then put in an oven at 80°C for 15 h. Finally, ground again for 30 min to make it fine powder using an agate mortar and using reference works sample was calcined at a temperature of 1350°C for 3 h; details are presented in **chapter 4**.

2.3.3 Replacing the synthetic iron oxide with extracted iron oxide in $Fe_xCu_{1-x}Cr_2O_4$ pigment

This section followed the same procedure in preparing complex inorganic colouring pigment with a general formula of $Fe_xCu_{1-x}Cr_2O_4$, except that synthetic iron oxide was replaced by extracted one. In the process, samples with different weight percentages were mixed using the attrition mill with acetone as a wetting medium.

Similarly, the samples were mixed using an agate mortar and pestle and then in the attrition mill for a period of 1:30 h at a revolution rate of 1000rpm. The slurry was then dried in an oven at 80°C for a period of 15h. Then ground using an agate mortar and pestle and then sieved to get a powder.

The powder was finally pressed into a pellet, and based on literature as a reference, it was calcined at 1350°C for 3h, and the pelletized sample was ground and sieved. Details are stated in **chapter 4.**

2.4 CHARACTERIZATION TECHNIQUES

The extracted samples' purity, particle size distribution, elemental and chemical composition, thermal property, crystalline properties, and optical and colouring properties were characterized using different instruments. Some of the advanced devices used in this experiment include:

2.4.1 TG-DTA

A thermal analyzer (TG-DTA) instrument was used at NML, Jamshedpur, India to study the changes in materials characteristics with the temperature. The instrument can measure the differential behaviour of solid samples to standard reference materials (in the O_2 atmosphere, alumina was employed as reference material during the programmed change in temperature using DTA and simultaneously measure any changes in mass using TG. Due to the uncontrolled nature of the extracted iron oxide, the thermal stability was investigated using TG-DTA, and based on the result; the sample powder was calcined before the characterization process; a detailed discussion is found in chapter 3.

2.4.2 X-Ray Diffraction

The crystallographic information of both extracted powder and synthesized samples was investigated from XRD data Using Origin 2019 and Xpert Highscore Plus software. The characterisation's first part (extracted iron oxide from steel slag) was conducted at the Department of Mechanical and Industrial Engineering, Tallinn University of Technology, Estonia. The next sample characterization was done at the College of Natural and computational science at Addis Ababa University, Addis Ababa, Ethiopia.

In both cases, the XRD data were collected by (RIGAKU, XRD machine with source λ=0.15406nm), but in the first case, the X-ray source was a copper-sealed 2 kW tube target producing Cu Kα and Kβ emission lines from a generator operating at 40 kV and 50mA [201], while the second one was copper-sealed 0.6kw Cu Kα emission lines from a generator operating at 40 kV and 15mA. The measurements were performed at room temperature; the scanning range, scanning size, and scanning rate was stated in detail in chapter 3, 4 and 5

2.4.3 XRF and ICPMS

The chemical composition of steel slag in the leached liquid was determined using ICP-MS. The experiment was done at NML Jamshedpur, India, with the instrument model: Perkin-Elmer/Elan DRCe, which is applicable for Trace and ultra-trace elemental analysis in metallurgical and water samples, having a lavele of edetection of 1ppb up to 100 ppm.

Then the chemical composition of the steel slag before and after was determined using XRF, Model Bruker/S8-Tiger, having an application for metallurgical elemental analysis with a lavele of edetection ranges 10 ppm to 100 ppm, working in solid, powder, and liquid standards [202].

2.4.4 SEM-EDS

Because of its versatility and great potential for morphology and chemical composition analysis, Field Emission Gun-scanning electron microscopy (FEG-SEM) equipped with energy-dispersive X-ray spectrometry (EDS) is one of the most commonly used spatially-resolved analytical methods [203]. As a result, in this experiment, FEG-SEM equipped with EDS was employed at different places for the first sample at the department of Mechanical and Industrial Engineering, Tallinn University of Technology, Tallinn, Estonia, and the complex inorganic colouring pigment was characterized at the Centre for Research in Nanotechnology and Science (CRNTS), Sophisticated Analytical Instrument Facility (SAIF), Indian Institute of Technology, Bombay, India. Detailed characterization of the samples was stated in chapters 3, 4, and 5.

2.4.5 DSL (particle size distribution analyzer)

The particle size distribution analysis was carried out at NML, Jamshedpur, India, with the help of the instrument depicted in Figure 2.4. The instrument is a Malvern MASTERSIZER2000part No. APA5007 with a resolution range of 0.02 to 2000 microns. It is comprised of a wet dispersion system, Hydro2000MU, a recirculation pump, an ultrasonic probe, a mechanical stirrer, a dry dispersion system, Sirocco2000, and application software.

It uses the optical principles of laser diffraction and LASER scattering to calculate particle size distribution in volume per cent. For example, the software computed d_{10}, d_{50}, and d_{90} values, to indicate the size of particles present in less than 10%, 50%, and 90% of the analysis, respectively. In addition, the software is available to display particle size distribution against a size scale in ASTM mesh size, Phi scale, and micron [202].

2.4.6 FTIR

The Fourier Transform Infrared (FTIR) spectroscopy was used at the Faculty of Natural Computational Science, Addis Ababa University, Addis Ababa, Ethiopia. It is widely established as a sensitive, fast, and non-destructive technique for material characterization of numerous samples for molecular species in various materials; FTIR provides information based on the chemical composition and physical state of the whole sample. In addition, the sensitivity and accuracy of FTIR detectors and a wide variety of software algorithms have dramatically increased the practical use of infrared for quantitative analysis [204].

The IR bands of spinel compounds are anticipated to be designated to the vibration of metallic ions in the crystal lattice, and the frequency of vibration is dependent on the quality and ionic radius of metallic ions. The IR spectra of a regular spinel structure will show two primary vibrations of metal-oxygen bonds [205]. As a result, vibration assigned to metal oxides has been investigated, and details are presented in Chapters 4 and 5.

2.4.7 UV-Vis Spectroscopy

The Refractive Index and colouring characteristics of extracted powder and synthesized samples were investigated using UV-VIS-NIR spectroscopy. First, the absorption spectra of the extracted Iron Oxide were done using (Carry 5000 UV-VIS-NIR spectrophotometer, Agilent technologies) at the wavelength range 200-800nm, in the Department of Mechanical and Industrial engineering, Tallinn University of Technology(TalTech), Tallinn, Estonia. Then, the second phase of work was conducted sing (Carry 100, UV-S-NIR spectrophotometer, Agilent technologies) at the Centre for Research in Nanotechnology and Science, Sophisticated Analytical Instrument Facility (CRNT-SAIF) at the Indian Institute of Technology, Bombay, India.

From the recorded UV-Visible spectroscopic data, the index of refraction value was obtained; this refractive index determines the density opacity of the pigment; this absorption spectra and the refractive index of the pigment affect the sample colour tone [206, 207]. In addition, the data in the second phase (synthesized CICP) were also used to calculate colouring coordinates using CIE-1931 colour space, using the CIExyz axis, and converted to spherical coordinates L*, a*, and b* [208].

2.4.8 CIEL*a*b* (Colorimetric measurement)

The colouring property of the extracted iron oxide powder was investigated at the University of Madrid, Spain, using L*a*b* coordinates the portable spectrophotometer (Konica Minolta CM 2600d/2500d) to acquire the data in the range of 300-800 nm. CIELAB is a uniform colour space (UCS) recommended by CIE in 1976; it is one of the most widely used colour spaces. It is used to describe a colour in perceptual correlations such as lightness, chroma, and hue and plot samples [209].

The data was defined through the parameters the L*a*b*, where L* represents Lightness ranging (L* = 100 white to L= 0 dark) while the two chromas a* denotes a change from green (negative values) to red (positive values); and b* the shift from blue (negative values) to yellow (positive values).

2.5 PROJECT DESIGN

This project was designed to develop black complex inorganic colouring pigments used to apply ceramic materials to ornamental decoration. The experiment has two main phases; extraction of iron oxide from industrial waste and applying it in copper-chromate pigment. In the process, the steel slag (industry waste) was collected from Steely RMI, Bishofu, Ethiopia, and the chemical composition was tested using XRF, and then the leaching process was done using the chemical sulfuric acid to extract the powder containing iron oxide as the main component (Detail methods are found in chapter 4). Next, the extracted iron oxide was calcined based on the TG-DTA result at four different temperatures; 700°C, 800°C, 900°C, and 1000°C (3 h each). Finally, the pigment's colouring and optical properties, crystallinity, chemical composition, and microstructure were investigated.

In the second part, the first part, $Fe_xCu_{1-x}Cr_2O_4$, was synthesized by mixing the Copper Oxide, Iron Oxide, and Chromium Oxide inorganic elements of laboratory-grade chemical purity without further purifying them. The result was compared with the commercial copper chromate black pigment and was taken as a reference. Then, the commercial iron oxide was replaced by the extracted iron oxide, and the colouring, optical properties, morphology, and microstructural property of the synthesized pigments were investigated. In the end, the results of the last synthesis were compared with the synthetic one. Each project phase is stated in **Figure 2.2**.

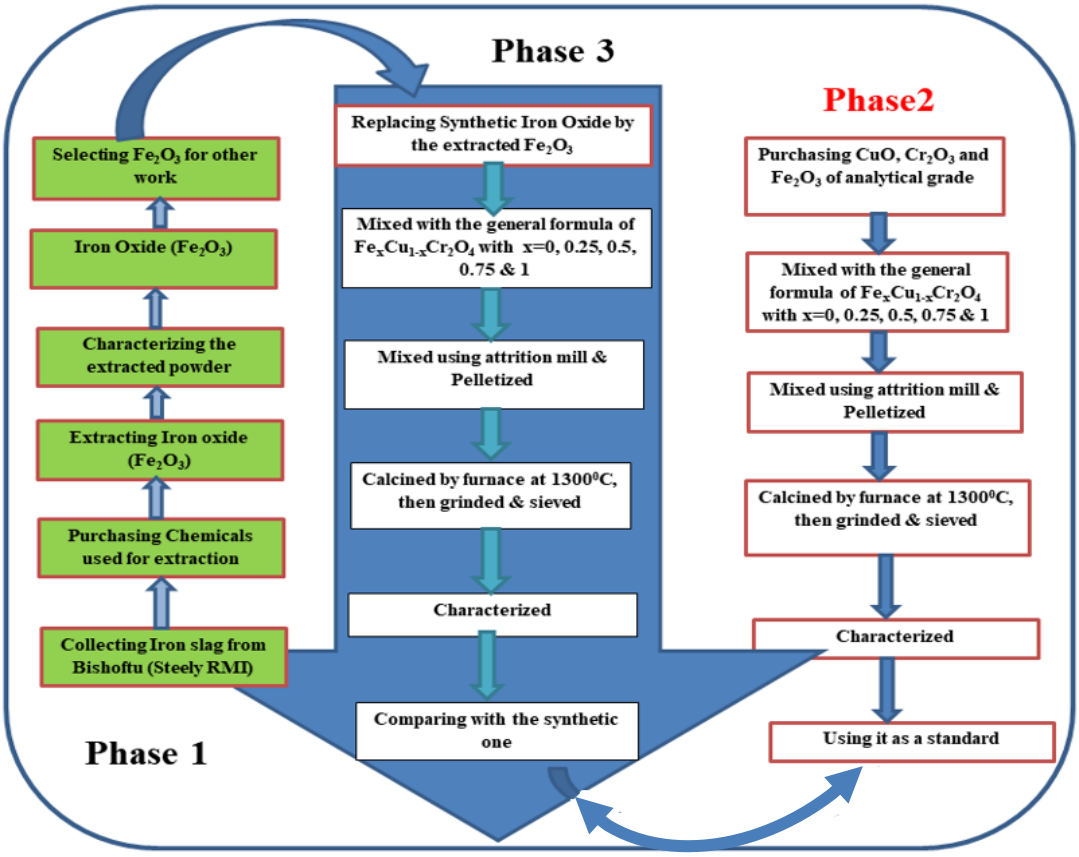

Figure 2. 2 The overall schematic diagram of the research work

CHAPTER THREE

EXTRACTION AND STUDYING THE EFFECT OF TEMPERATURE ON IRON OXIDE POWDER FROM STEEL SLAG

Zekarias G. Eticha, Rocio E. Rojas-Hernandez, Olu Emanuel Femi, Abubeker Yimam,, Irina Hussainova, Esayas Alemayehu.

ABSTRACT

Materials based on iron oxide are the most widely used red pigments. Although the synthetic iron oxide pigment industry has matured, great efforts are continuously applied for their environmentally friendly synthesis of the transition to a circular economy. This study uses a cost-effective hydrothermal method to produce brown-red pigment based on hematite extracted from mill-scale steel slag. The extraction was done using sulphuric acid as a leaching agent; the addition of hydrogen peroxide facilitated the oxidation of Fe^{2+} into Fe^{3+}. The total conversion in the process was tested using potassium dichromate. The pH was stabilized by ammonia; a brown precipitate was formed in the solution. The extracted powder was annealed in an air atmosphere at temperatures ranging from 700 to 1000°C. XRD, SEM with EDS, UV-VIS NIR, and CIE-L*a*b* were used to examine the annealing temperature effect on the colouring property of the extracted powder pigment. The results show that by adjusting the annealing temperature, a colour chart ranging from brown to red can be obtained, which means an increase in temperature causes the change in particle size and this change influences the pigment to be changed from a light-red-brown to a dark brown. In the end, the results presented here open new strategies to supply the range of red-brown to dark-brown pigment world production through a recycling strategy

Keywords: iron slag; extraction; pigment; hydrothermal; Waste; dark brown

3. INTRODUCTION

3.1 BACKGROUND AND JUSTIFICATION

Steel slag is the waste product of steel industries disposed of in large quantities, forming a hill of aggregate materials containing a large amount of iron in the form of oxide and other hazardous chemicals. This waste should be ground and sieved to achieve mill-scale slag [48]. The iron/steel processing industries release 5% of their total input materials as waste, which contains 60-72% iron in the form of oxides [210]. Due to the enormous demand for iron oxide for various uses, iron-reach industrial waste is crucial to obtain an alternate supply and alleviate shortages [211].

The circular economy concept gained stem when the Sustainable Development Goals (SDGs) were designed in 2015. Based on the report of McKinsey, 2015, the European economy was astoundingly wasteful, with only 5% of raw materials recycled and reused. He argued that if new technologies were adopted and unique production processes focused on sustainability, the European economy could add 1.8 trillion euros by 2030 [212]. According to the European Circular Economy Action Plan, industrial waste landfills could be a source for recovering vital raw materials and reducing environmental impact.

The European Commission issued an open call for input in July 2017 to assist in preparing guidance documents in extractive waste management plans, including topics relating to the circular economy [213, 214]. In addition, African Development Bank hopes to accelerate the circular economy in Africa with a waste management initiative funded by the KOREA-AFRICA ECONOMIC COOPERATION (KOAFEC). The circular economy is a model that aims to reduce waste and maximize resource value through the recovery and regeneration of products at the end of their typical service life [215].

Considering this opportunity, recycling industrial waste has become a focus research area. Among the solid wastes generated globally, the iron and steel industry is deemed to discharge significant waste as part of the manufacturing process. Based on the report [216], more than 400 million tons (Mt) of iron and steel slag (at a density ranging between 2.5 and 3.5 t/m^3) were produced worldwide in 2017. Furthermore, due to their durability, chemical stability, and wide use in several applications, such as photo-electrochemical sensors, cleaning environmental pollution, energy storage, pigments, optical, electrical, and bio-materials, iron and steel are referred to as the world's most recyclable materials [217-221].

According to Alison Rusell, in 1999, a total of 942,000 tonnes of pigments were produced worldwide, with iron oxides accounting for the majority (750,000 tonnes), with around 440,000 tonnes coming from natural ore and the rest from synthetic sources and the global market for pigments is expected to grow in lockstep with GDP [222].

Iron oxide pigments, in particular, have been used in various industrial applications, including ceramics, architectural features, paints, and surface coating paints. Moreover, its thermodynamic stability and wide range of colours evolved from its morphology, particle size distribution, and non-toxic nature, making it a globally selected pigment in the colour industry and becoming more critical in the research field [223-226]. As a result, producing iron oxide-based modern red pigments with vivid colour and better stability is still of great importance in iron pigment-related research, and focusing on recyclable waste is a robust approach.

The sustainable development agenda and circular economy promote resource longevity and rely partly on recycled waste as raw materials [227]. Therefore, different synthesis routes, parameters and precursors have been employed to obtain the desired requirements; particle size, degree of crystallinity, and morphology are among the results considered by the researcher in the synthesis process for specific applications [228].

Recent studies on recycling iron from industrial waste tried to answer the query of alternative processing routes applied by different researchers [229]. Most of them attested that the particle size change influences the colouring properties due to the annealing temperature employed [230-232]. However, the thermal treatment is not the only factor that influences the colour tone; instead, the other characteristics of the pigment, such as particle size and its distribution, the impurity found in the extracted powder, and the morphology, affect the colour of the end product(Miri, Khatami and Sarani, 2019) directly. Besides that, the ratio of Fe^{2+}/Fe^{3+} is another factor that has a decisive impact on the colour's chroma (colour intensity) [228].

The iron-red hybrid pigments with an impurity of kaolinite and quartz have been prepared from an oil shale semicoke waste using a one-pot hydrothermal method [124]. Also, iron with a composition of both ferric and ferrous precursors has been extracted from a blast furnace dust using acid leaching [193]. The development of environmentally benign iron oxide-containing composite pigments from mine drains waste and steel slag has revealed new types of colouring [233]. Notably, the efforts on iron recycling are mostly related to the extraction without any further modification; as a result, the pigment may end up with iron oxide phases due to ferric and ferrous

precursors. Besides, the pigment Hue (basic colour) and Chroma can be affected by the existence of different iron oxide phases [234].

As a result, this research work focused on extracting iron oxide from recycled mill-scale steel industry waste (slag), the extracted iron was calcined at 700, 800, 900, and 1000°C to investigate its property. In the end, the final colour of the extracted pigment was compared with a commercial hematite pigment. Although the finding shows a colour difference from the commercial one, the extracted hematite shows the synthesis of a wide range of colours by controlling the annealing temperature.

3.2 EXPERIMENTAL SECTION

3.2.1 Extraction method

The steel slag sample taken from Steely RMI was ground by agate mortar to a fine powder and sieved with #100-mesh size. First, the elemental composition of the solid slag was identified using XRF, and then hydrothermal extraction processes were used to extract iron oxide.

In the experiment, 100 g of slag was mixed with 100 ml of conc. Sulphuric acid and heated on a hot plate at 250°C with a continuous overhead stirrer stirring at 200rpm until all the liquid evaporated, as shown in **Figure 3.1a;** it was then washed using 400ml of deionized water and filtered using wattman filter paper. The filtered liquid solution shown in **Figure 3.1b** was measured to be 398ml, and then a sample liquid solution was taken to check the elemental composition using ICP-MS.

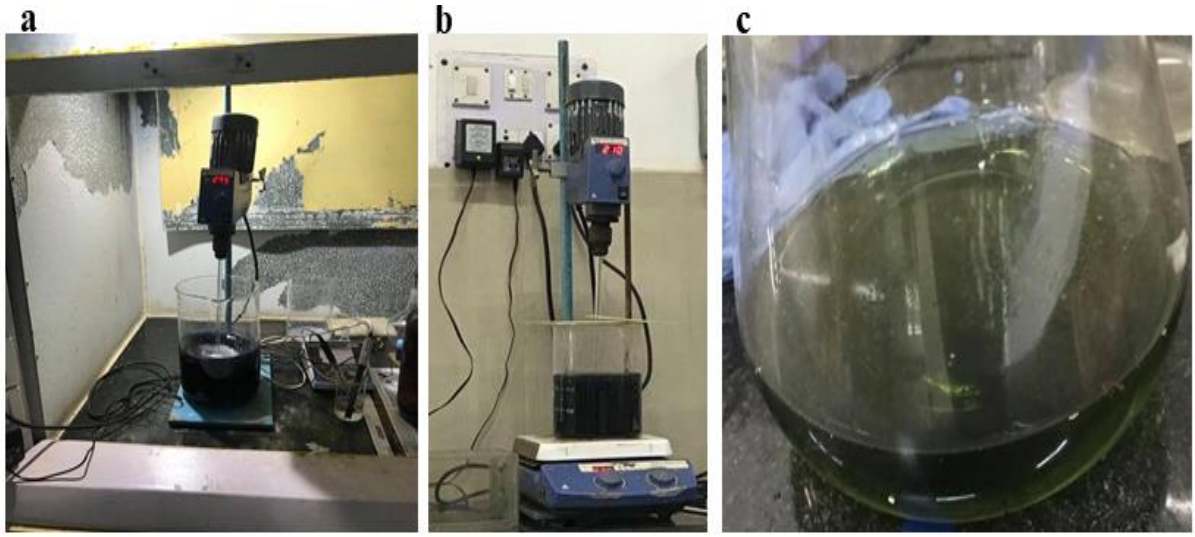

Figure 3. 1 (a) Steel slag digested in sulphuric acid, (b) the sample after filtration, and (c) The colour change of the solution confirms the complete change to Fe^{3+}

Titration was then used to determine the amount of Fe^{2+} in the solution. Based on the results, 30% H_2O_2 was added to facilitate the conversion, and the mixture was stirred for 30 minutes with an overhead stirrer at 200 rpm. Adding hydrogen peroxide facilitates the oxidation of Fe^{2+} to Fe^{3+} based on the Haber and Weiss equation [111, 235, 236].

$$2Fe^{2+} + H_2O_2 + 2H^+ \rightarrow 2Fe^{3+} + 2H_2O$$

The conversion process was checked using potassium dichromate, and the conversion of Fe^{2+} was confirmed with a change in colour of the solution totally to greenish, as shown in **Figure 3.1c** [236].

$$Cr_2O_7^{2-} + 6Fe^{2+} + 14H^+ \rightarrow 2Cr^{3+} + 6Fe^{3+} + 7H_2O$$

The pH of the solution at the beginning was 3.01, and ammonium was added until the pH reached 9. At this pH, the solution starts to form a brown precipitate. The precipitate was filtered using filter paper, and the cake was dried in an oven at 70°C; the dry sample was ground, sieved with a #100 mesh sieve, and stored for further processing. The process of extraction and calcination of the sample is listed in **Figure 3.2** below.

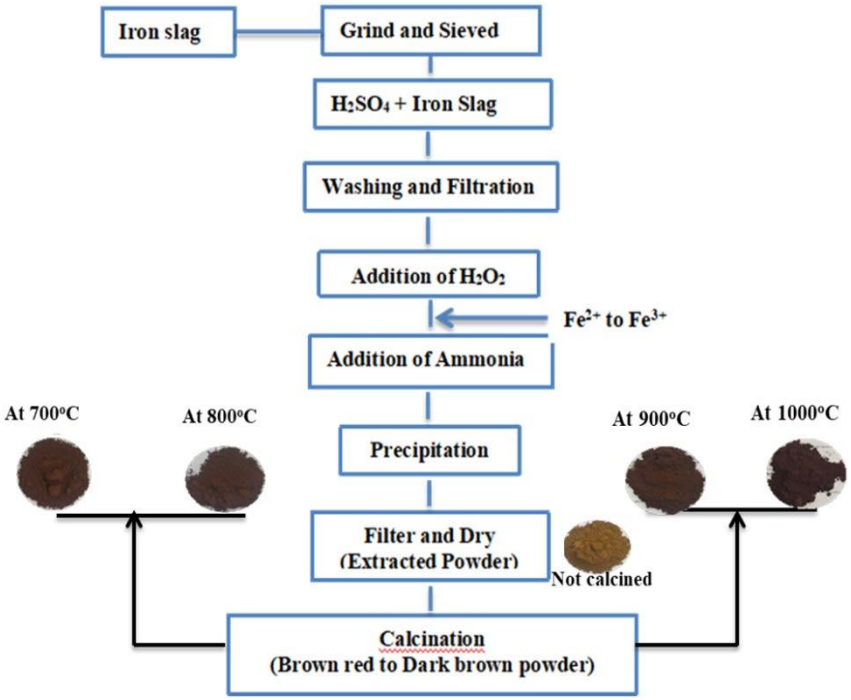

Figure 3. 2 Flow chart of iron extraction from mill scale iron slag using hydrothermal method

3.2.2 Chemical composition, microstructural and optical characterization

The chemical composition of the slag was analyzed using XRF, Bruker/SRS 3400. Besides, the amount of iron in the solution after the leaching process was determined using inductively coupled

plasma mass spectrometry (ICP-MS). The result obtained by ICP-MS shows the amount of iron in the liquid becomes 26.875 grams per litre (g/L), whereas the amount of other metals like aluminium and chromium was 8.2g/L and 0.5062g/L, respectively.

Differential thermal analysis (DTA) and thermogravimetric analysis (TG) of the material obtained from the extraction process were done using TG-DTA model STA-7300, Hitachi, Japan, up to 1200ºC (In the O_2 atmosphere, alumina was employed as reference material during the programmed change in temperature). The phase composition and crystalline material structure were characterized by analysing X-ray diffraction (XRD) data collected using a Rigaku Smart Lab SE with a D/teX Ultra 250 1D detector. The X-ray source is a copper-sealed 2 kW tube target producing Cu Kα and Kβ emission lines from a generator operating at 40 kV and 50 mA. The measurements were performed at room temperature from 20 to 90° (2θ) with a 0.01° step. The morphology of the samples was observed by a field emission scanning electron microscope (FEG-SEM, model EVO-MA15) together with EDS/INCA for elemental analysis. The particle size analysis was done using a Malvern laser diffraction particle size analyzer (Model: MASTERSIZER S, Malvern Instruments, and the UK). During this analysis, the proper dispersion was done using sodium hexametaphosphate as a dispersant and the application of ultrasonic vibration for 15 s. The powders synthesized were evaluated by UV-VIS-NIR spectrophotometer (Carry 5000 UV-VIS-NIR spectrophotometer, Agilent technologies) at the 200-800nm wavelength.

The energy band-gap of the hematite (α-Fe_2O_3) was determined according to Tauc expression [27], $(\alpha h\upsilon) = A(h\upsilon - E_g)^n$ Where α represents the absorption coefficient, A is a constant, hν is the photon energy (h is Planck's constant and ν is the light frequency), E_g Represent the optical band gap energy, and the exponent n is a constant that determines the type of optical transitions: for indirect allowed transition, n = 2; for indirect forbidden transition, n = 3.

The colour of the pigment was tested using CIEL*a*b* coordinates, the portable spectrophotometer (Konica Minolta CM 2600d/2500d) was used, and the data were acquired from 300-800 nm. Finally, the Chromatic and Hue values were calculated using the formula of [31] given by

$C = \sqrt{a^{*2} + b^{*2}}$, and the Hue angle is given by $H = \tan^{-1}(b/a)$

3.3 RESULT AND DISCUSSION

3.3.1 Hydrothermal Extraction Process

Since the raw impute of the steel rolling mill mainly used a scrab as an input, it is expected that more impurities to exist in the slag. The XRF analysis shown in **Table 3.1** confirmed that it contains Aluminum, Silicon, Titanium, Calcium, Iron, Sodium, Sulphur, Manganese and Chromium. But the amount of iron found in the slag is at a maximum level to extract for pigment application [193].

Initially, the amount of iron in the slag as a standard, and then the amount of iron leached in the liquid was investigated using the ICP-MS. The result shows 26.875 g/L was found to be iron, and the solid form of iron after filtration and drying was calculated as;

$$\text{Mass of Iron in 100 g slag} = \frac{398}{1000}\ L\ x 26.875\ g/L = 10.696\ \text{g}.$$

Where 398ml is the total liquid solution.

Table 3. 1 Chemical composition of steel slag investigated by XRF

Elements	Al	Si	Ti	Ca	Fe	Na	S	Mn	Cr
Percentage	8.31	13.64	1.01	1.58	58.3	0.39	0.06	10.60	6.11

Out of the total iron oxide, which is 26.875g/L in the solution, the titration result indicated that 24.0152g/L was Fe^{+2} in the solution, equivalent to 9.55g as calculated by the above equation, while the remaining is Fe^{3+}. Therefore, to completely change Fe^{2+} to Fe^{3+} oxidation process has been performed using hydrogen peroxide to get Fe^{3+} as innovative work to get only the hematite phase. According to the amount determination, 9.55 g (0.17mol) of Fe^{2+} in the solution requires 5.8187gm or 17.47 ml of 30% H_2O_2 for the oxidation process. Finally, the total transformation was checked using the addition of potassium dichromate as an indicator, which turns the solution purple when all ions in the solution are Fe^{3+}.

3.3.2 Thermal Property of the extracted Hematite powder

The thermal behaviour of the extracted powder was examined using TG-DTA, and the result is presented in **Figure 3.3.** The TG curve indicated that the weight loss of 32.27% occurs during heating from a room temperature up to 700°C, out of which 17.22% was lost when the sample was heated to 542.61°C, which is due to the removal of physically bonded water [237]. The next weight

loss occurred at around 15.05%, which was observed between 542.61°C and 643.43°C, ascribed to the organic sample's degradation and a transition phase hematite from goethite [238, 239].

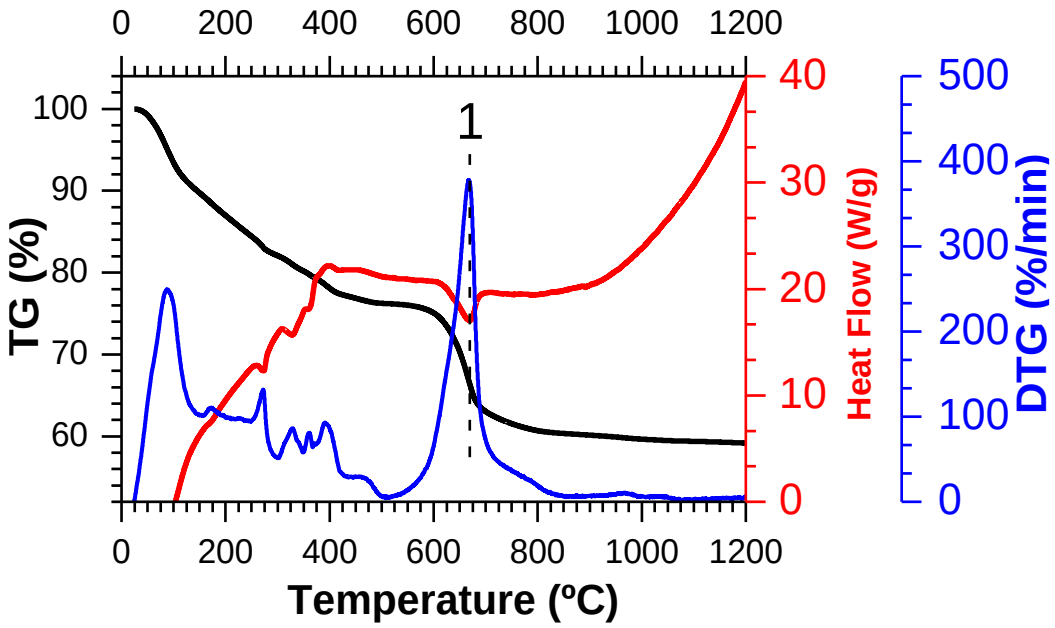

Figure 3. 3 DTA-TG-DTG curves of extracted iron oxide

Upon heating, the TGA profiles show an endothermic peak at around 270 and 320°C due to the organic sample degradation and transformation of goethite (γ-FeOOH) to hematite (α-Fe_2O_3) or detachment of hydroxyl group from iron and formation of hematite (α-Fe_2O_3). In contrast, the peak around 668°C is the endothermic peak (marked as 1 in **Figure 3.3**) formed due to the transformation of γ to α [240, 241]. After that, the TG axis graph line aligned parallel to the temperature axis, indicating the hematite powder's stability.

3.3.3 Crystallographic and Morphological property of Extracted Hematite

The XRD analysis of the extracted powder before and after thermal treatment is shown in **Figure 3.4 a-c**. The XRD result of the extracted sample shows no diffraction peaks, the powder after extraction presents as an amorphous phase, which does not display any peaks (shown in **Figure 3.4 a**). The amorphous structure happens at a lower temperature because at this temperature, there is/are dewatering of the molecule as well as phase transformation occurs; as a result, the particle will not be arranged well and have an amorphous structure [240], which is in agreement with the DT-TGA results. After the thermal treatment of mill slag-derived powder resulted in a hematite

phase, as detected by XRD and the diffraction data agree with the Joint Committee on Powder Diffraction Standards (JCPDS)(Powder Diffraction File (PDF)) card of JCPDS-PDF No. 01-084-0308. From the XRD peaks (**Figure 3.4**), the powders are crystalline when the temperature increases from 700 to 1000ºC, and the reflections of the hematite phase are marked with a pink square symbol. "▫". A small contribution of a second phase was also observed, marked reflections in the bottom with a blue square symbol "□" in **Figure 3.4 a,** and are assigned to Aluminum iron oxide with PDF No. 00-049-1657. **Figure 3.4 c** shows the photographs of the hematite particles after the thermal treatment at different temperatures under white light

Moreover, the XRD result in **Figure 3.4 (b)** shows the peak shift from 33.3 to 33.4 (2θ degree) and from 35.8 to 35.9 (2θ degree) after 800°C due to the crystal formation of aluminium iron oxide and overlapping with hematite. [225]. Besides, after 800°C, Aluminum iron oxide with PDF No 00-049-1657 has been identified in the diffractogram as a new peak. This overlapping of Fe^{3+} and Al^{3+} enhances the brightness effect of the pigment because the substitution of Al^{3+} helps to add a more yellowish colour to the pigment [242]. For an advanced structural investigation of the results, Xpert HighScore Plus has been used. The result indicated that the extracted sample is Rhombohedral with a space group of R-3c, group number 167, and a unit cell a= 5.0142Å = b, c=13.6733 Å, as identified by PDF number 01-084-0308.

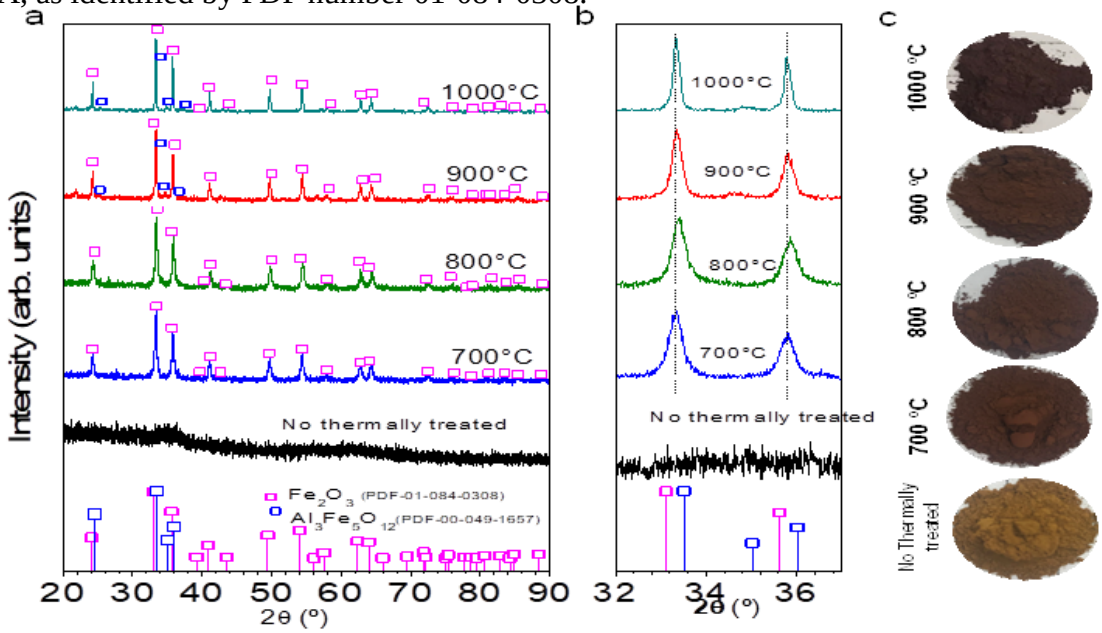

Figure 3. 4 (a) XRD analysis of the extracted powder before and after the thermal treatment at 700, 800, 900, and 1000°C. (b) Detail of the XRD in 32-37° 2θ range. (c) Photographs of the hematite particles under white light

Besides, the crystallite size was calculated from XRD data using the Debye Scherer formula given by [235];

$$D = \frac{k\lambda}{\beta cos\theta}$$

K=0.89 is the Scherer constant, λ=0.15406nm is the x-ray wavelength, β-the Full Wave Half Maximum (FWHM) in radian, and θ is the Bragg angle in radian. The crystallite size estimated from the Scherer equation also depends on the annealing temperature.

The crystallite size calculated using the Debye-Scherer equation and listed in **Table 3.2** increases as the annealing temperature, but the anomalous increase in the crystallite size occurs between 700°C and 800°C, as well as between 900°C and 1000°C. The first part (between 700°C and 800°C) might happen due to an incomplete crystal structure formation at the lower temperature, whereas the second part(between 900°C and 1000°C) is due to an overlapping of the crystallite structure of alumina iron and hematite, as detected in the XRD peak. Therefore, higher thermal treatments usually improve the crystallinity of the materials and imply the growth of the crystallite size due to the annealing.

Table 3. 2 Relation between thermal treatment and crystallite size of the powders after thermal treatment at 700, 800, 900 and 1000°C

Temperature	700°C	800°C	900°C	1000°C
Crystallite size	22.55	30.1	31.2	58.21

The morphology and size of extracted iron oxide powder have been investigated by field emission scanning electron microscopy (FE-SEM) in **Figure 3.5.**

The FE-SEM morphology shows that the powder is highly agglomerated. The agglomerates are formed by primary particles with an average size of ≤ 200 nm. This agglomeration occurred because of the large surface area energies due to smaller particles of the extracted powder [243]; however, it seems that the particles are not sintered.

Energy dispersive spectra (EDS) experiments are carried out to determine the chemical composition of the extracted sample after being thermally treated at 700,800, 900, and 1000ºC.

EDS analysis of the sample is summarized in **Table 3.3**. By selecting the total area of the micrograph, the elements detected are Fe, O, Al, Si, Na, Mg, Ca, Ti, Cr, Mn, and S, except iron, oxygen and alumina, which were detected in the XRD most of them are not in a traceable amount

and did not affect the pigment colour tone. These results are consistent with the findings by XRD, which confirms the presence of Fe_2O_3 and a secondary phase $Al_3Fe_5O_{12}$.

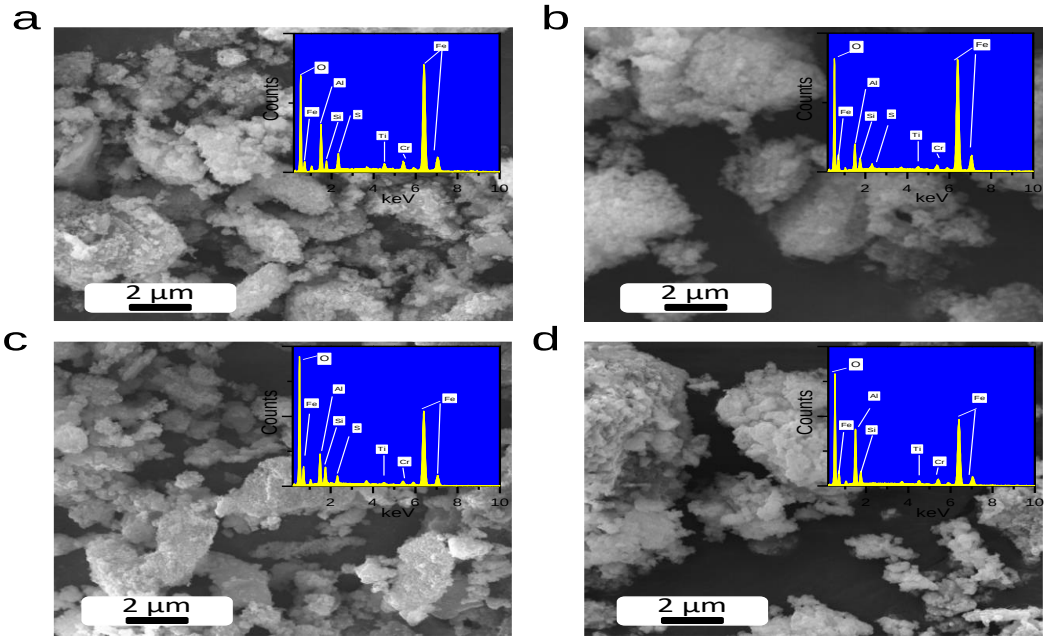

Figure 3. 5 SEM micrographs of extracted Fe_2O_3 sample pigment after thermal treatment with (a) 700°C, (b) 800°C, (c) 900°C and (d) 1000°C

EDS analysis shown in table 3.3 makes it possible to determine the remains of other elements that are not identified by the detection limit of the powder diffraction method.

Table 3. 3 Elemental analysis from the powder thermal treated at 700, 800, 900, and 1000°C in air

Elemental Composition in Weight %	Fe_2O_3 Theoretical	700°C	800°C	900°C	1000°C
Fe	69.94	55.72	46.62	55.02	41.34
O	30.06	26.44	38.78	32.24	38.26
Al	-	7.03	6.03	5.19	8.3
Si	-	1.09	2.75	2.09	4.44
Na	-	2.44	1.52	0.98	1.70
Mg	-	-	-	-	0.08
Ca	-	0.28	0.49	0.41	0.8
Ti	-	1.48	0.62	0.71	0.84
Cr	-	2.62	1.45	1.33	1.59
Mn	-	0.58	0.84	0.99	2.47

3.3.4 Particle size, Optical and colouring Property of Hematite Pigment

The particle size analysis was done by Dynamic Light Scattering (DLS), and the result of extracted powder and thermally treated at 700, 800, 900, and 1000ºC were presented as shown in **Table 3.4**. The result of the D-values (D0.10, D0.50 & D0.90) listed in Table 3.4 is also in agreement with the SEM result, that means as the annealing temperature increase, the particles tend to agglomerate, and the particle size becomes larger as a function of temperature [244].

Table 3. 4 The DLS result for particle diameter sample powder in µm

Temperature	Particle size distribution		
	D(V, 0.1)	D(V, 0.5)	D(V, 0.9)
700^0C	0.57	33.48	107.30
800^0C	1.70	35.98	104.87
900^0C	3.81	40.07	118.50
1000^0C	10.54	49.14	171.29

The UV-VIS-NIR absorbance spectra of extracted and annealed iron oxide are shown in **Figure 3.6**, with broadband between 250 and 600nm with the crystal structure of hematite.

The hematite structure, shown in **Figure 3.6(B),** has Fe (III) cations occupying interstices between the oxygen anions, thus forming an octahedral. These octahedral connected each other through the face's edge leading to different Fe-O bond lengths. This structure can be overlapped with Al(III) as it is a trivalent metal cation of a similar size. This overlapping modifies the properties of the Fe-O, like; crystallite size, spectrographic behaviour, solubility, dissolution kinetics, and colour [245]. The XRD result can deduce that the crystal formation of aluminium at 800^0C causes a slight change in the Chroma on the hematite pigment.

Moreover, **Figure 3.6(A)** confirmed that the absorption occurs at 250 nm, which is responsible for the ligand-to-metal charge transfer transitions [246], while the region between 300-550nm corresponds to the d-d transition, specifically at around 350nm. Near 550-800 nm, the peak is assigned to the $^6A_1 + {}^6A_1 \rightarrow {}^4T_1\ (^4G) + {}^4T_1\ (^4G)$ excitation of a $Fe^{2+} \rightarrow Fe^{3+}$. As to Olga Opuchovic et al., the dark red colouration of iron oxide is formed mainly due to the $2p(O^{2-}) \rightarrow 3d(Fe^{3+})$ charge transfer band [247]. In addition, the inter valance charge transfer band, at around 580 nm, shown

in **Figure 3.6,** implies that most of the optical bands are due to Fe^{3+} in α–Fe_2O_3 octahedral structure.

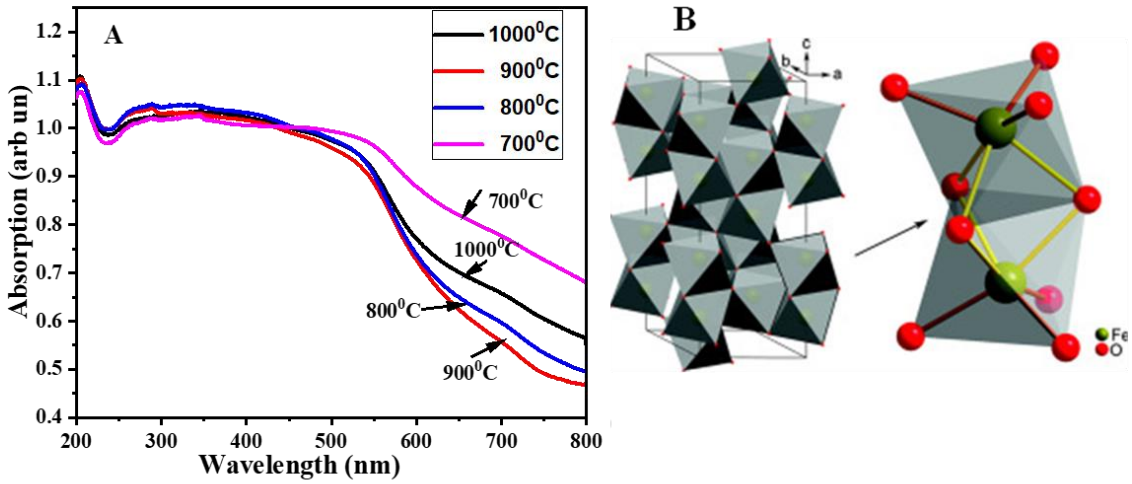

Figure 3. 6 (A) UV-VIS-NIR absorption of Hematite at different Temperature. (B) Crystal structure of hematite.

Besides, the energy bandgap change shown in **Table 3.5** is due to a change in temperature and the inclusion of aluminium impurity in it, which directly relates to the colouring property of the pigment. Furthermore, **Table 3.5** confirmed that the minimum energy band gap was observed at the temperature of 800°C; this may happen due to the overlapping of aluminium, which agrees with the XRD value.

In addition, the tonality of hematite colour powder strongly depends on its particle size and dispersibility: the colour of the powder looks red when the particle size is smaller, while it turns to dark grey as the particle size increases/annealing temperature increase [242], which is an agreement with **Table 3.2** and the colour of the pigment in **Figure 3.4b**.

Figure 3.7 and **Table 3.5** show the chromaticity CIE-L*a*b* analysis of the pigment extracted from slag with different annealing temperatures. Chromaticity in CIE-L*a*b* is an index that uses the values of brightness (L*), red/green (a*), and yellow/blue (b*).

A standard white calibration plate calibrated by NPL (National Physical Laboratory) is used as a white reference provided with the spectrophotometer. **Table 3.5** summarizes the values obtained for the CIE-L*a*b* coordinates and C and H values.

The calcination temperature influenced the CIE-L*a*b* values of pigments. When a* and b* values are positive, it is possible to deduce the degree of redness and yellowness. Moreover, **Table 3.5** indicates that a* value decreases continuously with increasing temperature. This is because an

increase in temperature causes the molecule of the powder sample to expand, resulting in the formation of larger molecules at a higher temperature. This expansion of the sample powder molecule causes it to display less red or brownish [242, 248].

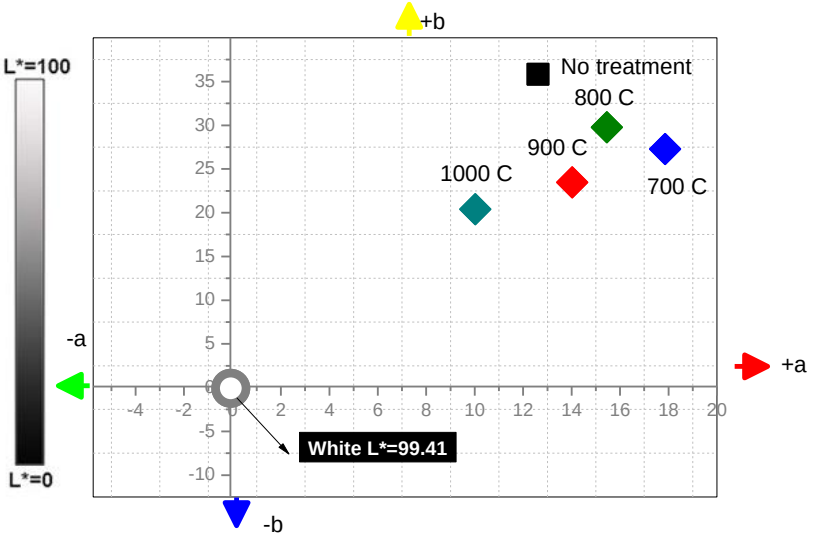

Figure 3. 7 Chromatic property CIE-L*a*b* as a function of temperature

Besides, **Figure 3.7** and **Table 3.5** clearly show that the b* value (yellow/blue) colour increases continuously towards yellowish and shifts towards bluish colour after 800°C. At the same time, the lightness of the colour increase till the temperature reaches 800°C. Even though a* value is relatively less at 800°C than at 700°C, it tends to show brighter colour at 800°C due to the highest value of yellowness b*. The colour change happened due to the overlapping of aluminium iron oxide in the hematite structure that caused the colour to be more yellowish, and the cumulative effect appeared as a brighter red-brown colour with better Chroma [119, 125]. The initial sample shows little red intensity when annealed at 700°C, but the redness decreases at 900 and 1000° C.

Table 3.5 CIEL*a*b* coordinates of the extracted powder, not annealed and treated at 700°C, 800°C, 900°C and 1000°C, and energy bandgap

Temperature	CIE-L*a*b* result					E_g (eV)
	L*	a*	b*	C	H^0	
No thermally treated	46.39	12.62	35.81	37.97	70.59	-
700ºC	29.61	17.86	27.27	32.60	56.8	1.68
800ºC	30.77	15.46	29.76	33.54	62.6	1.62
900ºC	28.04	14.02	23.47	27.34	59.1	1.81
1000ºC	24	10.02	20.4	22.73	63,8	1.92

Besides forming relatively larger crystallite size as a function of temperature, the colours are also influenced at elevated temperatures and become darker brown [242]. As a result, the lightness value decreases at the maximum temperature and the maximum lightness, and Chroma was registered at 800ºC. Moreover, the CIEL*a*b* results shown in **Table 3.5** clearly show that the extracted sample fulfils the colourimetric axis of the commercial hematite, except the hue (H) value at elevated temperature, which is affected due to the appearance of larger particle size of the sample[145].

3.4 CONCLUSIONS

Iron oxide powder has been extracted from mill-scale iron industry waste using a hydrothermal mechanism with sulphuric acid as a bleaching agent and ammonium used as a pH stabilizer. Innovative work has been done in transforming Fe^{2+} to Fe^{3+} to have a relatively pure hematite pigment from recycled waste. The extracted powders have different particle size distributions as a function of the annealing process; the particle size increases with the temperature and the crystallite size. Furthermore, the second phase causes this distortion because its peaks overlap with the hematite at 33.3 and 35.8 2theta at 800°C. A secondary phase assigned to aluminium iron oxide also appears after 800°C; as a result, the pigment possesses a brown-red colour due to the domination of calcined hematite, which has brown. Our observations demonstrate that it is possible to tune the colour of the particles with the annealing temperature to provide a chart for the pigment field. It is increasingly recognized that, although iron oxide pigments have been studied extensively, the extraction from mill-scale steel industry waste can open paths to obtain high-

demanding iron oxide pigments; moreover, it can act as a reference for extracting other industrial waste to substitute and conserve natural resources.

CHAPTER FOUR

EFFECTS OF DOPING SYNTHETIC IRON OXIDE ON THE COLORING PROPERTIES OF COPPER CHROMATE PIGMENT

Zekarias G. Eticha*, Thomas C Alex, Olu Emanuel Femi, Abubeker Yimam, Esayas Alemayehu*

ABSTRACT

Iron-doped copper chromate with ($Fe_xCu_{1-x}Cr_2O_4$) as a black ceramic decoration pigment is successfully synthesized using a solid-state synthesis method with a pure oxide precursor. The powder pigment was analysed using powder X-ray diffraction (PXRD), SEM with EDS, FTIR, UV-VIS, and colour-measuring instruments. The calcination temperature was determined from the literature and was calcined at 1350°C for 3 h. The result of the (PXRD) indicated that the sample contains a spinel structure; moreover, the addition of iron oxide caused the diffractogram peak to shift towards the lower angle due to the small ionic radius of iron compared to the replaced copper. The micrograph of the SEM result also indicated that agglomeration decreases as the amount of doped iron increases. As the amount of doped iron increases, the colour of the pigment L* tends to be darker, while the b* value tends more towards blue colour, but the intensity of the red colour ***a**** increases till the proportion is equal. In the end, the optimum colour, which is comparable with the commercial black pigment, was obtained when a similar weight percentage of iron replaced the copper

Keywords: Ceramic decoration, Black pigment, Copper chromite. Doping, Agglomeration

4. INTRODUCTION

4.1 BACKGROUND AND JUSTIFICATION

The chemical composition of the pigment impacts their qualities, such as solubility, thermal stability, resistance to sunshine, weather and atmosphere, abrasion resistance, and optical properties, and hence the pigment has been used for different applications like decoration, solar absorbent, cooling of the roof of the house and the like [66, 249, 250]. Pigments are responsible for the vibrant colours of coatings. Coatings now come in a variety of colours. Some of the factors to consider when selecting a pigment for special coatings are; hiding efficiency, refractive index, colour, density, hardness, and oil absorption.

Various research papers have reported on the use of various precursors and synthesis methods to produce the desired pigment. The pigment synthesis criteria are subjective and rely on cumulative light absorption by multiple chromophores. Pigment colours are achieved through nonlinear synthesis, and each chromophore has its optical bands that absorb a specific wavelength range; most of the time, the goal is to collect as many cations as possible to accomplish complete absorption in the visible spectrum [251].

The principal chromophores in pigments, including spinel, are transition metal ions such as Co^{2+}, Ni^{2+}, Fe^{2+}, Cr^{3+}, V^{3+}, Cu^{2+}, etc. They feature a partially filled electron valence shell and a good polarising ability. The colour changes due to oxygen polarisation, forming complexes with transition metal ions [252]. In general, chromophore refers to a transition metal ion in a specific ligand environment because the same cation will exhibit optical bands at different energies once octahedrally or tetrahedrally coordinated [253].

Considering the principal chromophores in the spinel pigment synthesis is beneficial, especially partial or complete inversion degrees develop transition elements with distinct valence states. As seen in **Figure 4.1**, the spinel structure is made up of a nearly perfect cubic arrangement of oxygen atoms that form tetrahedral (T) and octahedral (M) cavities [254, 255]. Unfortunately, this results in extraordinarily complicated optical spectra, with numerous bands and almost entirely filtering visible light, originating from d-d electronic transitions and metal-metal or metal-ligand charge transfer [256, 257].

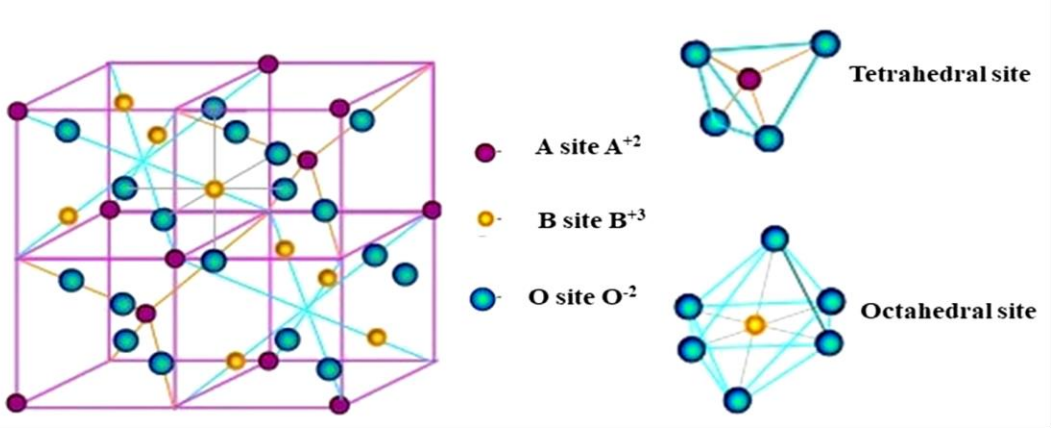

Figure 4. 1 Schematic diagram of spinel crystal structure with the general formula of AB_2O_4

Inorganic black pigments are among such chromophores and are commonly utilized as colourants in today's ceramics industry, either for ceramic bodies or glazes [251]. Black colours are becoming more popular due to their pure and dignified ornamental impact and their recognition as high-quality jewels. Metallic oxide doped chromate spinel powder has been used as a sun-absorbing pigment and decorative colour in ceramic industries over the previous decade due to its optical properties and lower oil absorption values than carbon soot and perylene black [258, 259].

The solid solutions of eskolaite-hematite $(Cr, Fe)_2O_3$ and sophisticated spinel compositions in the Co-Cr-Fe-Mn-Ni-(Cu-V) system are utilized to obtain the black pigment. Since eskolaite-hematite pigments are less stable in glazes and carbon black is less stable at a higher temperature, the spinel structure is used as the ceramic industry's most popular black colourant [256]. It contains a broad group of compounds with a general formula of AB_2O_4 that have two cations, A and B: an oxidation degree of A with 2+ representing (Mg, Cr, Mn, Fe, Co, Ni, Cu, Zn, Cd, and Sn) and the other an oxidation degree of 3+(Al, Ga, In, Ti, B, Cr, Mn, Fe, Co, Rh, and N) [159, 261, 262], they have a partially filled electron valence shell and high polarization ability [30].

The spinel structure accounts for 25wt% of the total usage of commercial black pigment formulations [34, 38], and the spinel chromites can be relatively easily obtained either by solid-state or wet synthesis mechanism with subsequent thermal treatment [262-264]. The physical properties of the spinel chromites are strongly dependent on the cation stiffness and distribution within the tetrahedral and octahedral sites in the spinel lattice [269]. Therefore, the process of synthesis directly influences the physicochemical properties of spinels. The most common

synthesis mechanisms reported by several researchers are co-precipitation [266-268], hydrothermal synthesis method [269], solid-state method [233, 251], sol-gel [270], and sol-gel combustion synthesis [2, 271].

Transition metals doped copper chromate black pigment was synthesized using co-precipitation and hydrothermal method [255], while Elham Pakzad et al., 2019 prepared pure copper chromate using sol-gel combustion as a spectrally selective absorber [263]. In addition, Qingfen Geng et al., 2012 produced a copper chromate pigment for selective absorbent using a low-temperature combustion method [272].

Similarly, different research activities have been attempted to synthesize an inorganic metal oxide spinel pigment using iron and manganese oxides; some of them are; Manganese Ferrite Black Spinel, (Fe, Mn)(Fe, Mn)$_2O_4$ (PBk26), Iron Manganese Oxide (Fe, Mn)$_2O_3$ (PBk33), which offers a dark brown-black. The synthesis of Iron-Cobalt Chromite Black Spinel (PBk27), Co(Fe, Cr)$_2O_4$, and Iron-Cobalt Black Spinel (PBk29), (Fe, Co)Fe_2O_4, on the other hand, have even made it more heat stable than $CuCr_2O_4$ blacks (PBk28) [273].

Even though different researchers have employed the wet chemical synthesis method, the method requires a greater understanding of each element's chemical reaction, precursor interaction method, surface stabilizing agent, and reagents used with growth and nucleation rate to control size and shape. Moreover, most are costly and time-consuming mechanisms [274].

As a result, the solid-state synthesis mechanism is considered suitable, especially for mass production. It has lower chemical waste; it is the most straightforward mechanism, has low cost, and has high product purity [251]. In addition, the colouring effect of iron oxide doped copper chromate synthesized by conventional solid-state mechanism is not reported yet. As a result, this paper reports the effect of adding iron oxide on $CuCr_2O_4$ spinel structure pigment synthesized by the conventional solid-state method to study the final product's colouring property, morphology, and crystallite size.

4.2 METHODOLOGY

4.2.1 Preparation of Composite pigment

The samples of $Fe_xCu_{1-x}Cr_2O_4$ (x=0, 0.25, 0.75, and 1) for all compositions have been synthesized with solid state technique. In the process, chromium oxide (99%), copper oxide (95%), and iron oxide (99.7%were used, and acetone was used as a wetting medium.

The required amount of the starting materials were mixed in an agate mortar and pestle and ground for 30min. Then, the mixed samples were placed in an attrition mill revolving at a rate of 1000rpm for further mixing using acetone as a wetting media for 1:30 h. After 1:30 h mixing in the attrition mill, the sample was dried in an oven at 80°C for 15 h. Finally, the dried sample was ground using an agate mortar and pestle for 1h. Finally, the powder sample was sieved using a #100 mesh size and kept in a plastic bag for further processing.

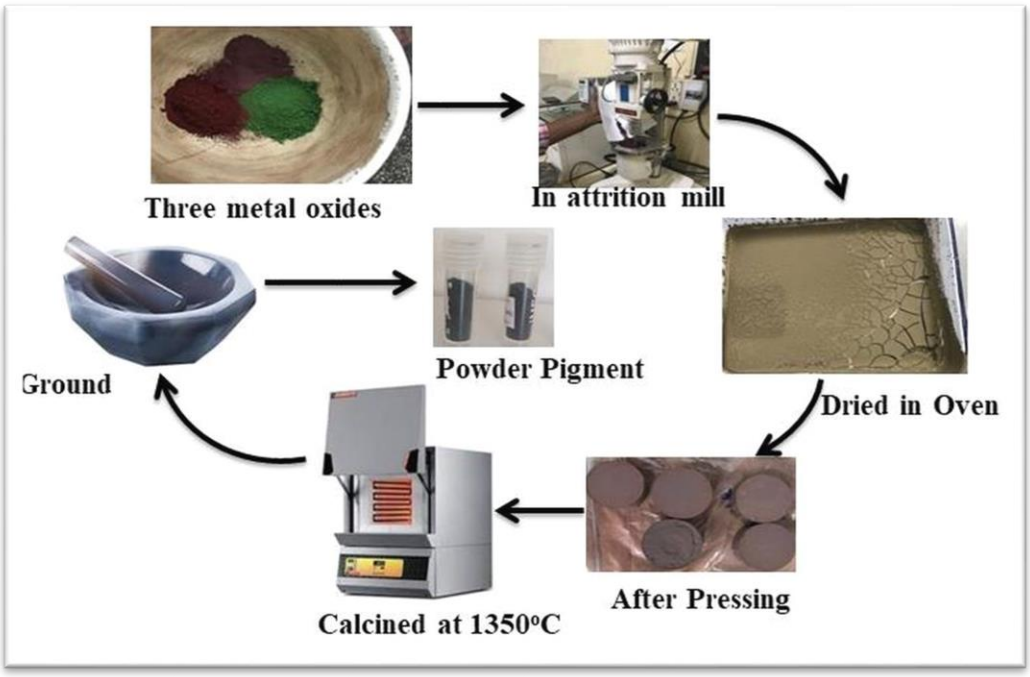

Figure 4. 2 Solid-state mixing of the three inorganic metals

The sample powder was then pelletized using a pressing machine at 18.133MPa (1ton) with a diameter of 25mm and calcined at a temperature of 1350^0C for 3 h, at a rate of rising and lowering of 50°C/min to ensure the reaction takes place properly [193]. Finally, the calcined pellets were ground using an agate mortar and pestle and sieved using #100 to get a powder labelled with code, as shown in **Table 4.1,** for further characterization.

Table 4. 1 Chemical composition and corresponding code of the composite pigment

No	Chemical Composition	Code
1	$FeCr_2O_4$	Z_1
2	$Fe_{0.75}Cu_{0.25}Cr_2O_4$	Z_2
3	$Fe_{0.5}Cu_{0.5}Cr_2O_4$	Z_3
4	$Fe_{0.25}Cu_{0.75}Cr_2O_4$	Z_4
5	$CuCr_2O_4$	Z_5

4.3 CHARACTERIZATION

The phase composition and crystalline materials structure was characterized using Rigaku powder x-ray diffraction (PXRD), and data were collected using continuous scanning. The X-ray source is copper-sealed 0.6kw Cu Kα emission lines from a generator operating at 40 kV and 15 mA. The measurements were performed at room temperature from 20 to 60° (2θ) with a 0.02° step and 0.12sec/step scanning rate.

The FT-IR was used on spectrum 65 FT-IR (PerkinElmer) in the range 4000-400cm^{-1} (resolution:4cm^{-1}, number of scale:4) using KBr pellets. The morphology of the samples was observed by a scanning electron microscope (ESEM, model Quanta 200, with a resolution up to 3nm), and the chemical composition was investigated using EDS. The particle size analysis was investigated using a Malvern laser diffraction particle size analyzer (Model: MASTERSIZER S, Malvern Instruments, and the UK). The proper dispersion was performed in the investigation using sodium hexametaphosphate as a dispersant, and the ultrasonic vibration was applied for 15 s as it was done in the former sample [201]. The optical property of the mixture sample pigment was evaluated using a UV-VIS spectrophotometer (carry 100 UV-VIS spectrophotometer, Agilent technologies) at the wavelength range of 200-800nm. The refractive index(n) of the synthetic iron-doped copper chromite was also calculated from the UV-VIS data using the formula [275]

$$n = \frac{1}{T_s} - \sqrt{\frac{1}{T_s} - 1}$$

Where, T_s – is per cent transmittance and is given by $T_s = 10^{-A}x100$, where A is the absorbance The colouring coordinate was calculated using CIE-1931 colour space, using CIExyz axis, and converted to spherical coordinates L*, a*, and b* using the formula

$$L^* = 116(^Y/_{Y_n})^{\frac{1}{3}} - 16 \quad (1)$$

$$a^* = 500((^X/_{X_n})^{\frac{1}{3}} - (^Y/_{Y_n})^{\frac{1}{3}}) \quad (2)$$

$$b^* = 200((^Y/_{Y_n})^{\frac{1}{3}} - (^Z/_{Z_n})^{\frac{1}{3}}) \quad (3)$$

$X_{n,}\, Y_n, and\ Z_n$ are specified white chromatic reference illuminated for the CIE1931(2*) and is given by; $X_n = 95.0489$, $Y_n = 100$ and $Z_n = 108.8840$ [208, 276]. The chroma a* and b* are given positive and negative values; it becomes red when a* is positive unless it becomes green; the yellowish colour is represented by positive b* while the negative is by the blue colour of the pigment in the colour measurement [201]. L* is the lightness of the pigment with a value (L* = 0 means dark, and L* = 100 is white).

Moreover, the Chroma (C) and hue (H) values are calculated from equations 4 and 5, respectively, as;

$$C = \sqrt{a^{*2} + b^{*2}} \quad \text{and} \quad (4)$$

$$H = \tan^{-1}(^{b^*}/_{a^*}) \quad (5)$$

4.4 RESULT AND DISCUSSION

The solid-state reaction containing Fe_2O_3, CuO, and Cr_2O_3 is supposed to occur above 1200°C [193]; as a result, the calcination was done at 1350°C for a period of 3 h to ensure a complete reaction.

4.4.1 Phase and Structural analysis of $Fe_xCu_{1-x}Cr_2O_4$ pigment

After Calcination took place at 1350°C for 3 h, the synthesized powders were analyzed using X-ray diffraction to get microstructural properties. The patterns of the samples were demonstrated as shown in **Figures 4.3 a** and **b**. The characterized peaks of the samples are indexed to the crystallographic planes of $FeCr_2O_4$ with the (Joint Committee on Powder Diffraction System-

Powder Diffraction File) JCPDS-PDF number 00-024-0512 and $CuCr_2O_4$, JCPDS-PDF number 00-021-0874 as reference. The results confirmed that the two samples have successfully attained the spinel oxide structure. The diffractogram shown in **Figures 4.3 a** and **b** indicated that the pure form of the spinel structure $FeCr_2O_4$ and $CuCr_2O_4$ best fit with the corresponding JCPDS-PDF No.

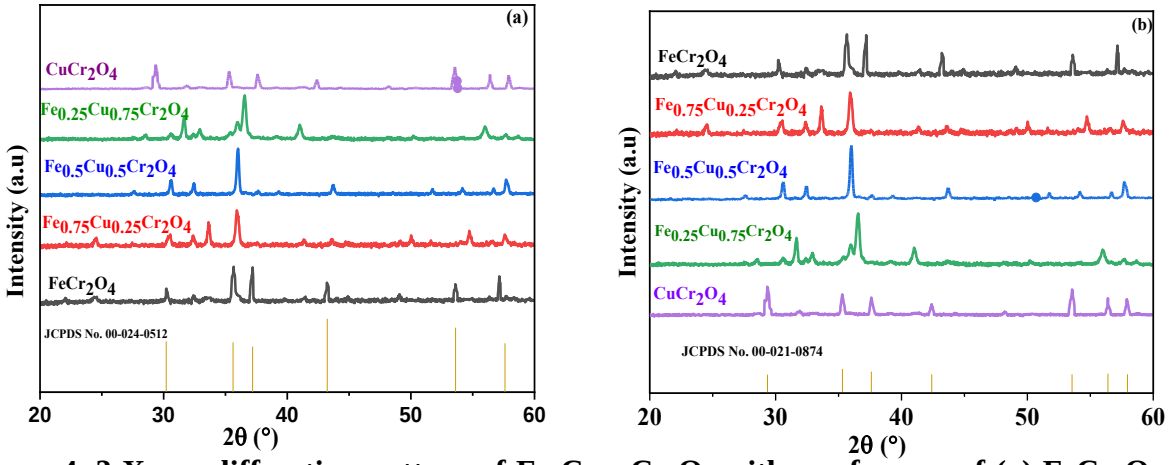

Figure 4. 3 X-ray diffraction pattern of $Fe_xCu_{1-x}Cr_2O_4$ with a reference of (a) $FeCr_2O_4$ (b) $CuCr_2O_4$

Moreover, it was evident that **Figure 4.4 b** shows a peak shift to a smaller Bragg angle as the amount of Fe added increases; this is due to the unit cell concentration induced by the partial substitution of Cu(II) with ionic radii (0.73Å) by smaller ionic radii Fe(II) of (0.7Å) than that of pure $CuCr_2O_4$ as indicated in **Figure 4.4C**.

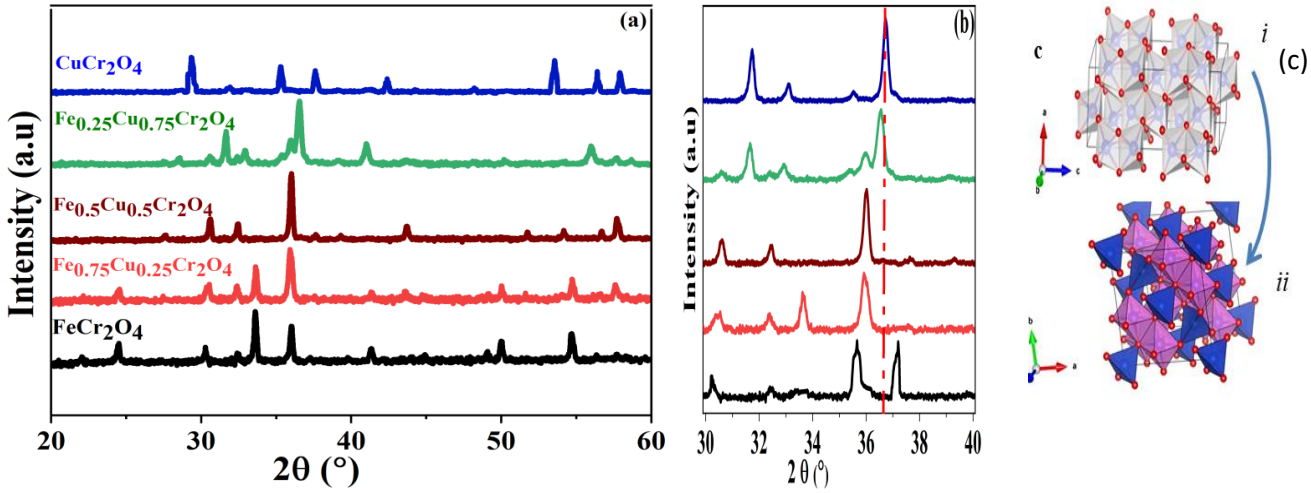

Figure 4. 4 XRD peak of (a) Different composition of iron on $CuCr_2O_4$ pigment (b) Shift in Bragg angle due to iron addition (c) Crystal structure of (i) Hematite and (ii) $CuCr_2O_4$

The average crystallite size of the powder pigment indicated in **Table 4.2** was calculated using the Debye Scherer equation:

$$D = \frac{k\lambda}{\beta \cos\theta}$$

The constant k-is shape factor k= 0.9, λ = 0.15406nm, is the wavelength of the XRD machine and β -the Full Wave Half Maximum (FWHM) in radian, and θ the Bragg angle in radian. The result shows an increase in size as the amount of iron oxide added to the copper chromate powder increases; it agrees with [277] and **Figures 4.5.** This can be happened due to a partial replacement of copper by iron which is less in ionic radius.

Doping may cause a change in the lattice parameters. Micro-strain is defined as the root-mean-square of variations in lattice parameters across individual crystallites, and it is calculated using the formula suggested by the formula given in [277],

$$\varepsilon = \frac{\beta \cos\theta}{4}$$

Where ε is microstrain.

The calculation result shown in **Table 4.2** indicated that the microstrain decreases from 0.0059 to 0.0027, indicating that the lattice defects decrease as smaller ionic radii (iron oxide) replace the more significant (copper oxide).

Table 4. 2 Crystallite size of each sample

Sample Powder	Z1	Z2	Z3	Z4	Z5
The average Crystallite size (nm)	12.81	10.67	10.61	10.17	10.02
Micro strain	0.0027	0.0029	0.0032	0.0057	0.0059

4.4.2 FTIR analysis of $Fe_xCu_{1-x}Cr_2O_4$

The vibrational spectra of $Fe_xCu_{1-x}Cr_2O_4$ spinel pigments (x=0, 0.25, 0.5, 0.75, and 1) in the infrared region (2500–400cm^{-1}) are shown in **Figure 4.5**. The spectra of spinel oxides containing transition metals with oxidation states of +2 and +3 usually feature four distinct bands: 800–650 cm^{-1} (ν_1), 600–500 cm^{-1} (ν_2), 450–300 cm^{-1} (ν_3), and 200–150 cm^{-1} (ν_4) [278].

The vibrational frequency of metallic ions in the crystal lattice is allocated to the IR bands of spinel, and the vibrational frequency is determined by the quality and ionic radius of metallic ions. Absorption bands in the 600-500cm^{-1} range correspond to the inherent stretching vibration of the M_{tetra}–O band at the tetrahedral site (Cu-O and Fe-O) [272], whereas bands in the 499-385cm^{-1} range relate to octahedral metal ion stretching (Cr-O) [279].

Moreover, **Figure 4.5** shows that all samples' IR absorption bands for metal-oxygen bonds are about 700 and 500cm^{-1} due to coupled vibrations of metal-oxygen bonds in both tetrahedral and tetragonal locations. The Fe-O vibration is represented by the absorption bands at 806. The typical absorption bands became more evident as the iron content increased in the produced pigment.

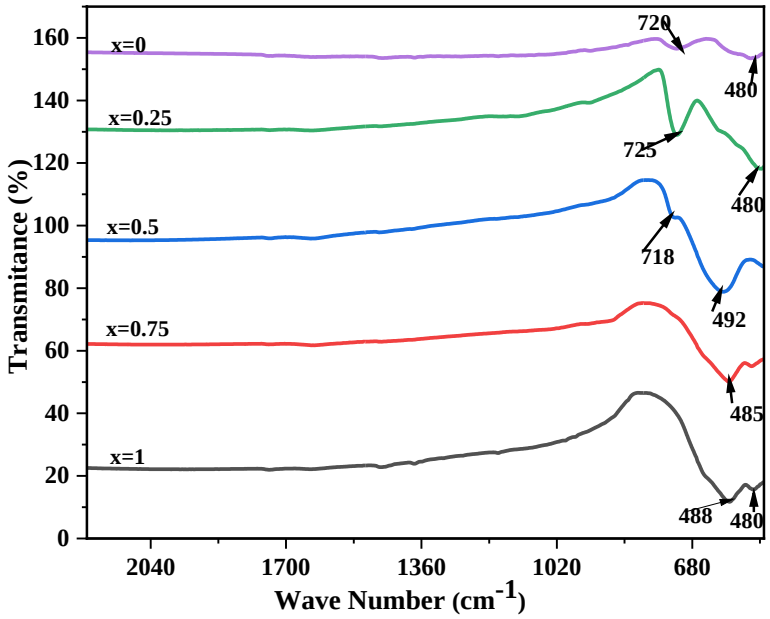

Figure 4. 5 FTIR spectra of the sample $Fe_xCu_{1-x}Cr_2O_4$ (x= 0, 0.75. 0.5. 0.25)

4.4.3 SEM with EDS result of $Fe_xCu_{1-x}Cr_2O_4$

Figure 4.6 shows a scanning electron microscope (SEM) image of the sample pigment with varying weight percentages of iron oxide added to copper chromate. The pigment powder is characterized by a more spherical shape with some irregular shapes, as is observed. Moreover, the EDS result confirms the purity of the raw sample, except for introducing carbon in a smaller amount.

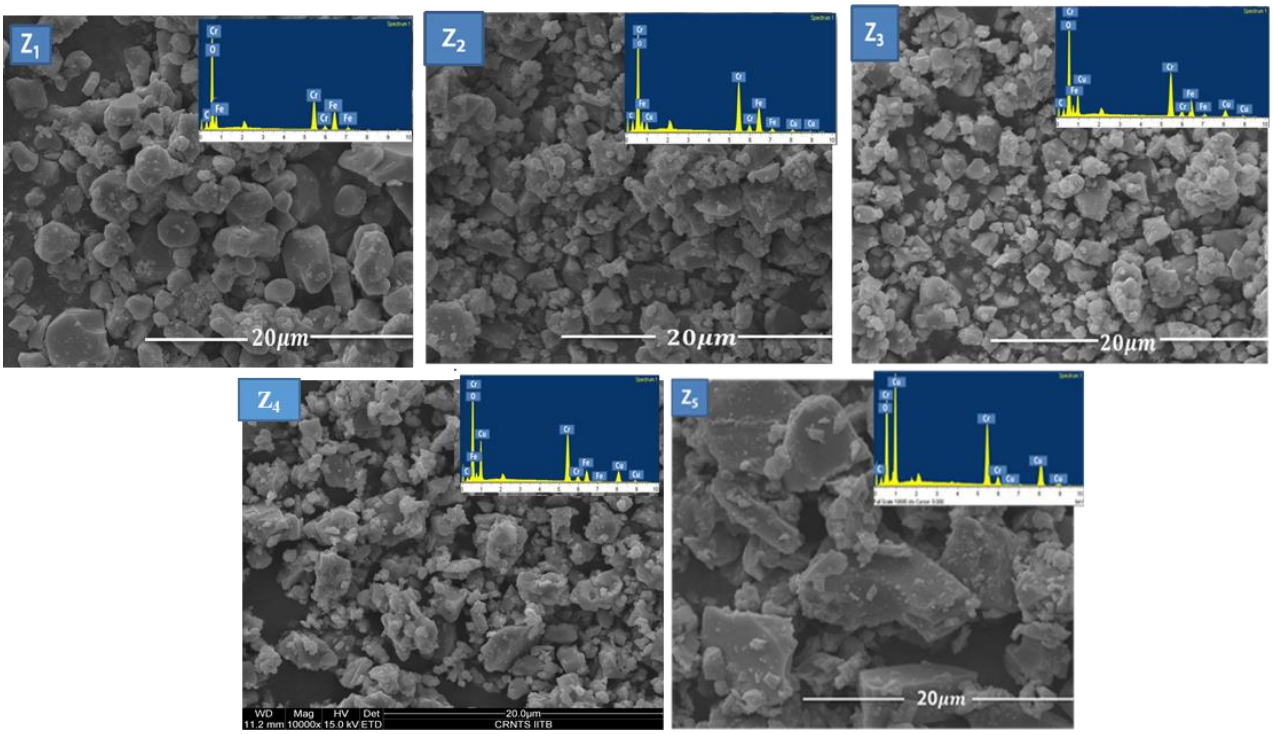

Figure 4. 6 SEM image of $Fe_xCu_{1-x}Cr_2O_4$ sample

The particle size was evaluated using Dynamic Light Scattering (DLS) with proper dispersion performed using sodium hexametaphosphate as a dispersant, and the ultrasonic vibration was applied for 15 s. The results showed a wide range of particle sizes, as given in **Table 4.3**. The result shows a non-uniform particle size distribution, indicating that more grinding and sieving with a minimal sieve size are required to achieve a uniform size distribution. Furthermore, **Table 4.3** result agrees with **Figure 4.6,** as it contains a particle in the nanometer and micrometre ranges. The larger particle size distribution may occur due to improper grinding and sieving.

Table 4. 3 Particle size distribution of the sample (identified by DLS)

Sample	Distribution	Size (μm)
Z_1	D(v, 0.1)	0.24
	D(v, 0.5)	73.71
	D(v, 0.9)	276.41
Z_2	D(v, 0.1)	0.32
	D(v, 0.5)	46.96
	D(v, 0.9)	176.29
Z_3	D(v, 0.1)	0.77
	D(v, 0.5)	82.13
	D(v, 0.9)	217.43
Z_4	D(v, 0.1)	0.81
	D(v, 0.5)	4.85
	D(v, 0.9)	133.89
Z_5	D(v, 0.1)	1.86
	D(v, 0.5)	55.32
	D(v, 0.9)	266.24

4.4.4 Optical and Coloring Property of $Fe_xCu_{1-x}Cr_2O_4$

The optical response of $CuCr_2O_4$ with an addition of iron oxide towards UV-Vis radiation is tested by ultra-violate visible spectroscopy (UV-VIS Spectroscopy) in the wavelength range from 200 nm to 800 nm.

The UV-vis absorbance spectra of those black pigments in **Figure 4.7** demonstrate that the absorption curve is horizontal for samples Z1 through Z5, indicating that the samples have uniform absorption of all the incoming intensity of light in the visible light spectrum range [280]. Hence it is a confirmation that the synthesized pigment is a perfect black comparable with the commercial one as well as with carbon black pigments[1].

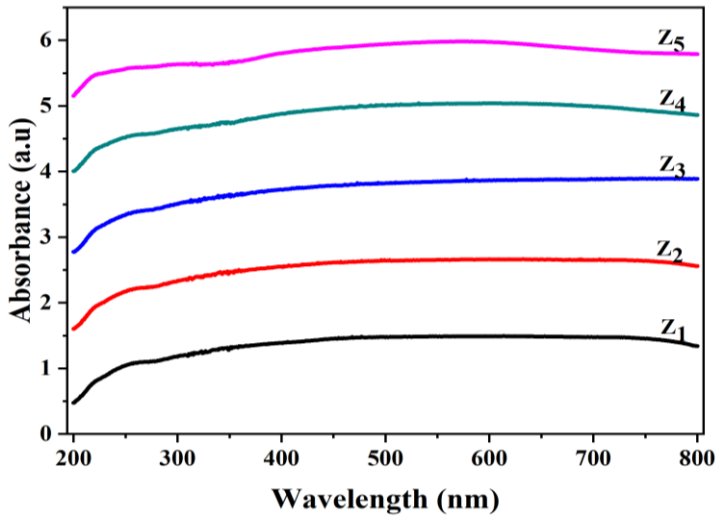

Figure 4. 7 UV-VIS spectroscopic results of iron oxide added copper chromate pigment

The refractive index of iron oxide doped copper chromate is shown in Figure 4.8, as shown below. The pigment's purpose is to provide colour while also protecting the substrate. Therefore, the pigment must create opacity in the coating to give it colour. When a coating is opaque, the pigment particles scatter or absorb light so it does not reach the substrate. The pigment's ability to impart opacity is determined by two properties: refractive index and particle size [281].

Figure 4.8 revealed that the refractive index of the pigment powder increases as the doped iron amount increases. Since the ionic radii of iron are smaller than copper's, the illustration in **Figure 4.8** agrees with scientific truth because pigment with tiny particles has more surface molecules per gram than coarse particles. Moreover, a black pigment calcined above 1200°C exhibits an index of refraction between 1.5 and 2.6 [282].

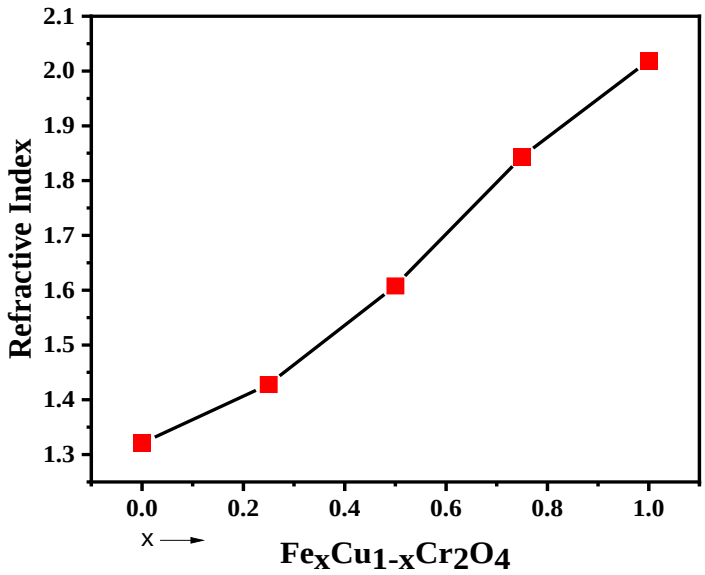

Figure 4. 8 The value of the Index of refraction of the copper chromate pigment function as the doped iron oxide.

Table 4.4 summarizes the comparison results with commercial black pigment and their synthetic black pigments.

According to equations 1-3, the chromatic characteristics of the synthesized $Fe_xCu_{1-x}Cr_2O_4$ pigment particles were assessed using CIE 1931 colour coordinates with CIExyz values and then converted to CIEL*a*b*. Equations 4 and 5 were used to calculate the chroma and hue values, and the colour coordinates (L*, *a**, b*) of the pigment show that the synthesized pigment is darker in colour, and the picture of the pigment is shown in **Figure 4.9 b.**

The comparative study in **Table 4.4** indicated that the Lightness of the as-synthesized pigment shows a relatively comparable result with the commercial one, the experimental result value depicts darker than the commercial black, and an optimized result was registered at Z_3. In contrast, the experimental result is better Chroma and Hue than CP-2 but slightly lower chroma than CP-1. Furthermore, the commercial pigment calcined at 1200°C turned a more reddish and yellowish colour than the experimental one; as a result, it may develop a colour towards a brown intensity than the experimental result.

Table 4. 4 The chromaticity of the five samples and the commercial black pigment

Sample	Colourimetric Values						Reference
	Composition	L*	*a**	b*	C	H	
Z1 (x=1)	$Fe_xCu_{1-x}Cr_2O_4$	32.3	1.20	1.07	2.34	41.7	Research result
Z2 (x=0.75)	$Fe_xCu_{1-x}Cr_2O_4$	32.4	1.11	1.09	2.29	44.48	Research result
Z3 (x=0.5)	$Fe_xCu_{1-x}Cr_2O_4$	32.96	1.01	1.41	3.03	54.39	Research result
Z4 (x=0.25)	$Fe_xCu_{1-x}Cr_2O_4$	32.49	1.04	1.25	2.60	50.2	Research result
Z5 (x=0)	$Fe_xCu_{1-x}Cr_2O_4$	32.52	0.94	1.41	2.93	56.3	Research result
S2	Chromium-rich leather sludge	30.47	0.91	0.72	1.43	38.35	[193]
Cp-1	Commercial Black Pigment at 1200°C	33.04	1.24	1.76	4.33	54.8	[193]
CP-2	Commercial (Fe-Cr) Black Pigment	33.0	1.0	0.5	1.25	26.6	[283]
$Zn_1Co_6Sb_2O_{12}$	Synthetic Black containing cobalt	32.1	1.8	3.4	13.36	62.1	[205]

In addition, **Figure 4.9 (b)** shows that the colour looks similar when we detect it in the necked eye. However, the colourimetric measurement confirmed that as the amount of iron oxide added to the copper chromate pigment increase, the colour attains a more reddish intensity (increase the value of a*) and decreases the b* value, as indicated in **Figure 4.9 (a) [275, 280]**.

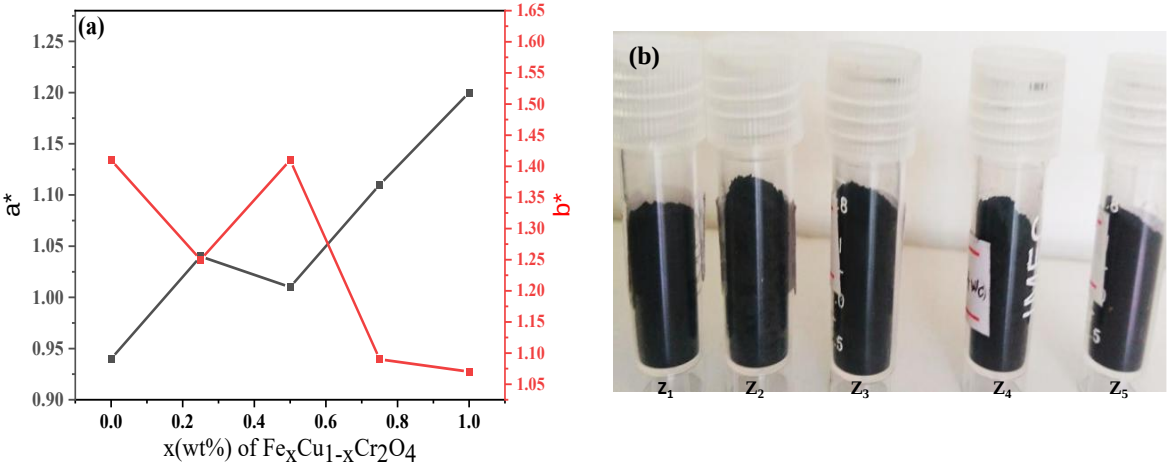

Figure 4. 9 Relationship between amounts of iron oxide added to the copper chromate and Chroma of the Pigment (a) graphically (b) the photograph of the powder.

4.5 CONCLUSION

$Fe_xCu_{1-x}Cr_2O_4$ (x=0, 0.25, 0.5, 0.75, and 1) were prepared by the solid-state method effectively to examine the colour performance of $CuCr_2O_4$ black pigment. Crystallography, morphological, optical, and colouring characteristics of the materials were assessed using XRD, SEM, FTIR, UV-Vis, and chromaticity. The results show that the substitution of Cu by Fe in $CuCr_2O_4$ resulted in the formation of a black pigment comparable to commercially available copper chromate, with no impurity phases. The iron oxide added copper chromate pigment had been an appealing method for preparing black pigment with $Fe_xCu_{1-x}Cr_2O_4$ spinel structure, fine grain, and good dispersion that can replace commercially available copper chromate pigment used in the ceramic industry. The charge transform and the d-d transition in Fe increase absorption in visible light (380 nm to 780 nm), decrease the L* value and exhibits good blackness. The colouring axis a* increases as the amount of iron oxide doped increases; this agrees with the former chapter; the iron oxide gives a reddish shade to the pigment. Besides, the proper placement of iron in the position of copper caused the pigment to be more opaque and enhanced the index of refraction, as the ionic radii of iron are smaller than that of copper. Moreover, this index of refraction is in good agreement with other experiments. Finally, compared to the commercial one, the $Fe_{0.5}Cu_{0.5}Cr_2O_4$ has the optimal chromaticity values of L*=32.96, a*=1.01, and b*=1.41.

CHAPTER FIVE

EFFECT OF ADDING EXTRACTED IRON OXIDE ON THE COLORING PROPERTY OF COPPER CHROMATE; A COMPARATIVE STUDY.

Zekarias G. Eticha*, Thomas C Alex, Olu Emanuel Femi, Abubeker Yimam, Esayas Alemayehu*

ABSTRACT

Industrial waste is now being recognized as a viable replacement for some raw materials in industrial ceramic pigments. The root cause of improved colour tonalities is the synthesis route, starting materials, and external factors. In this study, iron oxide extracted from steel slag has been added to synthetic copper chromite pigment to create a spinel structure of $Fe_xCu_{1-x}Cr_2O_4$ ($0 < x \leq 1$) black pigment comparable with synthetic iron doped copper chromate pigment using a solid state mechanism. In a similar fashion to the former experiment, the starting materials were mixed using agate mortar and pestle, then further using an attrition mill. The reaction of the compounds was then facilitated by pelletizing using a pressing machine and calcined at 1350°C for 3 h. Then, the pelleted sample was ground and sieved to get a proper-sized powder. In the end, the sample's crystallographic, morphological, optical, and colouring properties were investigated using characterization instruments; XRD, FTIR, SEM with EDS, and UV VIS NIR. XRD data and the analysis revealed the presence of some new peaks as well as the shift in peak position to the lower Bragg angle due to the increase in doped iron. Similarly, increasing the doped iron on copper chromate causes the microstrain to decrease, which agrees with the previous result. Furthermore, the SEM image shows smaller agglomerations, but they are better than the synthetic iron-doped copper chromate, with sizes ranging from nano to micro. The UV-VIS result confirmed the formation of black pigment, while the FTIR reveals the synthesized pigment is a spinel structure. In addition colouring axis best fit with the synthetic iron-doped copper chromate.

Keywords: Spinel structure, black pigment, circular economy, extracted iron oxide

5. INTRODUCTION

5.1 Background and Justification

Inorganic black pigments are frequently used to suit various purposes in a wide range of industrial applications, such as as a starting raw material in porcelain tile and sanitary ware body formulations and glaze compositions. The contemporary use of these pigments has increased dramatically due to increased demand and aesthetic considerations in the ceramic industries [34, 126]. As a result, inorganic black pigments account for roughly 25% of total market consumption. Most pigments were synthesized from synthetic precursors, salts or metal oxides, and those precursors are highly purified and expensive, raising the production cost [181, 284, 285].

$CuCr_2O_4$ inorganic black pigments, Iron-Cobalt Chromate and Chrome-Iron Nickel, as representative of spinel-type oxides, can be considered one of the best black pigments made from synthetic starting materials, often used in the ceramic industry due to their excellent stability [254, 287]. But, the recent increase in the price of cobalt-bearing black pigments and the most frequent usage and broad application of iron oxide made researchers extensively study alternative sources to prepare ceramic pigments [222, 192].

Contemporary trends are changing the research area towards utilising less expensive alternative raw resources, such as various types of industrial waste. Although such materials do not generally have good chemical purity, they are widely investigated as starting materials since they may produce a favourable result [287]. Furthermore, the use of recycled industrial waste as a raw material for another product is a focusing area that has a circular economy idea, where industrial production is focused on recycling materials, and this concept is attested to and has gained significant attention by European Circular Economy [288-290].

Various efforts have been made to turn industrial waste into raw ingredients for ceramic pigment industrial applications. For example, the green pigment was synthesized by Krysztafkiewicz et al.2008, [291] using post-galvanic sludge and other industrial wastes [292], while prim et al. prepared a pink pigment from sheet metal treatment waste together with pure hematite [217].

On the other hand, different research outputs have been reported in preparing black and brown pigment using industrial wastes [293, 294]. For example, black spinel pigment was synthesized by incorporating iron oxide (Fe_2O_3) powder into the dried electroplating sludge, and the waste was transformed into black spinel pigment ($FeCr_2O_4$) [295]. Similarly, copper and steel slag by

managing the Fe/Cr molar ratio, iron waste from the steel rolling industry in combination with chromium ore, electroplating sludge containing Cr/Ni, and residual sludges from Cr/Ni/Cu plating dried and calcined at higher temperature are some of the results in the black pigment preparation. The findings indicated that the use of less pure raw materials becomes a cause of compositional instability and are unable to keep the chromatic value constant [285, 149, 296, 297].

Yet, this process requires proper pre-treatment of the industrial waste before combining it with the synthetic metal to obtain pigments with the intended property. As a result, this experimental work reports the effect of adding extracted iron oxide from steel slag with relatively less impurity on the copper chromate pigment using the solid-state mechanism and compares its property with the one synthesized using pure synthetic precursor.

5.2 MATERIALS AND METHODOLOGY

5.2.1 Preparation of synthetic iron-doped copper chromate pigment

Synthetic iron-doped copper chromate with a structure $Fe_xCu_{1-x}Cr_2O_4$ (x= 0.25, 0.75, and 1) was synthesized using a solid-state method. The powders were mixed with the stated stoichiometric weight percentage proportion and ground in an agate mortar and pestle for 30 min. Next, the ground powders were added to an attrition mill for further mixing using acetone as a wetting medium for 1:30 h at 1000 rpm. After mixing in the attrition mill, the mixed sample was dried in an oven at 80°C for 15 h, and finally, the dried sample was ground using an agate mortar and pestle for 1 h. The powder sample was sieved using #100 mesh size, and it was then Pelletized using a pressing machine at 18.133MPa (1ton) with a diameter of 25mm. The pellets were calcined at 1350°C for 3 h at a rate of rising and lowering temperature of 50°C/min.

The calcined pellets were ground using an agate mortar and pestle for 1hr, sieved using #100 to get a powder, and labelled with code as shown in **Table 5.1** for further characterization.

Table 5. 1 Elemental composition and corresponding code of extracted iron oxide added copper chromite with $Fe_xCu_{1-x}Cr_2O_4$

No	Chemical Composition	Code
1	x= 1	A_1
2	x=0.75	A_2
3	x=0.5	A_3
4	x=0.25	A_4

5.3 CHARACTERIZATION

PXRD at room temperature with a Rigaku X-ray diffraction (XRD) was used to assess the produced samples' crystalline nature and phase purity. Data was gathered utilizing continuous scanning. The X-ray source consists of copper-sealed 0.6KW Cu K emission lines from a 40 kV/15mA generator. The measurements ranged from 20 to 60°, with a 0.02° step and a 0.12 s/step scanning rate. The data were analyzed using origin 19, and the diffractogram peak was matched using Xpert Highscore Plus software with a Joint Committee for Powder Diffraction System-Powder Database File (JCPDS-PDF) database.

The FT-IR was utilized on spectrum 65 FT-IR (PerkinElmer) in the range 4000-400cm^{-1} (resolution: 4cm^{-1}, number of scale:4) with KBr pellets. The morphology of the materials was examined using a scanning electron microscope (ESEM, model Quanta 200, with a resolution of up to 3nm), and the chemical composition was determined using EDS.

The optical property of the synthesized powder pigment was analyzed using a UV-VIS spectrophotometer (carry 100 UV-VIS spectrophotometer, Agilent technologies) in the wavelength range of 200-800nm.

Similarly, the refractive index(n) of the extracted iron-doped copper chromite was calculated from the UV-VIS data, and the colouring coordinate was determined using CIE-1931 colour space using the CIExyz axis and transformed to spherical coordinates L*, a*, and b* using the equations described in **Chapter 4**.

5.4 RESULT AND DISCUSSION

5.4.1 XRD Analysis Results of Extracted Fe-Doped Copper Chromite

The XRD patterns of extracted iron oxide added spinel copper chromate black inorganic pigment is shown in **Figure 5.1** below.

According to the substitution principle, Fe replaces Cu to form $Fe_xCu_{1-x}Cr_2O_4$, where x = 0.25, 0.5, 0.75, and 1%. The coordination number of Fe is 6 [298], according to the Pauling rule, resulting in the [FeO_6] octahedron and doping influencing cation distribution, like substituting one or more ions from a spinel lattice with any other metal ions. Substituent ions alter host materials' structural, electrical, colouring, and magnetic properties as they could occupy different lattice sites depending on their preferences.

The main peaks of pure iron chromate ($FeCr_2O_4$) and extracted iron-doped copper chromate pigment have similar peaks with the synthetic iron-doped copper chromate peaks, as shown in **Chapter 4 (Figure 5.1 b)**. Besides, the crystallographic plane indexed with the $FeCr_2O_4$ shows some extra peaks shown in **Figure 5.1**, which may happen due to the impurity in the extracted iron oxide, as depicted in **chapter 3**.

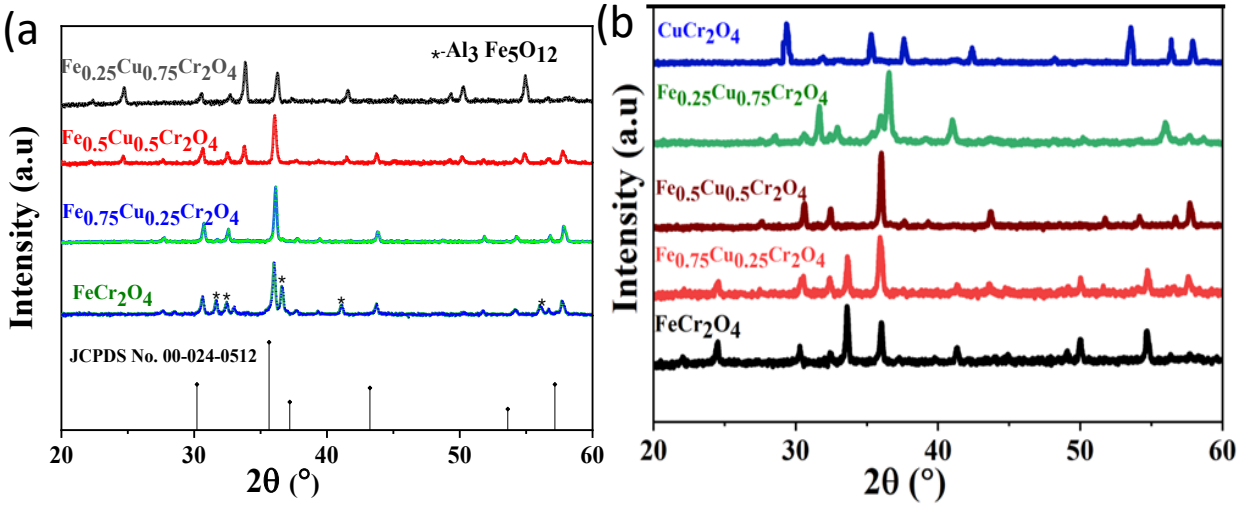

Figure 5. 1 X-ray diffraction pattern of $Fe_xCu_{1-x}Cr_2O_4$ with (a) extracted iron-doped copper chromate with JCPDS-PDF No of $FeCr_2O_4$ (b) synthetic iron-doped copper chromate

At the same time, the diffraction peak shown in **Figure 5.2** shifted slightly to a smaller angle as the Fe doping increased [299]; this agrees with **chapter 4** since the copper with higher ionic radii was replaced by the smaller ionic radii iron [278, 279].

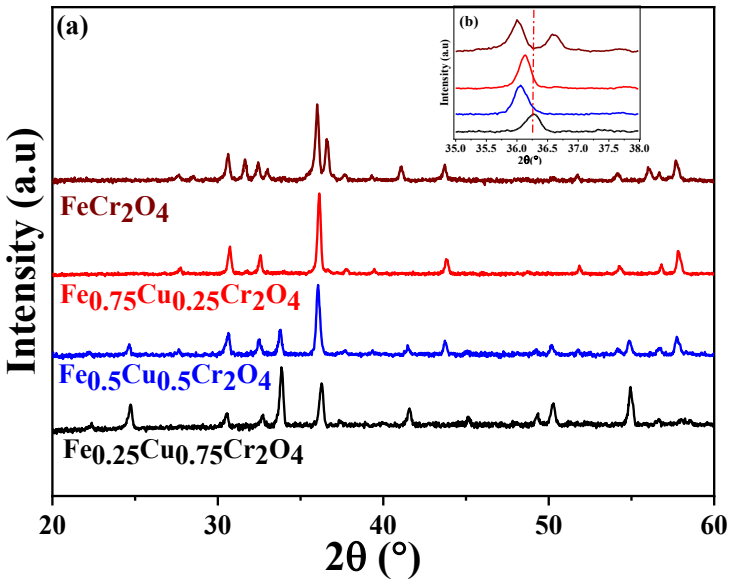

Figure 5. 2 XRD peak of (a) Different composition of extracted iron-on $CuCr_2O_4$ pigment (b) Shift in Bragg angle due to extracted iron oxide addition

The average crystallite size of extracted iron oxide doped to copper chromite was computed using the Debye Sherrer equation [300, 301]:

$$\boldsymbol{D = \frac{k\lambda}{\beta cos\theta}}$$

The constant k-is shape factor k= 0.9, λ=0.15406nm, is the wavelength of the XRD machine and, β-the Full Wave Half Maximum (FWHM) in radian, and θ the Bragg angle in radian. The result in **Table 5.2** confirmed an increase in crystallite size as the amount of extracted iron was added to the copper chromite pigment, which agrees with [302] and **chapter 4** result.

Similarly, the lattice parameters were changed due to doping. Micro-strain is defined as the root mean square of variations in lattice parameters across individual crystallites and is calculated using the proposed formula.

$$\varepsilon = \frac{\beta cos\theta}{4}$$

Where $\boldsymbol{\varepsilon}$ is the microstrain, $\boldsymbol{\beta}$ is the Full Wave Half Maximum (FWHM in Radians), and $\boldsymbol{\theta}$ is the Bragg angle in radians. The results in **Table 5.2** show that the Microstrain decreases as the amount of extracted iron oxide added to the synthetic copper chromate increases. Moreover, the reduction in the microstrain due to the doped extracted iron oxide distorts the microstructure [260].

Table 5. 2 Crystallite size and microstrain of each sample

Sample Powder	A_1	A_2	A_3	A_4
The average Crystallite size (nm)	12.12	11.93	10.64	10.56
MicroStrain (10^{-3})	2.793	3.036	3.30	3.40

It also agrees with the XRD peak shift crystallite size and ionic radii relationship since the ionic radii of iron oxide are lower than copper's [280, 304].

5.4.2 FTIR Analysis of Extracted Fe-Doped Copper Chromite

The FT-IR transmittance spectra of $Fe_xCu_{1-x}Cr_2O_4$ (x= 0.25, 0.5, 0.75 and 1) powder pigment measured at room temperature are shown in **Figure 5.3.** The spinel oxide spectra containing transition metals with oxidation states of +2 and +3 typically have four distinct brands: 800–650 cm^{-1} (ν_1), 600–500 cm^{-1} (ν_2), 450–300 cm^{-1} (ν_3), and 200–150 cm^{-1} (ν_4) [299].

In similar ways to the previous experiment in chapter 4, absorption bands in the 600-500cm-1 range correspond to the inherent stretching vibration of the Mtetra-O band at the tetrahedral site (Cu-O and Fe-O) [272]. In contrast, bands in the 499-385cm-1 range correspond to octahedral metal ion stretching (Cr-O) [279]. Hence, peaks in FTIR of the extracted iron-doped copper chromate also assure the formation of a spinel structure.

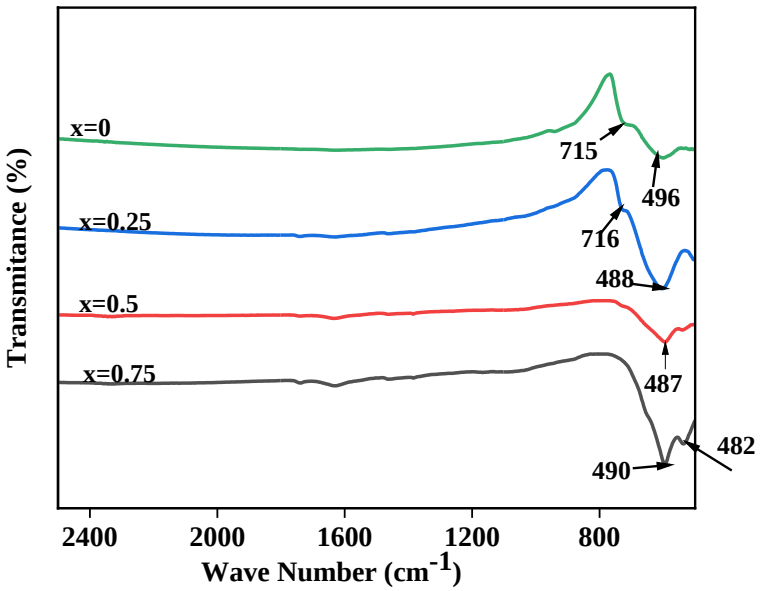

Figure 5. 3 FTIR spectra of extracted iron oxide were added sample with a general formula of $Fe_xCu_{1-x}Cr_2O_4$ (x= 0, 0.75. 0.5. 0.25)

5.4.3 SEM with EDS Analysis of Extracted Fe-Doped Copper Chromite

The microstructure and elemental composition of the sample containing extracted iron oxide added copper chromite were investigated by SEM/EDS, shown in **Figure 5.4.**

FEG-SEM images of selected samples were taken to examine the morphology of prepared samples. **Figure 5.4** shows the FE-SEM photograph of $Fe_xCu_{1-x}Cr_2O_4$ samples. The sample looks at a uniform particle size distribution with some agglomerates but better particle distribution than the synthetic iron-doped chromate, as observed in **Figure 5.4**. The milling process and the selection of sieve size cause a considerable decline in the particle size of the powders. Moreover, as a witness, some impurities from doped extracted iron oxide were introduced in the EDS result shown in **Figure 5.4**.

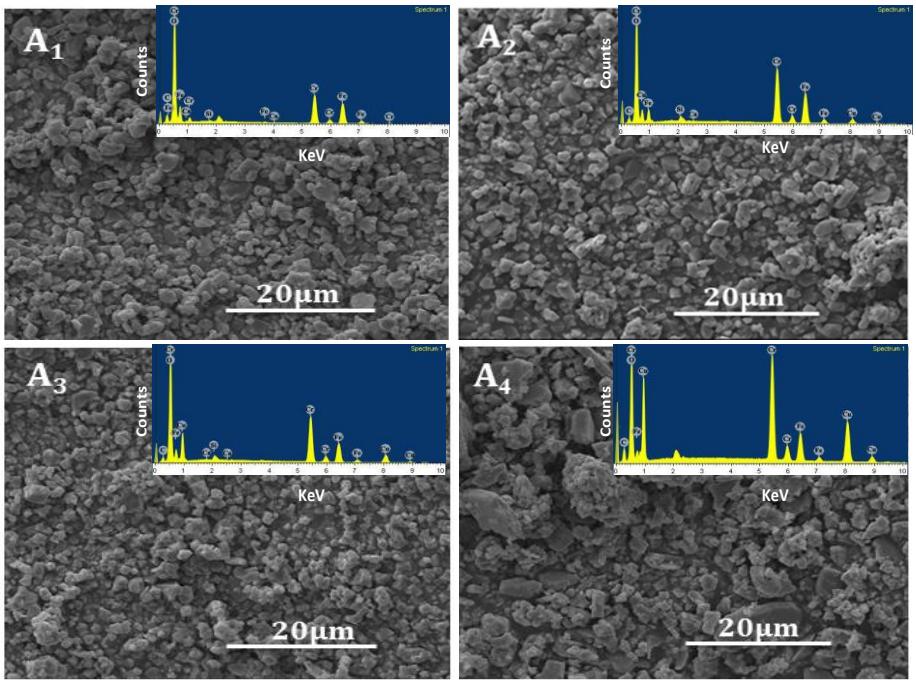

Figure 5. 4 SEM images and EDX spectra of the black pigments, with a composition of $Fe_xCu_{1-x}Cr_2O_4$, having A_1 x=1, A_2 x=0.75, A_3 x=0.5 and A_4 x=0.25

5.4.4 Optical Property of Extracted Fe-Doped Copper Chromite

The optical transmission spectra of $Fe_xCu_{1-x}Cr_2O_4$ black powders were measured in the visible range from A_1 to A_4, as shown in **Figure 5.5.** The absorption edge is found to be almost parallel to the wavelength axis, and the increase in peak has been observed at a lower wavelength as the amount of the extracted iron oxide added to synthetic copper chromite increases, which is in agreement with the literature [304].

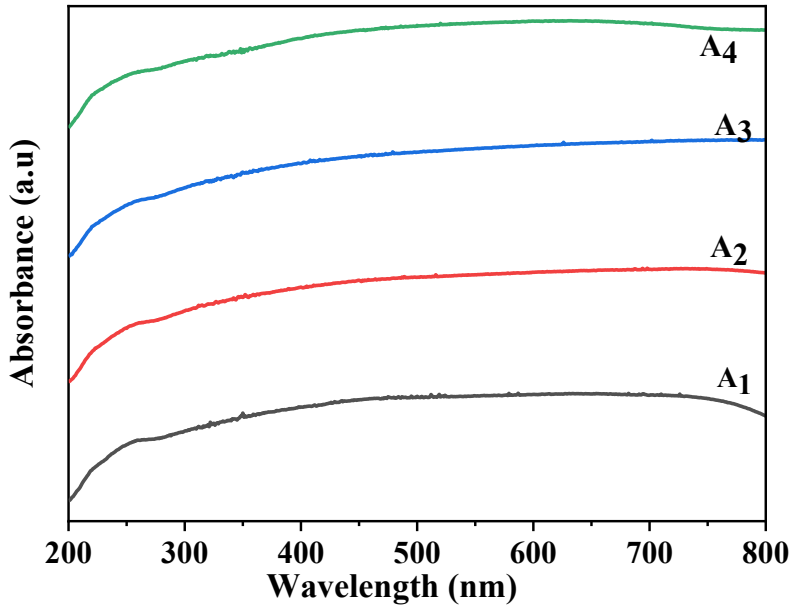

Figure 5. 5 UV-VIS Spectroscopy of $Fe_xCu_{1-x}Cr_2O_4$

Moreover, the absorption spectra obtained by adding extracted iron oxide to the synthetic copper chromite to get $Fe_xCu_{1-x}Cr_2O_4$ are similar to the results obtained in **chapter 4**. In addition, the refractive index shown in **Figure 5.6** better agrees with the commercial one [282] and the one synthesized using synthetic iron-doped copper chromate earlier in **chapter 4**.

The refractive index increases as the amount of doped iron oxide increases; the result is in good agreement till the doped iron oxide becomes 0.75 and with **chapter 4**.

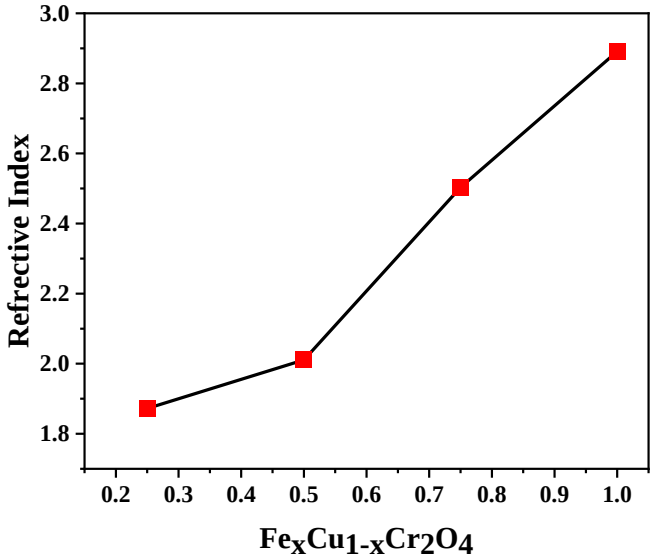

Figure 5. 6 The relationship between the refractive index and the amount of extracted iron oxide doped on copper chromate.

The pigment must create opacity in the coating. When a coating is opaque, the pigment particles scatter and absorb light, preventing it from reaching the substrate. In addition, since the smaller radii replace the larger radii, the powder becomes denser and a potential absorbent of the pigment as its refractive index increases.

5.4.5 Coloring Property of Extracted Fe-Doped Copper Chromite

The chromatic properties of the synthesized $Fe_xCu_{1-x}Cr_2O_4$ (x = 0, 0.25, 0.50, 0.75 and 1) powder pigments were assessed from their UV-VIS diffuse reflectance CIE 1931 colour coordinate values depicted in **Table 5.3.** The systematic doping of iron in $CuCr_2O_4$ causes the increase in a* value from 1.02 to 1.27; this implies the addition of iron oxide gives a reddish tonality to the synthesized pigment. On the other hand, the increase in iron causes the b* value to decrease hence getting more bluish in tone. As a result, the Chromatic value and Hue reach the maximum value at 0.5% weight percentage mixing of iron oxide. In addition, the lightness value of the pigment lies in the range of black colour, which is comparable with the synthetic black pigment shown in **Chapter 4** and comparable with the commercial black pigment [192, 305].

Table 5. 3 the colour coordinate of $Fe_xCu_{1-x}Cr_2O_4$ (x = 1, 0.75. 0.5 and 0.25)

Compound	L*	a*	b*	C	H
$FeCr_2O_4$	32.34	1.27	1.12	2.52	41.4
$Fe_{0.75}Cu_{0.25}Cr_2O_4$	32.4	1.13	1.20	2.57	46.7
$Fe_{0.5}Cu_{0.5}Cr_2O_4$	32.48	1.06	1.38	2.96	52.47
$Fe_{0.25}Cu_{0.75}Cr_2O_4$	32.49	1.02	1.39	2.43	53.73
$FeCr_{2O4}$	32.3	1.20	1.07	2.34	41.7
$Fe_{0.75}Cu_{0.25}Cr_2O_4$	32.4	1.11	1.09	2.29	44.48
$Fe_{0.5}Cu_{0.5}Cr_2O_4$	32.96	1.01	1.41	3.03	54.39
$Fe_{0.25}Cu_{0.75}Cr_2O_4$	32.49	1.04	1.25	2.60	50.2
$CuCr_2O_4$	32.52	0.94	1.41	2.93	56.3

5.5 CONCLUSION

This work reported a successful preparation of ceramic pigment by adding extracted iron oxide in different weight percentages to the synthetic copper chromate using a solid-state mechanism. The final result was investigated using various instruments, which showed the formation of a black colour with a spinel structure of $Fe_xCu_{1-x}Cr_2O_4$. The XRD result indicated a slight shift in diffractogram towards the lower Bragg angle as the amount of doped iron oxide increases, which agrees with the synthetic iron-doped copper chromate. The occurrence of peak shift is an indication of the mismatch in the ionic radii of copper and iron ion. Furthermore, some peaks were detected on the graph, indicating some impurities in the extracted iron oxide, as was determined in chapter 4. The impurity in the iron oxide does not affect the colouring property but brings some shift in the colouring axis. The SEM result shows a slight uniformity, better than the synthetic iron-doped copper chromate; still, it requires the utilization of a suitable sieve to get a uniform particle size distribution. The result displayed in the FTIR also confirmed the interaction of metal and ligands and the formation of spinel structure. Finally, the UV-VIS result indicated that the peak forms a parallel line to the horizontal axis, which suggests light absorption in the whole wavelengths (property of black pigment). Furthermore, an increase in refractive index causes the pigment to scatter and absorb light sufficiently to prevent it from reaching the substrate or making the coating opaque (higher refractive index). In the end, the refractive index of the synthesized pigment agrees with the commercial black pigment and with the synthetic iron-doped copper chromate until the doped iron oxide becomes 0.75.

CHAPTER-SIX

GENERAL DISCUSSION, CONCLUSION, AND RECOMMENDATION

6.1 GENERAL DISCUSSION

Customers require various colours for different purposes and applications to decide what they like and dislike. They elicit various emotional responses, such as excitement, energy, and calmness. Colour emotions are the feelings elicited by specific colours or colour combinations [306]. Colours are never seen in isolation in our daily lives but are always presented in conjunction with other colours; this is true when we examine our surroundings, ranging from the inside of a building to an entire cityscape [307].

Black pigments are used extensively in today's ceramic buildings because they can give pleasure and withstand dirt and other external factors. In addition, those black inorganic pigments are used in various industrial applications to colour ceramic tile and bricks, accounting for approximately 25% of total inorganic pigment consumption [308]. Iron-chromite and Co-or Ni-containing spinels are examples of commercial inorganic black pigments [296]. However, since Cobalt-containing raw materials are expensive and hazardous to human health, iron-containing chromite spinels, synthesized at temperatures above 1000°C from a mixture of iron and chromium oxides, are widely concerned [34].

Recently, several researchers investigated the synthesis of inorganic black iron-chromite and copper chromate pigment with iron- or chromium-containing industrial wastes. It was then introduced into the ceramic matrix to produce black ceramic tiles [38, 285]. In addition, different researchers have investigated structural factors spinel, optical bandgap particle size, and the like to produce a pigment with a property compared with the commercial one in colour (chroma).

This report presented two main parts; extracting iron oxide and synthesising black inorganic pigments. The first part of the research reported the extracted iron oxide from steel processing industry waste (steel slag). The study investigated the chemical composition, the purity of the extracted powder, structural properties, the relationship of the firing temperature with the crystallite size, and colouring properties. In the second investigation, the three inorganic metal oxides, copper oxide, chromium oxide, and iron oxide, were mixed using the solid-state method. The microstructure, optical and colouring properties were used to identify and compare with the commercial. Finally, the synthetic iron oxide has been replaced by the extracted iron oxide, the

black spinel colouring pigment has been synthesized, and its properties have been investigated and compared with the synthetic one. In the spinel pigment's synthesis process, the different weight proportion of the copper has been replaced by the iron oxide to get the comparable property of the commercial one.

Most importantly, the research output will address the challenges in the steel industry waste and open the door to finding a substitute for commercial black pigments as it is used widely. In addition, the different extraction process has been critically investigated from the literature to select the suitable one for the process we employed.

In chapter one, the classification of pigments based on the chemical composition, their pros and cons, historical background of the pigment usage, and criteria for selection of inorganic pigment like cost, ease of use, and environmental friendliness are stated. The problem statement, overall aim, research objectives, scope of the research, and conceptual/theoretical frameworks were presented.

Chapter two stated the basic definition of pigment and basic classes, types of colourants, and pigment properties. In addition, the principle of colour formation with the wavelength of each colour in the visible light spectrum of the light, the relationship between energy bandgap and colouring of metallic materials, the effect of metallic cation interaction as well as metal and ligand interaction, coordination number and geometrical structure has been elaborated. Moreover, the synthesis mechanism with pros and cons stated the principle of colour measurement. In the end, research that has been done so far and the research gaps were stated in-depth.

In chapter three, the materials and methodology were stated. The experimental synthesis methods, materials, and instrumentations used in this section of the dissertation are presented and demonstrated thoroughly. The theoretical background of the instrumentation and working principle were also stated, which can clarify better for the reader. In addition, the basic instrumentations utilized in this research work were briefly demonstrated through the schematic diagram and photographic images.

As briefly stated in chapter four, iron oxide was extracted from steel slag using the hydrothermal method. In the process, sulphuric acid was used to leach iron from steel slag. Ammonia was applied to precipitate the leachate in the liquor. Finally, Hydrogen peroxide was used to favour the oxidation process so that all the samples remain with Fe^{3+}, which becomes Fe_2O_3 through an oxidation process. The stable temperature of extracted iron oxide was determined using

Thermogravimetric analysis (TG-DTA). The sample was calcined at 700°C, 800°C, 900°C, and 1000°C, and the result confirmed that the hematite form of iron oxide is stable under the mentioned temperature. Then, the sample powder crystallographic structure was examined by XRD, while its particle size, chemical composition, morphology, optical, and colouring properties were investigated using DLS, ICPMS/XRF, SEM-EDS, UV-VIS-NIR Spectroscopy, and Colorimetry, respectively.

In Chapter Five, synthetic inorganic black spinel pigment has been synthesized using iron oxide added to copper chromite by a solid-state method. In the process, synthetic iron oxide, copper oxide, and chromium oxide were used, and they were mixed by solid-state method to get a black spinel pigment with a general composition of $Fe_xCu_{1-x}Cr_2O_4 (0 \leq x \leq 1)$. First, the samples were mixed using an agate mortar and pestle and then an attrition mill for further mixing; acetone was used for mixing purposes. Then the sample was pelletized using a pressing machine and calcined at 1350°C for 3 h, and It was then ground and sieved using #100 mesh size. Next, the sample powder crystallographic structure was examined by XRD. At the same time, particle size, chemical composition, morphology, optical, and colouring properties were investigated using DLS, SEM-EDS, FTIR, UV-VIS-NIR Spectroscopy, and Colorimetry. Finally, the output colouring property was compared with the commercial spinel black pigment.

In chapter six, the synthetic iron oxide was replaced by the extracted one (Discussed in chapter 4), and the same steps in chapter 4 have been applied. Based on the result obtained in chapter 5, after pelletization, the sample was calcined with an annealing temperature of 1350°C for 3 h; it was then ground using an agate mortar and pestle and sieved using #100 mesh size. Except for the particle size analysis using DLS, the crystallographic property, chemical composition, morphology, and optical and colouring properties were investigated using XRD, SEM-EDS, FTIR, UV-VIS-NIR Spectroscopy, and Colorimetry, respectively. Finally, the output colouring property was compared with the result obtained in chapter 4.

6.2 CONCLUSION

In conclusion, after performing all the experiments mentioned above, the significant findings obtained are as follows;

Findings in the article "Effect of Annealing Temperature of Brownish-Red Pigment Based on Iron Oxide Extracted by Hydrothermal Route from Mill-Scale Steel Slag" are

- The chemical composition of the steel slag has been identified using XRF, and effective extraction of iron oxide was done using the hydrothermal method. (composition of iron oxide in the leached liquor was investigated using ICPMS). The colouring properties of the pigment were also investigated in relation to the annealing temperatures. Moreover, the crystallographic peak confirmed that the extracted powder is hematite with smaller impurities observed at 900°C and 1000°C. The FEG-SEM result and the DLS confirmed that the extracted samples agglomerated. In the end, the UV-VIS-NIR result indicated the d-d electron transition, while the colouring axis confirmed the formation of a chart of colour due to the variation in annealing temperature, which is a good insight for the pigment industry.

Findings on the "Effects of Adding Iron Oxide (doping) on the Coloring Properties of Copper Chromate Pigment" are:

- The as-synthesized $Fe_xCu_{1-x}Cr_2O_4$ using XRD data, the phase and structural analysis indicated that the pure form of $CuCr_2O_4$ and $FeCr_2O_4$ obtained compared to their corresponding JCPDS No. when x=0 and x=1, respectively. Doping synthetic iron to the synthetic copper chromate cause the Bragg angle shift to the lower angle; it is a confirmation that the smaller ionic radii iron takes the position of the relatively larger ionic radii copper's position. The perfect doping or replacement of copper by iron in the copper chromate pigment was also proved by its micro strain results, and the microstrain decreases as the amount of iron-doped in copper chromate increases. The FTIR result indicated the occurrence of the peak between 600-500cm^{-1} that is due to the stretching of metals at the tetrahedral site with oxygen(M_{tetra}- O), that is (Cu-O and Fe-O) and in the range of 499-385$cm^{-1}$is due to (M_{oct}-O) that is (Cr-O) stretching. These stretchings are a confirmation of spinel structure formation. The SEM-EDS confirmed a relatively better powder particle distribution with no impurity introduced in it. In the end, the UV-VIS-NIR and colouring

measurement confirmed the formation of Black pigment comparable with the commercial one with an optimized result of L* = 32.96 as the pigment composition is $Fe_{0.5}Cu_{0.5}Cr_2O_4$.

The research article is “Effect of adding extracted iron oxide on the colouring property of copper chromate; a comparative study.”

- The extracted iron was doped effectively on the copper chromate pigment using a solid-state synthesis mechanism to form a black spinel pigment with $Fe_xCu_{1-x}Cr_2O_4$ ($1 \leq \boldsymbol{x} < \mathbf{0}$). The crystallographic, morphology, optical and colouring properties were investigated and compared with the synthetic one produced earlier. The crystallographic peaks obtained from XRD data indicated the existence of some peaks due to the impurity of extracted iron. But in a similar manner, the peak shifted towards the lower Bragg angle, which is a confirmation of the lower ionic radii of iron replacing the relatively larger ionic radii of copper. The pictogram obtained from SEM confirmed the best particle distribution were exist; moreover, the EDS result indicated those impurities come from extracted iron. The FTIR result showed that the peaks that occurred indicated the existence of M_{tetra}-O and M_{octa}-O stretching, which is the confirmation of spinel structure formation. In the end, the optical, colouring and refractive index obtained from UV-VIS-NIR data indicated that the pigment is black, comparable with the synthetic one and the index of refraction increases as the amount of iron-doped increases.

Finally, our findings are believed to provide insights into the alternative use of recycled raw materials for the colouring pigments industry. As was witnessed by different researchers, spinel structure black is more stable than the hematite-eskolite and other structures. Furthermore, the sieve size also affects the particle size distribution, which has influenced the application of this pigment.

6.3 RECOMMENDATION AND FUTURE DIRECTION

Other research has been conducted on extracting pigment powder from industrial wastes. But a challenging part is applying them to the market value, as it becomes inefficient in the amount of pigment obtained from the waste and impurity issue. Sometimes the impurity issue may not affect the research output as it brings some chart of colours for the pigment, but some salts in the powder may end up deteriorating quickly. In this regard examining the impurities found in the extracted powder, studying the effects on the Chroma and its long-lasting effect, and withstanding the advert environment should be considered. In this regard, the research output recommends the following

- Proper treatment and mechanism of the de-agglomeration process should be done on the extracted powder to get uniform particle size distribution.
- Considering effects of impurities found in the extracted powder should be investigated by comparing its property with pure commercial hematite.
- The cost-benefit analysis should be done on the extraction of iron oxide pigment to show clearly its benefit in environmental remediation and economic support.
- Recycling and applying other industrial wastes, for example, the leather industry, textile industry, sugar industry waste and the like for pigment application, should be considered.
- Further investigation should be done to apply the extracted pigment for corrosion protection mechanisms.
- Effects of the leaching agent concentration, leaching time and stirring rate on the amount of extracted powder pigment and purity should be considered.
- Different mechanisms should be implemented to study the effect of doping iron oxide on copper chromate pigment as a comparative study.
- In-depth research on the CICPs is required to apply for enhancing the cooling effects of the pigment for room paint, to enhance the visible light reflecting ability of the pigment and the like.

REFERENCE

[1] A. Marzec *et al.*, "Characterization and properties of new colour-tunable hybrid pigments based on layered double hydroxides (LDH) and 1,2-dihydroxyanthraquinone dye," *J. Ind. Eng. Chem.*, vol 70, pp. 427–438, 2019, Z.

[2] J. Zhou *et al.*, "Combustion synthesis of ZnFe2-xCrxO4 nanocrystallites for ceramic digital decoration," *Mater. Chem. Phys.*, 2020.

[3] G. Palczewska *et al.*, "Human infrared Vision is triggered by two-photon chromophore isomerization," *Proc. Natl. Acad. Sci. U. S. A.*, vol. 111, pp. E5445–E5454, 2014, http://doi.org/10.1073/pnas.1410162111.

[4] M. V. Orna and T. College, "Historic Mineral Pigments : Colorful Benchmarks of Ancient Civilizations," in *American chemical society*, pp. 17–69, 2015, http://doi.org/10.1021/bk-2015-1211.ch002.

[5] F. Hund, "Inorganic Pigments: Bases for Colored, Uncolored, and Transparent Products," *Angew. Chemie Int. Ed. English*, vol. 20, pp. 723–730, 1981, http://doi.org/10.1002/anie.198107231.

[6] M. Luisa *et al.*, "Multianalytical characterization of pigments from funerary artefacts belong to the Chupicuaro Culture (Western Mexico): Oldest Maya blue and cinnabar identified in Pre-Columbian Mesoamerica," *Microchem. J.*, vol. 150, p. 104101, 2019, http://doi.org/10.1016/j.microc.2019.104101.

[7] J. R. Barnett, S. Miller, and E. Pearce, "Colour and art: A brief history of pigments," *Opt. Laser Technol.*, vol. 38, pp. 445–453, 2006, http://doi.org/10.1016/j.optlastec.2005.06.005.

[8] S. D. Solomon, *et al*., "Synthesis of Copper Pigments, Malachite and Verdigris: Making Tempera Paint," *J. Chem. Educ.*, pp. 1694–1697, 2011, http://doi.org/10.1021/ed200096e.

[9] D. Johnson-Mcdaniel, *et al*., "Nanoscience of an ancient pigment," *J. Am. Chem. Soc.*, vol. 135, no. DOI: 10.1021/ja310587c, pp. 1677–1679, 2013, http://doi.org/10.1021/ja310587c.

[10] G. D. Hatton, A. J. Shortland, and M. S. Tite, "The production technology of Egyptian blue and green frits from the second millennium BC Egypt and Mesopotamia," *Archaeol. Sci.*, vol. 35, pp. 1591–1604, 2008, http://doi.org/10.1016/j.jas.2007.11.008.

[11] R. Dang *et al.*, "Influence of illumination on inorganic pigments used in Chinese traditional paintings based on Raman spectroscopy," *Light. Res. Technol.*, vol. 51, pp. 402–416, 2019, http://doi.org/10.1177/1477153518766972.

[12] R. Dang *et al.*, "Chromaticity shifts due to light exposure of inorganic pigments used in traditional Chinese painting," *Light. Res. Technol.*, vol. 49, pp. 818–828, 2017, http://doi.org/10.1177/1477153516644866.

[13] F. Ciesielczyk, "Pigment, Inorganic," *Encycl. Color Sci. Technol.*, pp. 1–21, 2020, http://doi.org/10.1007/978-3-642-27851-8.

[14] G. Accorsi *et al.*, "The exceptional near-infrared luminescence properties of cuprorivaite (Egyptian blue)," *R. Society Chem.*, pp. 3392–3394, 2009, http://doi.org/10.1039/b902563d.

[15] P. B. Zaneta Dohnalova, and Petra Sulcova, "Pink NIR pigment based on Cr-doped $SrSnO_3$," *J. Therm. Anal. Calorim.*, 2019, http://doi.org/10.1007/s10973-019-08522-z.

[16] J. Luxova, "The effect of partial substitution of Bi on colour properties and thermal stability of $Bi_xPr_{1-2\,x}FeO_3$ pigments," *J. Therm. Anal. Calorim.*, 2019, http://doi.org/10.1007/s10973-019-08686-8.

[17] Markowicz *et al.*, "Quality management and method Validation in EDXRF analysis," *X-Ray Spectrom.*, vol. 36, pp. 27–34, 2007, http://doi.org/10.1002/xrs.

[18] A. D. Broadbent, "Basic Principles of Textile Coloration," Society of Dye and Colour, 184-196, 2001.

[19] L. Pereira, and M. Alves, "Dyes-environmental impact and remediation," *Environ. Prot. Strategy. Sustain. Dev.*, pp. 111–162, 2012, http://doi.org/10.1007/978-94-007-1591-2_4.

[20] Pigments Market Report, Ceresana, 2022, https://www.ceresana.com/en/market-studies/chemicals/pigments/ceresana-market-study-pigments.html.

[21] M. Rostampour, and S. Eavani, "Synthesis and characterization of the novel nano-composite pigments using $CoWO_4$ on different silica sources : A comparative study," *Powder Technol.*, vol. 363, pp. 86–94, 2020, http://doi.org/10.1016/j.powtec.2020.01.031.

[22] M. Salavati-Niasari, M. Farhadi-Khouzani, and F. Davar, "Bright blue pigment $CoAl_2O_4$ nanocrystals prepared by modified sol-gel method," *J. Sol-Gel Sci. Technol.*, vol. 52, pp. 321–327, 2009, http://doi.org/10.1007/s10971-009-2050-y

[23] F. Deganello, and A. Kumar, "Solution combustion synthesis, energy and environment : Best parameters for better materials," *Prog. Cryst. Growth Charact. Mater.*, vol. 64, pp. 23–61, 2018, http://doi.org/10.1016/j.pcrysgrow.2018.03.001

[24] R. K. Gupta *et al.*, "Facile synthesis and characterization of nanostructured chromium oxide," *Powder Technol.*, vol. 254, pp. 78–81, 2014, http://doi.org/10.1016/j.powtec.2014.01.014.

[25] M. Yoneda *et al.*, "Influence of aluminium source on the colour tone of cobalt blue pigment," *Powder Technol.*, 2016, http://doi.org/10.1016/j.powtec.2016.06.021.

[26] D. R. Swiler, "Pigments, Inorganic," *Kirk-Othmer Encycl. Chem. Technol.*, pp. 1–37, 2005, http://doi.org/10.1002/0471238961.0914151814152215.a01.pub2.

[27] S. D. Dolić *et al.*, "Improved colouristic properties and high NIR reflectance of environment-friendly yellow pigments based on bismuth vanadate," *Ceram. Int.*, 2018, http://doi.org/10.1016/j.ceramint.2018.09.057.

[28] X. Zhang *et al.*, "Synthesis and characterization of environmentally friendly $BiVO_4$ yellow pigment by non-hydrolytic sol-gel route," *J. Sol-Gel Sci. Technol.*, vol. 91, pp. 127–137, 2019, http://doi.org/10.1007/s10971-019-05026-y.

[29] Pfaff, *Industrial Organic Pigments*, WILEY-VCH Verlag gmbh & Co., 2005.

[30] L.Frolova, A. Pivovarov, and T. Butyrina "Synthesis of pigments in Fe_2O_3-Al_2O_3-CoO by co-precipitation method," *Pigment Resin Technol.*, 2017.

[31] P. K. Thejus and K. G. Nishanth, "Rational approach to low-cost synthesis $BiVO_4$–ZnO complex inorganic pigment for energy-efficient buildings," *Sol. Energy Mater. Sol. Cells*, vol. 200, p. 109999, 2019, http://doi.org/10.1016/j.solmat.2019.109999.

[32] S. Cerro, *et al.*, "Cool and photocatalytic yellow ceramic pigments; from lead-tin to Cr doped scheelite pigments," *Ceram. Int.*, 2018, http://doi.org/10.1016/j.ceramint.2018.11.150.

[33] M. Fortuño-Morte, H. Beltrán-Mir, and E. Cordoncillo, "Study of the role of praseodymium and iron in an environment-friendly reddish orange pigment based on Fe doped $Pr_2Zr_2O_7$: A multifunctional material," *J. Alloys Compd.*, vol. 845, 2020, http://doi.org/10.1016/j.jallcom.2020.155841.

[34] J. A. Labrincha, "Synthesis of black ceramic pigments from secondary raw materials," *Dye. Pigment.*, vol. 77, pp. 137–144, 2008, http://doi.org/10.1016/j.dyepig.2007.04.006.

[35] L. M. Plyasova *et al.*, "The interaction of copper-containing spinels $CuFe_2O_4$ and $CuFeCrO_4$ with hydrogen," *Mater. Res. Bull.*, vol. 118, pp. 1–8, 2019, http://doi.org/10.1016/j.materresbull.2019.05.006.

[36] M. Yusuf, M. Shabbir, and F. Mohammad, "Natural Colorants: Historical, Processing and Sustainable Prospects," *Nat. Products Bioprospect.*, vol. 7, pp. 123–145, 2017, http://doi.org/10.1007/s13659-017-0119-9.

[37] R. R. Marcello *et al.*, "Inorganic pigments made from the recycling of coal mine drainage treatment sludge," *J. Environ. Manage.*, vol. 88, no. 4, pp. 1280–1284, 2008, http://doi.org/10.1016/j.jenvman.2007.07.005.

[38] Z. Chen, *et al.*, "Synthesis of black pigments containing chromium from leather sludge," *Ceram. Int.*, pp. 1–6, 2015, http://doi.org/10.1016/j.ceramint.2015.04.001.

[39] G. Tian *et al.*, "Novel environment-friendly inorganic red pigments based on attapulgite," *Powder Technol.*, vol. 315, pp. 60–67, 2017, http://doi.org/10.1016/j.powtec.2017.03.044.

[40] R. Ianoş, *et al.*, "Solution combustion synthesis and characterization of magnetite, Fe_3O_4, nanopowders," *J. Am. Ceram. Soc.*, pp. 1–5, 2012, http://doi.org/10.1111/j.1551-2916.2012.05159.x.

[41] M. Radepont, *et al.*, "Thermodynamic and experimental study of the degradation of the red pigment mercury sulfide," *J. Anal. At. Spectrom.*, vol. 30, no. 3, pp. 599–612, 2015, http://doi.org/10.1039/c4ja00372a.

[42] C. Tian, "Effects of Structural Factors of Hydrated TiO_2 on Rutile TiO_2 Pigment Preparation via Short Sulfate Process," *Sci. Rep.*, vol. 10, pp. 1–9, 2020, http://doi.org/10.1038/s41598-020-64976-4.

[43] M. Zhao *et al.*, "Preparation and characterization of Fe3+ doped Y2Ce2O7 pigments with high near-infrared reflectance," *Sol. Energy*, vol. 97, pp. 350–355, 2013, http://doi.org/10.1016/j.solener.2013.08.007.

[44] I. Gonzalo-Juan, and R. Riedel, "Ceramic synthesis from condensed phases," *ChemTexts*, vol. 2, no. 2, 2016, http://doi.org/10.1007/s40828-016-0024-6.

[45] R.C.Klet *et al.*, "Evidence for Redox Mechanisms in Organometallic Chemisorption and Reactivity on Sulfated Metal Oxides," *J. Am. Chem. Soc.*, vol. 140, no. 20, pp. 6308–6316, 2018, http://doi.org/10.1021/jacs.8b00995.

[46] S. El-Haggar, *Sustainable Industrial Design and Waste Management*, Elsevier Academic Press, June. 2007.

[47] M. Schwarz et al., "Utilisation of industrial waste for ferrite pigments production," *Chem. Pap.*, vol. 66, no. 4, pp. 248–258, 2012, http://doi.org/10.2478/s11696-012-0154-2.

[48] L. Bian *et al.*, "Enhanced Photovoltage Response of Hematite-X-Ferrite Interfaces (X = Cr, Mn, Co, or Ni)," *Nanoscale Res. Lett.*, vol. 12, no. 1, pp. 2–7, 2017, http://doi.org/10.1186/s11671-017-1885-3.

[49] P. Das *et al.*, "Journal of Environmental Chemical Engineering Waste to wealth : Recovery of value-added products from steel slag," *J. Environ. Chem. Eng.*, vol. 9, no. 4, pp. 1–21, 2021, http://doi.org/10.1016/j.jece.2021.105640.

[50] M. L. P. Reddy, "$YIn_{0.9}Mn_{0.1}O_3$-ZnO nano-pigment is exhibiting intense blue colour with impressive solar reflectance," *Dye. Pigment.*, 2015, http://doi.org/10.1016/j.dyepig.2015.09.014.

[51] J. Mandapati, N. Materials, and T. Development, "Solution Combustion Synthesis of Fe_2O_3/C, Fe_2O_3-SnO_2/C, Fe_2O_3-ZnO/C Composites and their Electrochemical Characterization in Non-Aqueous Electrolyte for Supercapacitor Application," Int. Journal of Electr. Chem. Science, Vol 4, page 878-886,2009.

[52] P. Meenakshi and M. Selvaraj, "Bismuth titanate as an infrared reflective pigment for cool roof coating," *Sol. Energy Mater. Sol. Cells*, vol. 174, pp. 530–537, 2018, http://doi.org/10.1016/j.solmat.2017.09.048.

[53] S. Jose *et al*., "Recent advances in infrared reflective inorganic pigments," *Sol. Energy Mater. Sol. Cells*, vol. 194, pp. 7–27, 2019, http://doi.org/10.1016/j.solmat.2019.01.037.

[54] A. Zhang et al., "Applied Clay Science Microwave hydrothermal assisted preparation of $CoAl_2O_4$ / kaolin hybrid pigments for reinforcement colouring and mechanical property of acrylonitrile butadiene styrene," *Appl. Clay Sci.*, vol. 175, pp. 67–75, 2019, http://doi.org/10.1016/j.clay.2019.04.005.

[55] M. Łączka and K. Cholewa, "Chromium, cobalt, nickel and copper as pigments of sol-gel glasses," *J. Alloys Compd.*, vol. 218, pp. 77–85, 1995, http://doi.org/10.1016/0925-8388(94)01362-4.

[56] Libre Texts chemistry, 2021 https://chem.libretexts.org/ Bookshelves /General_Chemistry /Map%3A_General_Chemistry_(Petrucci_et_al.)/24%3A_Complex_Ions_and_Coordination_Compounds/24.07%3A_Color_and_the_Colors_of_Complexes.

[57] L. Cao et al., "Preparation of phthalocyanine blue/rutile TiO_2 composite pigment with a ball milling method and study on its NIR reflectivity," *Dye. Pigment.*, vol. 173, p. 107879, 2020, http://doi.org/10.1016/j.dyepig.2019.107879.

[58] L. Yuan et al., "Synthesis and characterization of novel nontoxic $BiFe_{1-x}Al_xO_3$/mica-titania pigments with high NIR reflectance," *Ceram. Int.*, 2017, http://doi.org/10.1016/j.ceramint.2017.09.032.

[59] M. Moreno and J. A. Aramburu, "Origin of the Anomalous Color of Egyptian and Han Blue Historical Pigments: Going beyond the Complex Approximation in Ligand Field Theory," *J. Chem. Educ.*, 2015, http://doi.org/:10.1021/acs.jchemed.5b00288.

[60] A. Heuer-Jungmann *et al.*, "The role of ligands in the chemical synthesis and application of inorganic nanoparticles," *Chem. Rev.*, 2018, http://doi.org/10.1021/acs.chemrev.8b00733.

[61] M. A. Abreu and S. M. Toffoli, "Characterization of a chromium-rich tannery waste and its potential use in ceramics," *Ceram. Int.*, vol. 35, pp. 2225–2234, 2009, http://doi.org/10.1016/j.ceramint.2008.12.011.

[62] R. M. Novais et al., "Hidden value in low-cost inorganic pigments as potentially valuable magnetic materials," *Elsevier Ltd Techna Gr. S.r.l. All Rights Reserved.*, no. Ceram. Int., pp. 1–8, 2016, http://doi.org/10.1016/j.ceramint.2016.03.045.

[63] M. Lau, "Synthesis of Nanoscale $CoAl_2O_4$ Pigments," *Univ. Alberta, Edmonton, Canada*, pp. 1–9, 2010.

[64] H.M.Smith, *High-Performance Pigments*, vol. 8. 1975.

[65] M. Comstock, T. Shepherd, and C. Company, "Past, present, and future of high-performance inorganic pigments," The Shepherd Color Company, Cincinnati, Ohio, 2017.

[66] G. . Maslennikova, "Pigments of the spinel type," *Glas. Ceram.*, vol. 58, pp. 216–220, 2001.

[67] X. Duan et al., "Synthesis, structure and optical properties of $CoAl_2O_4$ spinel nanocrystals," *J. Alloys Compd.*, vol. 509, no. 3, pp. 1079–1083, 2011, http://doi.org/10.1016/j.jallcom.2010.09.199.

[68] A. Armoni, M. Piai, and A. Teimouri, "Correlators of circular Wilson loops from holography," *Phys. Rev. D - Part. Fields, Gravit. Cosmol.*, vol. 88, no. 6, pp. 92–95, 2013, http://doi.org/10.1103/PhysRevD.88.066008.

[69] H. Agarwal *et al.*, "Cation distribution in nanocrystalline (Co, Ni)Al_2O_4 Spinel," *Ceram. Int.*, pp. 8–11, 2016, http://doi.org/10.1016/j.ceramint.2016.08.193.

[70] A. Sutka *et al.*, "Effect of nickel addition on the colour of nanometer spinel zinc ferrite pigments," *J. Aust. Ceram. Soc.*, vol. 48, pp. 150–155, 2012.

[72] K. H. W. Herbst, "*Industrial Inorganic Pigment*." 1998.

[71] A. K. H. C. Chambers, "*Modern Inorganic Chemistry*." 1975

[73] G. T. S. Herman F. Mark et al., "Encyclopedia of Chemical Technology," vol. 14, p. 95655, 1981.

[74] K. W. Borth et al., "Structural and morphological behaviour and study of the colourimetric and reflective properties of commercial inorganic pigments," *South African J. Chem.*, vol. 72, pp. 215–221, 2019, http://doi.org/10.17159/0379-4350/2019/V72A28.

[75] M. Comstock, "Complex Inorganic Colored Pigments: Comparison of options and relative properties when faced with elemental restrictions," 2017.

[76] H. R. Hedayati *et al.*, "Synthesis and characterization of $Co_{1-x}Zn_xCr_{2-y}Al_yO_4$ as a near-infrared reflective colour tunable nano-pigment," *Dye. Pigment.*, vol. 113, pp. 588–595, 2015, http://doi.org/10.1016/j.dyepig.2014.09.030.

[77] "Technical Information," *Build. Res. Inf.*, vol. 1, pp. 1–6, 2007, http://doi.org/10.1080/09613219408727368.

[78] P. N. Medeiros *et al.*, "Influence of variables on the synthesis of $CoFe_2O_4$ pigment by the complex polymerization method," *J. Adv. Ceram.*, vol. 4, pp. 135–141, 2015, http://doi.org/10.1007/s40145-015-0145-1.

[79] R. Korifi *et al.*, "CIEL*a*b*; colour space predictive models for colourimetry devices – Analysis of perfume quality," *Talanta*, vol. 104, pp. 58–66, 2013, http://doi.org/10.1016/j.talanta.2012.11.026.

[80] M. Comstock *et al.*, "Spectral properties of the UV absorbing and near-IR reflecting blue pigment, $YIn_{1-x}Mn_xO_3$," *Dye. Pigment.*, vol. 133, pp. 214–221, 2016, http://doi.org/10.1016/j.dyepig.2016.05.029.

[81] W. Bao *et al.*, "Synthesis and characterization of Fe^{3+} doped $Co_{0.5}Mg_{0.5}Al_2O_4$ inorganic pigments with high near-infrared reflectance," *Powder Technol.*, 2016, http://doi.org/10.1016/j.powtec.2016.01.013.

[82] I. Hunter Associates Laboratory, "Colour Hunter CIE L* a* b* Color Scale," *HunterLab*, vol. 8, no. 7, pp. 1–4, 1996, http://www.hunterlab.com.

[83] M. Comstock, "Complex Inorganic Colored Pigments : Comparison of options and relative properties when faced with elemental restrictions," *J. Surf. Coatings Aust.*, pp. 10–30, 2017.

[84] B. J. Ng *et al.*, "Hybridized Nanowires and Cubes : A Novel Architecture of a Heterojunctioned $TiO_2/SrTiO_3$ Thin Film for Efficient Water Splitting," *Mater. View*, vol. 20, pp. 4287–4294, 2010, http://doi.org/10.1002/adfm.201000931.

[85] A. K. V Raj *et al.*, "Terbium doped Sr_2MO_4 [M = Sn and Zr] yellow pigments with high infrared reflectance for energy saving applications," *Powder Technol.*, vol. 311pp. 52–58, 2017, http://doi.org/10.1016/j.powtec.2017.01.089.

[86] M. Takesue *et al.*, "Formation mechanism and luminescence appearance of Mn-doped zinc silicate particles synthesized in supercritical water," *J. Solid State Chem.*, vol. 181, pp. 1307–1313, 2008, http://doi.org/10.1016/j.jssc.2008.02.036.

[87] R. Ricceri *et al.*, "Ceramic pigments obtained by sol-gel techniques and by mechanochemical insertion of colour centres in Al_2O_3 host matrix," *J. Eur. Ceram. Soc.*, vol. 22, pp. 629–637, 2002, http://doi.org/10.1016/S0955-2219(01)00376-4.

[88] E. Grazenaite *et al.*, "Sol-gel and sonochemically derived transition metal (Co, Ni, Cu, and Zn) chromites as pigments: A comparative study," *Ceram. Int.*, vol. 42, pp. 9402–9412, 2016, http://doi.org/10.1016/j.ceramint.2016.02.163.

[89] L. Liu *et al.*, "Synthesis and characterization of Al^{3+} doped $LaFeO_3$ compounds: A novel inorganic pigments with high near-infrared reflectance," *Sol. Energy Mater. Sol. Cells*, vol. 132, pp. 377–384, 2015, http://doi.org/10.1016/j.solmat.2014.08.048.

[90] Y. Zhang *et al.*, "Sol-gel synthesis and properties of europium-strontium copper silicates blue pigments with high near-infrared reflectance," *Dye. Pigment.*, vol. 131, pp. 154–159, 2016, http://doi.org/10.1016/j.dyepig.2016.04.011.

[91] N. Zhou *et al.*, "Synthesis and characterization of $Zn_{1-x}Co_xO$ green pigments with low content cobalt oxide," *J. Alloys Compd.*, vol. 711, pp. 406–413, 2017, http://doi.org/10.1016/j.jallcom.2017.04.015.

[92] P. Sulcová *et al.*, "New purple-blue ceramic pigments based on $CoZr_4(PO_4)_6$," *Dye. Pigment.*, vol. 98, pp. 393–404, 2013, http://doi.org/10.1016/j.dyepig.2013.03.004.

[93] T. I. Dimitrov, T. H. Ibreva, and I. G. Markovska, "Synthesis and Investigation of Ceramic Pigments in the System MnO. $ZnO.SiO_2$," *Glas. Ceram. Russ. Orig.*, vol. 76, pp. 216–218, 2019, http://doi.org/10.1007/s10717-019-00168-5.

[94] N. Srisawad *et al.*, "Formation of $CoAl_2O_4$ nanoparticles via low-temperature solid-state reaction of fine gibbsite and cobalt precursor," *J. Nanomater.*, vol. 2012, pp. 1–8, 2012, http://doi.org/10.1155/2012/108369.

[95] R. Laz *et al.*, " Combustion synthesis of a blue Co-doped zinc aluminate near-infrared reflective pigment," *Dye. Pigment.*, vol. 142, pp. 24–31, 2017, http://doi.org/10.1016/j.dyepig.2017.03.016.

[96] A. A. Ali, E. El Fadaly, and I. S. Ahmed, "Near-infrared reflecting blue inorganic nano-pigment based on cobalt aluminate spinel via combustion synthesis method," *Dye. Pigment.*, 2018, http://doi.org/10.1016/j.dyepig.2018.05.058.

[97] T. Adschiri, Y. Hakuta, and K. Arai, "Hydrothermal synthesis of metal oxide fine particles at supercritical conditions," *Ind. Eng. Chem. Res.*, vol. 39, pp. 4901–4907, 2000, http://doi.org/10.1021/ie0003279

[98] T. Adschiri and K. Arai, "Hydrothermal Synthesis of Metal Oxide Nanoparticles Under Supercritical Conditions," *Tohoku Univ. Sendai, Japan*, 2002.

[99] H. Hayashi and Y. Hakuta, "Hydrothermal Synthesis of metal oxide nanoparticles in supercritical water," *Materials (Basel).*, vol. 3, pp. 3794–3817, 2010, http://doi.org/10.3390/ma3073794

[100] X. Li *et al.*, "One-pot hydrothermal synthesis of micaceous iron oxide pigment from jarosite waste," *J. Coatings Technol. Res.*, vol. 16, pp. 213–220, 2019, http://doi.org/10.1007/s11998-018-0098-8.

[101] H. Hayashi and K. Torii, "Hydrothermal synthesis of titania photocatalyst under subcritical and supercritical water conditions," *J. Mater. Chem.*, vol. 12, pp. 3671–3676, 2002, http://doi.org/10.1039/b207052a.

[102] Y. Chen *et al.*, "Hydrothermal synthesis, hierarchical structures and properties of blue pigments $SrCuSi_4O_{10}$ and $BaCuSi_4O_{10}$" *CrystEngComm*, vol. 15, pp. 5418–5423, 2014, http://doi.org/10.1039/c3ce42394h.

[103] X. Liu *et al.*, "Hydrothermal synthesis and characterization of α-FeOOH and α-Fe_2O_3 uniform nanocrystalline," *J. Alloys Compd.*, vol. 433, pp. 216–220, 2007, http://doi.org/10.1016/j.jallcom.2006.06.029.

[104] D. Chen, X. Jiao, and G. Cheng, "Hydrothermal synthesis of zinc oxide powders with different morphologies," *Solid State Commun.*, vol. 113, pp. 363–366, 1999, http://doi.org/10.1016/s0038-1098(99)00472-x.

[105] R. Ianos and R. Laza, "Synthesis of $Mg_{1-x}Co_xAl_2O_4$ blue pigments via combustion route," *Adv. Powder Technol.*, vol. 22, pp. 396–400, 2011, http://doi.org/10.1016/j.apt.2010.06.006.

[106] A. Sutka, and G. Mezinskis, "Sol-gel auto-combustion synthesis of spinel-type ferrite nanomaterials," *Front. Mater. Sci.*, vol. 6, pp. 128–141, 2012, http://doi.org/10.1007/s11706-012-0167-3.

[107] R. Rosa, P. Veronesi, and C. Leonelli, "A review on combustion synthesis intensification by means of microwave energy," *Chem. Eng. Process. Process Intensif.*, vol. 71, pp. 2–18, 2013, http://doi.rog/10.1016/j.cep.2013.02.007.

[108] A. Varma *et al.*, "Solution Combustion Synthesis of Nanoscale Materials," *Chem. Rev.*, pp. 14493–14586, 2016, http://doi.org/10.1021/acs.chemrev.6b00279.

[109] R. Naik, R. Pothu, and S. C. Prashantha, "Energy-Saving Synthesis of Mg_2SiO_4 : RE^{3+} Nanophosphors for Solid-State Lighting Applications," in *Environmental chemistry for a sustainable world*, 2019, pp. 122–129.

[110] C. Păcurariu *et al.*, "New synthesis methods of $MgAl_2O_4$ spinel," *J. Eur. Ceram. Soc.*, vol. 27, pp. 707–710, 2007, http://doi.org/10.1016/j.jeurceramsoc.2006.04.050.

[111] A. A. Ali and I. S. Ahmed, "Sol-gel auto-combustion fabrication and optical properties of cobalt orthosilicate: Utilization as a colouring agent in polymer and ceramic," *Mater. Chem. Phys.*, vol. 238, p. 121888, 2019, http://doi.org/10.1016/j.matchemphys.2019.121888.

[112] N. Zhou *et al.*, "Synthesis of high near-infrared reflection wurtzite structure green pigments using Co-doped ZnO by combustion method," *Ceram. Int.*, 2018, http://doi.org/10.1016/j.ceramint.2018.10.241.

[113] V. S. Vishnu, S. Jose, and M. L. Reddy, "Novel environmentally benign yellow inorganic pigments based on solid solutions of samarium-transition metal mixed oxides," *J. Am.*

Ceram. Soc., vol. 94, no. 4, pp. 997–1001, 2011, http://doi.org/10.1111/j.1551-2916.2011.04422.x.

[114] I. S. Ahmed *et al.*, "Synthesis and spectral characterization of $Co_xMg_{1-x}Al_2O_4$ as a new nano-colouring agent of ceramic pigment," *Spectrochim. Acta - Part A Mol. Biomol. Spectrosc.*, vol. 74, pp. 665–672, 2009, http://doi,.org/10.1016/j.saa.2009.07.024.

[115] M. Shafiei and C. Behrooz, "Solution combustion synthesis (SCS) of chrome alumina as a high-temperature pink pigment," no. June, pp. 203–209, 2017, http://doi.org10.1111/ijac.12770.

[116] E. A. Chavarriaga *et al.*, "Gel combustion synthesis and magnetic properties of $CoFe_2O_4$, $ZnFe_2O_4$, and $MgFe_2O_4$ using 6-aminohexanoic acid as a new fuel," *J. Magn. Magn. Mater.*, p. 166054, 2019, http://doi.org/10.1016/j.jmmm.2019.166054.

[117] S. Rasouli, and Sh.Saket "One Step Rapid Synthesis of Nano-Crystalline ZnO by Microwave-Assisted Solution Combustion Method" progress in colour, colourants and coatings. Vol 3, pp.19-25, 2014.

[118] V. I. Popkov, and O. V Almjasheva, "Yttrium Orthoferrite $YFeO_3$ Nanopowders Formation under Glycine-Nitrate Combustion Conditions," vol. 87, no. 2, pp. 167–171, 2014, http://doi.org/10.1134/S1070427214020074.

[119] E. Novitskaya *et al.*, "A review of solution combustion synthesis: an analysis of parameters controlling powder characteristics," *Int. Mater. Rev.*, pp. 1–27, 2020, http://doi.org/10.1080/09506608.2020.1765603

[120] G. Kumar et al., "Electric and dielectric study of cobalt substituted MgMn nano ferrites synthesized by solution combustion technique," *Ceram. Int.*, vol. 39, pp. 4813–4818, 2013, http://doi.org/10.1016/j.ceramint.2012.11.071.

[121] A. I. Ivanets et al., "Magnesium ferrite nanoparticles as a magnetic sorbent for the removal of Mn^{2+}, Co^{2+}, Ni^{2+} and Cu^{2+} from aqueous solution," *Ceram. Int.*, vol. 44, no. 8, pp. 9097–9104, 2018, http://doi.org/10.1016/j.ceramint.2018.02.117.

[122] F. Liu, J. Huang, and J. Jiang, "Synthesis and characterization of red pigment $YAl_{1-y}CryO_3$ prepared by the low-temperature combustion method," *J. Eur. Ceram. Soc.*, vol. 33, pp. 2723–2729, 2013, http://doi.org/10.1016/j.jeurceramsoc.2013.04.001.

[123] U. G. Akpan, and B. H. Hameed, "The advancements in sol-gel method of doped-TiO_2 photocatalysts," *Appl. Catal. A Gen.*, vol. 375, pp. 1–11, 2010, http://doi.org/10.1016/j.apcata.2009.12.023.

[124] M. Rajabi, P. Kharaziyan, and M. Montazeri-Pour, "Microwave-assisted processing of cobalt aluminate blue nano-ceramic pigment using sol-gel method," *J. Aust. Ceram. Soc.*, vol. 55, pp. 219–227, 2019, http://doi.org/10.1007/s41779-018-0226-z.

[125] S. Mann *et al.*, "Sol-Gel Synthesis of Organized Matter," *Chem. Mater.*, vol. 9, pp. 2300–2310, 1997, http://doi.org/10.1021/cm970274u.

[126] A. E. Danks, S. R. Hall, and Z. Schnepp, "The evolution of 'sol-gel' chemistry as a technique for materials synthesis," *Mater. Horizons*, vol. 3, no. 2, pp. 91–112, 2016, http://doi.org/10.1039/c5mh00260e.

[127] A. E. Gash *et al.*, "New sol-gel synthetic route to transition and main-group metal oxide aerogels using inorganic salt precursors," *J. Non. Cryst. Solids*, vol. 285, pp. 22–28, 2001, http://doi.org/10.1016/S0022-3093(01)00427-6.

[128] S. Mishra *et al.*, "Molecular engineering of metal alkoxides for solution phase synthesis of high-tech metal oxide nanomaterials," *Chem. - A Eur. J.*, 2020, http://doi.org/10.1002/chem.202000534.

[129] G. Da Costa Cunha *et al.*, "*Recycling of chromium wastes from the tanning industry to produce ceramic nano pigments"*, vol. 18, no. 19. 2016. http://doi.org/10.1039/c6gc01562j.

[130] G. Valverde Aguilar, "A Brief Semblance of the Sol-Gel Method in Research," pp. 3–8, 2019, http://doi.org/10.5772/intechopen.82487.

[131] R. Corrie *et al.*, "Preparation of Monolithic Binary Oxide Gels by a Nonhydrolytic Sol-Gel Process," *Chem. Mater.*, vol. 4, pp. 961–963, 1992, http://doi.org/10.1021/cm00023a001.

[132] S. Esposito, "'Traditional' sol-gel chemistry as a powerful tool for the preparation of supported metal and metal oxide catalysts," *Materials (Basel).*, vol. 12, pp. 1–25, 2019, http://doi.org/10.3390/ma12040668.

[133] I. Bilecka, and M. Niederberger, "New developments in the nonaqueous and/or non-hydrolytic sol-gel synthesis of inorganic nanoparticles," *Electrochim. Acta*, vol. 55, pp. 7717–7725, 2010, http://doi.org/10.1016/j.electacta.2009.12.066.

[134] M. A. Ahmadzadeh, S. F. Chini, and A. Sadeghi, "Size and shape tailored sol-gel synthesis and characterization of lanthanum phosphate ($LaPO_4$) nanoparticles," *Mater. Des.*, vol. 181, p. 108058, 2019, http://doi.org/10.1016/j.matdes.2019.108058.

[135] C. Bogatu *et al.*, "The Influence Of Parameters In Silica Sol-Gel Process," *Bull. Transilv. Univ. Braşov*, vol. 4, no. 53, pp. 1–9, 2011.

[136] F. Ciesielczyk *et al.*, "The sol-gel approach as a method of synthesis of $xMgO_ySiO_2$ powder with defined physicochemical properties including crystalline structure," *J. Sol-Gel Sci. Technol.*, vol. 71, pp. 501–513, 2014, http://doi.org/10.1007/s10971-014-3398-1

[137] Y. El Jabbar *et al.*, "Structure, microstructure, optical and magnetic properties of cobalt aluminate nanopowders obtained by sol-gel process," *J. Non. Cryst. Solids*, vol. 542, pp. 1–8, 2020, http://doi.org/10.1016/j.jnoncrysol.2020.120115.

[138] Á. Triviño-Peláez et al., G. C. "$SrZr_{0.9}Y_{0.1}O_{3-\delta}$ thin films by in-situ synthesis of triple alkoxide for protonic ceramic electrolyser membranes," *J. Sol-Gel Sci. Technol.*, vol. 95, pp. 661–669, 2020, http://doi.org/10.1007/s10971-020-05338-4.

[139] J. Li, and M. A. Subramanian, "Inorganic pigments with transition metal chromophores at trigonal bipyramidal coordination: $Y(In, Mn)O_3$ blues and beyond," *J. Solid State Chem.*, vol. 272, pp. 9–20, 2019, http://doi.org/10.1016/j.jssc.2019.01.019.

[140] D. K. Nguyen, H. Lee, and I. T. Kim, "Synthesis and thermochromic properties of Cr-doped Al_2O_3 for a reversible thermochromic sensor," *Materials (Basel).*, vol. 10, pp. 1–14, 2017, http://doi.org/10.3390/ma10050476.

[141] S. Ke *et al.*, "Effect of mechanical activation on solid-state synthesis process of neodymium disilicate ceramic pigment," *Dye. Pigment.*, 2017, http://doi.org/10.1016/j.dyepig.2017.06.005.

[142] R. C. Olegário *et al.*, "Synthesis and characterization of Fe^{3+} doped cerium-praseodymium oxide pigments," *Dye. Pigment.*, vol. 97, pp. 113–117, 2013, http://doi.org/10.1016/j.dyepig.2012.12.011.

[143] C. M. Álvarez-Docio *et al.*, "2D particles forming a nanostructured shell: A step forward cool NIR reflectivity for $CoAl_2O_4$ pigments," *Dye. Pigment.*, vol. 137, pp. 1–11, 2017, http://doi.org/10.1016/j.dyepig.2016.09.061.

[144] C. Gori *et al.*, "Colour of $Ca(Co_x\ Mg_{1-x})Si_2O_6$ pyroxenes and their technological behaviour as ceramic colourants," *Ceram. Int.*, vol. 44, pp. 12745–12753, 2018, http://doi.org/10.1016/j.ceramint.2018.04.078.

[145] A. M. Gueli *et al.*, "Effect of particle size on pigments colour," *Color Res. Appl.*, vol. 42, no. 2, pp. 236–243, 2017, http://doi.org/10.1002/col.22062.

[146] Ş. Telem *et al.*, "Synthesis of $MnFe_2O_4$ nanocrystals by wet-milling under atmospheric conditions," *Ceram. Int.*, pp. 10–13, 2014, http://doi.org/10.1016/j.ceramint.2013.12.144.

[147] D. Guo *et al.*, "The influence of micronization on the properties of Pr-$ZrSiO_4$ pigment," *Dye. Pigment.*, 2018, http://doi.org/10.1016/j.dyepig.2018.01.049.

[148] W. Hajjaji, M. P. Seabra, and J. A. Labrincha, "Dyes and Pigments Recycling of solid wastes in the synthesis of Co-bearing Calcium Hexa-Aluminate pigment," *Dye. Pigment.*, vol. 83, pp. 385–390, 2009, http://doi.org/10.1016/j.dyepig.2009.06.004.

[149] W. Hajjaji *et al.*, "An overview of using solid wastes for pigment industry," *J. Eur. Ceram. Soc.*, vol. 32, pp. 753–764, 2012, http://doi.org/10.1016/j.jeurceramsoc.2011.10.018.

[150] Y. Lu et al., "Synthesis of iron red hybrid pigments from oil shale semi-coke waste," *Adv. Powder Technol.*, vol. 31, pp. 2276–2284, 2020, http://doi.org/10.1016/j.apt.2020.03.020.

[151] T. Elyn *et al.*, "Iron-based inorganic pigments from residue: Preparation and application in ceramic, polymer, and paint," *Dye. Pigment.*, 2017, http://doi.org/10.1016/j.dyepig.2017.09.025.

[152] W. Hajjaji, M. P. Seabra, and J. A. Labrincha, "Evaluation of metal-ions containing sludges in the preparation of black inorganic pigments," *J. Hazard. Mater.*, vol. 185, pp. 619–625, 2011, http://doi.org/10.1016/j.jhazmat.2010.09.063.

[153] S. Zhang, Z. Pan, and Y. Wang, "Synthesis and characterization of (Ni, Sb)-co-doped rutile ceramic pigment via mechanical activation-assisted solid-state reaction," *Particuology*, vol. 41, pp. 20–29, 2018, http://doi.org/10.1016/j.partic.2017.12.016.

[154] S. Jose and M. L. Reddy, "Lanthanum strontium copper silicates as intense blue inorganic pigments with high near-infrared reflectance," *Dye. Pigment.*, vol. 98, pp. 540–546, 2013.

[155] S. Zhang *et al.*, "Synthesis and characterization of mica / γ-$Ce_{2-x}Y_xS_3$ composite red pigments with UV absorption and high NIR reflectance," 2016, http://doi.org/10.1016/j.ceramint.2016.07.111.

[156] C. P. Aby *et al.*, "Doped oxides of cerium as inorganic colourants," *Color. Technol.*, vol. 123, no. 6, pp. 374–378, 2007, http://doi.org/10.1111/j.1478-4408.2007.00111.x.

[157] T. Shepherd, and C. Company, "options and relative properties when faced with elemental restrictions Complex Inorganic Colored Pigments : Comparison of," no. December, pp. 10–30, 2016.

[158] G. George, V. S. Vishnu, and M. L. P. Reddy, "The synthesis, characterization and optical properties of silicon and praseodymium doped Y_6MoO_{12} compounds: Environmentally benign inorganic pigments with high NIR reflectance," *Dye. Pigment.*, vol. 88, no. 1, pp. 109–115, 2011, http://doi.org/10.1016/j.dyepig.2010.05.010.

[159] M. Cai *et al.*, "New environmental-friendly yellow pigments $Y_{4-x}A_xMoO_{9+d}$ (A = Ta, Tb)," *J. Rare Earths J.*, vol. 37, pp. 741–749, 2019, http://doi.org/10.1016/j.jre.2018.12.008.

[160] J. Chen *et al.*, "Sustainable cool pigments based on iron and tungsten co-doped lanthanum cerium oxide with high NIR reflectance for energy saving," *Dye. Pigment.*, vol. 154, pp. 1–7, 2018, http://doi.org/10.1016/j.dyepig.2018.02.032.

[161] C. Xiong *et al.*, "The far-infrared emissivity and near-infrared reflectance of $Mg_{1-x}Mn_xFe_2O_4$ synthesized by xerogel-microwave method," *J. Alloys Compd.*, vol. 836, pp. 2–10, 2020, http://doi.org/10.1016/j.jallcom.2020.155516.

[162] Y. Xiao *et al.*, "Novel Bi^{3+} doped and Bi^{3+}/Tb^{3+} co-doped $LaYO_3$ pigments with high near-infrared reflectances," *J. Alloys Compd.*, vol. 762, pp. 873–880, 2018, http://doi.org/10.1016/j.jallcom.2018.05.233.

[163] Y. Li *et al.*, "Effect of Sr^{2+} and Dy^{3+} co-doping on colouration and temperature stabilization of a γ-Ce_2S_3 red pigment," *J. Rare Earths*, vol. 38, pp. 213–218, 2020, http://doi.org10.1016/j.jre.2019.02.015.

[164] S. Tamilarasan *et al.*, "Exploring the colour of transition metal ions in irregular coordination geometries: New coloured inorganic oxides based on the spiroffite structure, $Zn_{2-x}M_xTe_3O_8$ (M = Co, Ni, Cu)," *Inorg. Chem.*, vol. 52, pp. 5757–5763, 2013, http://doi.org/10.1021/ic302557j.

[165] M. S. C. Da Câmara *et al.*, "Spectroscopic properties of pigment $Li_{2-x}Zn_{1-x}Pr_xTi_3O_8$," *Mater. Res.*, vol. 19, no. 4, pp. 824–828, 2016, http://doi.org/10.1590/1980-5373-MR-2015-0635.

[166] C. Cardell *et al.*, "Pigment-size effect on the Physico-chemical behaviour of azurite-tempera dosimeters upon natural and accelerated photo-ageing," *Dye. Pigment.*, vol. 141, pp. 53–65, 2017, http://doi.org/10.1016/j.dyepig.2017.02.001.

[167] J. Zou and P. Zhang, "Ni-doped $BaTi_5O_{11}$: New brilliant yellow pigment with high NIR reflectance as solar reflective fillers," *Ceram. Int.*, vol. 46, pp. 3490–3497, 2020, http://doi.org/10.1016/j.ceramint.2019.10.063.

[168] M. Abdullah, Y. Slimani, and A. Baykal, "Synthesis and characterization of $Co_{1-2x}Ni_xMn_xCe_yFe_{2-y}O_4$ nanoparticles," *J. Rare Earths*, pp. 1–7, 2019, http://doi.org/10.1016/j.jre.2019.07.005.

[169] X. Wang *et al.*, "Preparation of high-performance bismuth yellow hybrid pigments by doping with inorganic oxides," *Powder Technol.*, vol. 373, pp. 411–420, 2020, http://doi.org/10.1016/j.powtec.2020.06.063.

[170] F. Z. Akika *et al.*, "Structural and optical properties of Cu-doped $ZnAl_2O_4$ and its," *Surfaces and Interfaces*, 2019, http://doi.org/10.1016/j.surfin.2019.100406.

[171] X. Zhao *et al.*, "Synthesis and characterization of neodymium-doped yttrium molybdate high NIR reflective nano pigments," *Dye. Pigment.*, 2015, http://doi.org/10.1016/j.dyepig.2015.01.018

[172] C. D. Lin Yuan *et al.*, "Synthesis and characterization of environmentally benign inorganic pigments with high NIR reflectance : Lanthanum-doped $BiFeO_3$," *Dye. Pigment.*, vol. 148, pp. 137–146, 2018, http://doi.org/10.1016/j.dyepig.2017.09.008.

[173] Y. Li *et al.*, "Preparation, characterization, and properties of a Ba^{2+}–Sm^{3+} co-doped γ-Ce_2S_3 red pigment," *Solid State Sci.*, vol. 106, 2020, http://doi.org/10.1016/j.solidstatesciences.2020.106332.

[174] X. Wang et al., "Effects of different pH regulators on the colour properties of attapulgite/ $BiVO_4$ hybrid pigment," *Powder Technol.*, vol. 343, pp. 68–78, 2019, http://doi.org/10.1016/j.powtec.2018.11.003.

[175] R. Yang et al., "The influence of Mn/N-codoping on the thermal performance of $ZnAl_2O_4$ as high near-infrared reflective inorganic pigment," *J. Alloys Compd.*, 2016, http://doi.org/10.1016/j.jallcom.2016.12.100.

[176] Z. Xu et al., "Preparation and characterization of Mg^{2+} doped $CaCu_3Ti_4O_{12}$ pigment with high NIR reflectance," *Ceram. Int.*, 2020, http://doi.org/10.1016/j.ceramint.2020.06.324.

[177] E. Cordoncillo, M. Jovaní, and A. Sanz, "New red-shade environmental-friendly multifunctional pigment based on Tb and Fe doped $Y_2Zr_2O_7$ for ceramic applications and cool roof coatings ctor Beltr a," *Dye. Pigment.*, vol. 133, pp. 33–40, 2016, http://doi.org/10.1016/j.dyepig.2016.05.042.

[178] M. Calatayud et al., "Dyes and Pigments Hydrothermal-mediated synthesis of orange Cr, Sb-containing TiO_2 nano-pigments with improved microstructure Jos e," *Dye. Pigment.*, vol. 139, pp. 33–41, 2017, http://doi.org/10.1016/j.dyepig.2016.12.020.

[179] X. Li, Y. Wang, and Z. Pan, "Synthesis and colour properties of neodymium-doped holmium molybdate pigments with allochroic effect," *Ceram. Int.*, vol. 45, no. 17, pp. 21596–21607, 2019, http://doi.org/10.1016/j.ceramint.2019.07.155.

[179] P. Sulcová *et al.*, "Dyes and Pigments New purple-blue ceramic pigments based on $CoZr_4(PO_4)_6$," *Dye. Pigment.*, vol. 98, pp. 393–404, 2013, http://doi: 10.1016/j.dyepig.2013.03.004.

[180] H. Ovčačíková *et al.*, "Metallurgy dust as a pigment for glazes and engobes," *Ceram. Int.*, vol. 43, pp. 7789–7796, 2017, http://doi.org/10.1016/j.ceramint.2017.03.091.

[181] E. Ozel, and S. Turan, "Production and characterisation of iron-chromium pigments and their interactions with transparent glazes," *J. Eur. Ceram. Soc.*, vol. 23, no. 12, pp. 2097–2104, 2003, http://doi.org/10.1016/S0955-2219(03)00036-0.

[182] W. Chang *et al.*, "Influence of heat-treating temperature upon the light absorption for," *Mater. Lett.*, vol. 299, p. 130091, 2021, http://doi.org/10.1016/j.matlet.2021.130091.

[183] A. Kareiva *et al.*, "Evaluation of carbon-based nanostructures suitable for the development of black pigments and glazes," *Colloids Surface A*, vol. 580, pp. 1–10, 2019, http://doi.org/10.1016/j.colsurfa.2019.123718.

[184] S. Chen *et al.*, "Synthesis and chromatic properties of zircon encapsulated ceramic black pigment with carbon sphere as carbon source," *J. Eur. Ceram. Soc.*, vol. 38, no. 4, pp. 2218–2227, 2018, http://doi.org/10.1016/j.jeurceramsoc.2017.12.009.

[185] J. Beetsma, "Optical Properties of Pigments : Absorption and Scattering," *https://knowledge.ulprospector.com/5871/pc-pigment-optical-properties-absorption-scattering/*, pp. 2–5, 2022.

[186] R. A. Candeia *et al.*, "$MgFe_2O_4$ pigment obtained at low temperature," *Mater. Res. Bull.*, vol. 41, pp. 183–190, 2006, http://doi.org/10.1016/j.materresbull.2005.07.019.

[187] S. R. Prim *et al.*, "Synthesis and characterization of hematite pigment obtained from a steel waste industry," *J. Hazard. Mater.*, vol. 192, pp. 1307–1313, 2011, http://doi.org/10.1016/j.jhazmat.2011.06.034.

[188] F. Andreola, L. Barbieri, and F. Bondioli, "Agricultural waste in the synthesis of coral ceramic pigment," *Dye. Pigment.*, vol. 94, pp. 207–211, 2012, http://doi.org/10.1016/j.dyepig.2012.01.007.

[189] H. Ovčačíková *et al.*, "Characterization of waste sludge pigment from production of $ZnCl_2$," *Minerals*, vol. 11, pp. 1–17, 2021, http://doi.org/10.3390/min11030313.

[190] V. Zalyhina *et al.*, "Pigments from spent Zn, Ni, Cu, and Cd electrolytes from electroplating industry," *Environ. Sci. Pollut. Res.*, vol. 28, no. 25, pp. 32660–32668, 2021, http://doi.org/10.1007/s11356-021-13007-4.

[191] N. Klllnç Mirdall, "Inorganic wastes in glaze recipes and their effects on microstructure," *J. Aust. Ceram. Soc.*, vol. 53, no. 2, pp. 713–718, 2017, http://doi:10.1007/s41779-017-00840.

[192] M. Du *et al.*, "Synthesis and characterization of black ceramic pigments by recycling of two hazardous wastes," *Appl. Phys. A*, vol. 575, pp. 1–7, 2017, http://doi.org/10.1007/s00339-017-1181-1.

[193] L. Shen *et al.*, "Preparation of nanometer-sized black iron oxide pigment by recycling of blast furnace flue dust," *J. Hazard. Mater.*, vol. 177, pp. 495–500, 2010, http://doi.org/10.1016/j.jhazmat.2009.12.060.

[194] P. K. Thejus *et al.*, "NIR reflective, anticorrosive magenta pigment for energy saving sustainable building coatings," *Sol. Energy*, vol. 222, pp. 103–114, 2021, http://doi.org/10.1016/j.solener.2021.05.017.

[195] Y. Zhou *et al.*, "Synthesis and properties of novel turquoise-green pigments based on $BaAl_{2-x}Mn_xO_{4+y}$," *Dye. Pigment.*, vol. 155, pp. 212–217, 2018, http://doi.org/10.1016/j.dyepig.2018.03.042.

[196] T. Business, G. Newswire, and T. Business, "Synthetic Pigments Market Overview – Size, Segmentation, Company Growth Strategies By The Business Research Company," *https//www.globenewswire.com/news-release/2021/09/29/2305610/0/en/Synthetic-Pigment. Res.*, pp. 6–9, 2021.

[197] O. Guirdham, "Insights into the global synthetic pigments market 2022-2030 forecast period" tbrc business research Pvt. ltd., *https://www.thebusinessresearchcompany.com/report/toluene-global-market-report*, 2022.

[198] M. A. Legodi and D. de Waal, “The preparation of magnetite, goethite, hematite and maghemite of pigment quality from mill scale iron waste,” *Dye. Pigment.*, vol. 74, pp. 161–168, 2007, http://doi.org/10.1016/j.dyepig.2006.01.038.

[199] A. Sutka *et al.*, “Effect of nickel addition on the colour of nanometer spinel zinc ferrite pigments,” *J. Aust. Ceram. Soc.*, vol. 48, no. 2, pp. 150–155, 2012.

[200] W. A. Dollase, “*Solid state chemistry and its applications by A. R. West”* , vol. 41, no. 6. 1985. http://doi.org/10.1107/s0108768185002476.

[201] Z. G. Eticha *et al.*, “Effect of Annealing Temperature of Brownish-Red Pigment Based on Iron Oxide Extracted by Hydrothermal Route from Mill-Scale Steel Slag,” *J. Sustain. Metall.*, vol. 8, no. 1, pp. 218–227, 2022, http://doi.org/10.1007/s40831-021-00470-z.

[202] “Equipment Facility at CSIR NML,” 2021.

[203] D. Moro, G. Ulian, and G. Valdrè, “SEM-EDS nanoanalysis of mineral composite materials: A Monte Carlo approach,” *Compos. Struct.*, p. 113227, 2020, http://doi.org/10.1016/j.compstruct.2020.113227.

[204] R. M. Amir *et al.*, “Application of Fourier transform infrared (FTIR) spectroscopy for the identification of wheat varieties,” *J. Food Sci. Technol.*, vol. 50, no. 5, pp. 1018–1023, 2013, http://doi.org/10.1007/s13197-011-0424-y.

[205] M. Ye *et al.*, “Synthesis and characterization of Mn-doped copper chromite black pigments,” *Adv. Mater. Res.*, vol. 602–604, pp. 71–75, 2013, http://doi.org/10.4028/www.scientific.net/AMR.602-604.71.

[206] E. B. and G. P. G.Pfaff, *Industrial Inorganic Pigment*. 2005.

[207] A. R. Mirhabibi, “Ceramic Coatings for Pigments,” *Ceram. Coatings - Appl. Eng.*, no. February 2012 2012, http://doi.org/10.5772/30010.

[208] A. R. Robertson, “Historical development of CIE recommended colour difference equations,” *Color Res. Appl.*, vol. 15, no. 3, pp. 167–170, 1990, http://doi.org/10.1002/col.5080150308.

[209] M. R. Luo, "*Encyclopedia of Science and Technology*", vol. 16, no. 3. 2002. http://doi.org/10.1108/rr.2002.16.3.27.138.

[210] F. A. Lo, J. M. Torralba, and M. I. Martı, "Production of sponge iron powder by reduction of rolling mill scale," *Ironman. Steelmak.*, vol. 39, no. 3, pp. 155–163, 2012, http://doi.org/10.1179/1743281211Y.0000000078.

[211] N. M. Gaballah *et al.*, "Production of Iron from Mill Scale Industrial Waste via Hydrogen," *Open J. Inorg. Non-metallic Mater.*, vol. 03, no. 03, pp. 23–28, 2013, http://doi.org/10.4236/ojinm.2013.33005.

[212] T. Bertelsmann-Scott., "The circular economy : Including Africa in Europe" s circle,"*https://saiia.org.za/research/the-circular-economy-including-africa-in-europes-circle/.*, 2020.

[213] N. Mehta *et al.*, "Assessment of the possible reuse of extractive waste coming from abandoned mine sites: A case study in Gorno, Italy," *Sustain.*, vol. 12, no. 6, pp. 1–22, 2020, http://doi.org/10.3390/su12062471.

[214] N. Mehta *et al.*, "Extractive waste management: A risk analysis approach," *Sci. Total Environ.*, vol. 622–623, pp. 900–912, 2018, http://doi.org/10.1016/j.scitotenv.2017.11.260.

[215] T. Facility, "African Development Bank Group to launch new trust fund for the circular economy," p. https://www.afdb.org/en/news-and-events/press-rele, 2022.

[216] Y. Schoeman, P. Oberholster, and V. Somerset, "A decision-support framework for industrial waste management in the iron and steel industry: A case study in Southern Africa," *Case Stud. Chem. Environ. Eng.*, vol. 3, no. January, p. 100097, 2021, http://doi.org/10.1016/j.cscee.2021.100097.

[217] S. R. Prim *et al.*, "Synthesis and characterization of hematite pigment obtained from a steel waste industry," *J. Hazard. Mater.*, vol. 192, pp. 1307–1313, 2011, http://doi.org/10.1016/j.jhazmat.2011.06.034.

[218] H. Hashimoto *et al.*, "Bright Yellowish-Red Pigment Based on Hematite/Alumina Composites with a Unique Porous Disk-like Structure," *ACS Omega*, vol. 5, no. 8, pp. 4330–4337, 2020, http://doi.org/10.1021/acsomega.9b04297.

[219] F. Feng *et al.*, "Boosting hematite photoelectrochemical water splitting by a decoration of TiO2 at the grain boundaries," *Chem. Eng. J.*, vol. 368, pp. 959–967, 2019, http://doi.org/10.1016/j.cej.2019.03.005.

[220] T. Ma *et al.*, "Highly Porous Double-Shelled Hollow Hematite Nanoparticles for Gas Sensing," *ACS Appl. Nano Mater.*, vol. 2, no. 4, pp. 2347–2357, 2019, http://doi.org/10.1021/acsanm.9b00228.

[221] A. Miri, M. Khatami, and M. Sarani, "Biosynthesis, Magnetic and Cytotoxic Studies of Hematite Nanoparticles," *J. Inorg. Organomet. Polym. Mater.*, no. i, 2019, http://doi.org/10.1007/s10904-019-01245-6.

[222] A. Russell, "Inorganic pigments industry worldwide," *Mater. Technol.*, vol. 14, pp. 227–230, 1999, http://doi.org/10.1080/10667857.1999.11752843.

[223] Y. V. Kurkova, and V. B. Kuskov, "Development of technology for the production of natural red iron oxide pigments," *Inc. Miner.*, vol. 2017, no. 1, pp. 217–220, 2017, http://doi.org/10.29227/IM-2017-01-34.

[224] Mengke Liu *et al.*, "Preparation of Black Ceramic Tiles Using Waste Copper Slag and Stainless Steel Slag of Electric," *Materials (Basel).*, vol. 13, pp. 1–12, 2020.

[225] T. Leskelä, and M. Leskelä, "Preparation of yellow and red iron oxide pigments from iron(II) sulfate by alkali precipitation," *Thermochim. Acta*, vol. 77, pp. 177–184, 1984, http://doi.org/10.1016/0040-6031(84)87056-2.

[226] P. K. Thejus, K. V. Krishnapriya, and K. G. Nishanth, "A cost-effective intense blue colour inorganic pigment for multifunctional-cool roof and anticorrosive coatings," *Sol. Energy Mater. Sol. Cells*, vol. 219, p. 110778, 2021, http://doi.org/10.1016/j.solmat.2020.110778.

[227] M. Grohol *et al.*, "*Report on Critical Raw Materials and the Circular Economy"*, 2018, http://doi.org/10.2873/167813.

[228] E. Castagnotto *et al.*, "Characterization of the Caput Mortuum purple hematite pigment and synthesis of a modern analogue," *Dye. Pigment.*, vol. 185, no. PA, p. 108881, 2021, http://doi.org/10.1016/j.dyepig.2020.108881.

[229] V. Akinwekomi *et al.*, "Synthesis of magnetite from iron-rich mine water using sodium carbonate," *J. Environ. Chem. Eng.*, vol. 5, no. 3, pp. 2699–2707, 2017, http://doi.org/10.1016/j.jece.2017.05.025.

[230] F. Q. Mariani *et al.*, "Sustainable, innovative method to synthesize different shades of iron oxide pigments," *Dye. Pigment.*, vol. 137, pp. 403–409, 2017, http://doi.org/10.1016/j.dyepig.2016.10.024.

[231] M. J. Ryan, A. D. Kney, and T. L. Carley, "A study of selective precipitation techniques used to recover refined iron oxide pigments for the production of paint from a synthetic acid mine drainage solution," *Appl. Geochemistry*, vol. 79, pp. 27–35, 2017, http://doi.org10.1016/j.apgeochem.2017.01.019.

[232] X. Li *et al.*, "Bacteria-assisted preparation of nano α-Fe_2O_3 red pigment powders from waste ferrous sulfate," *J. Hazard. Mater.*, 2016, http://doi.org/10.1016/j.jhazmat.2016.06.021.

[233] B. Liu *et al.*, "Synthesis and Characterization of Micaceous Iron Oxide Pigment from Oily Cold Rolling Mill Sludge," *Procedia Environ. Sci.*, vol. 31, pp. 653–661, 2016, http://doi.org/10.1016/j.proenv.2016.02.121.

[234] V. Akinwekomi *et al.*, "Beneficiation of acid mine drainage (AMD): A viable option for the synthesis of goethite, hematite, magnetite, and gypsum – Gearing towards a circular economy concept," *Miner. Eng.*, vol. 148, pp. 1–9, 2020, http://doi.org/10.1016/j.mineng.2020.106204.

[235] R. N. K. Taylor *et al.*, "Painting by numbers: Nanoparticle-based colourants in the post-empirical age," *Adv. Mater.*, vol. 23, pp. 2554–2570, 2011, http://doi.org/10.1002/adma.201100541.

[236] T. C. Costa *et al.*, "Industrial steel waste as an iron source to promote heterogeneous and homogeneous oxidation/reduction reactions," *J. Clean. Prod.*, vol. 211, pp. 804–817, 2019, http://doi.org/10.1016/j.jclepro.2018.11.201.

[237] A. Lassoued *et al.*, "Control of the shape and size of iron oxide (α- Fe_2O_3) nanoparticles synthesized through the chemical precipitation method," *Results Phys.*, vol. 7, pp. 3007–3015, 2017, http://doi.org/10.1016/j.rinp.2017.07.066.

[238] H. X. and W. L. Bin Xiang, "Effects of Calcination Temperature on the performance of nano-sized iron oxide catalysts for ethylbenzene dehydrogenation", *Akad. Kiado, Budapest Springer, Dordr.*, vol. 94, pp. 175–182, 2008.

[239] O. Ozdemir, and S. K. Banerjee, "High-Temperature Stability of Maghemite," *Geophys. Res. Lett.*, vol. 11, no. 3, pp. 161–164, 1984.

[240] D. P. Nguyen *et al.*, "Crystallization and magnetic properties of amorphous iron-chromium oxide nanoparticles synthesized by sonochemistry," *Adv. Nat. Sci. Nanosci. Nanotechnol.*, vol. 3, no. 1, 2012, http://doi.org/10.1088/2043-6262/3/1/015017.

[241] N. H. H. N D Phu, D T Ngo, and L H Hoang, "Crystallization process and magnetic properties of amorphous iron oxide nanoparticles," *J. Phys. D. Appl. Phys.*, vol. 44, pp. 1–7, 2011, http://doi.org/10.1088/0022-3727/44/34/345002.

[242] K. Tamura *et al.*, "High-Quality Inorganic Red Pigment Prepared by Aluminum Deposition on Biogenous Iron Oxide Sheaths," *ACS Appl. Bio Mater.*, 2020, http://doi.org/10.1021/acsabm.0c00476.

[243] A. Lassoued *et al.*, "Synthesis, structural, morphological, optical and magnetic characterization of iron oxide (α-Fe_2O_3) nanoparticles by precipitation method: Effect of varying the nature of precursor," *Phys. E Low-Dimensional Syst. Nanostructures*, vol. 97, pp. 328–334, 2018, http://doi.org/10.1016/j.physe.2017.12.004.

[244] A. Dehbi *et al.*, "Hematite iron oxide nanoparticles (α-Fe_2O_3): Synthesis and modelling adsorption of malachite green," *J. Environ. Chem. Eng.*, vol. 8, p. 103394, 2020, http://doi.org/10.1016/j.jece.2019.103394.

[245] V. Vi and T. A. World, "Encyclopedia of Encyclopedia of," *Anc. World*, vol. V, pp. 1–3, 1950.

[246] A. H. Kamel, A. M. Abdallah, and H. Y. El-Baradei, "The effect of temperature on the properties of calcined red iron oxide pigments," *J. Appl. Chem. Biotechnol.*, vol. 22, no. 12, pp. 1209–1215, 2007, http://doi.org/10.1002/jctb.5020221202.

[247] O. Opuchovic, and A. Kareiva, "Historical hematite pigment: Synthesis by an aqueous sol-gel method, characterization and application for the colouration of ceramic glazes," *Ceram. Int.*, vol. 41, pp. 4504–4513, 2015, http://doi.org/10.1016/j.ceramint.2014.11.145.

[248] L. Drăguţ, and A. Dornik, "Land-surface segmentation as a method to create strata for spatial sampling and its potential for digital soil mapping," *Int. J. Geogr. Inf. Sci.*, vol. 30, no. 7, pp. 1359–1376, 2016, http://doi.org/10.1080/13658816.2015.1131828.

[249] Wendusu, T. Masui, and N. Imanaka, "Novel environment-friendly inorganic red pigments based on (Bi, Er, Y, Fe)$_2O_3$ solid solutions," *J. Asian Ceram. Soc.*, vol. 2, pp. 195–198, 2014, http://doi.org/10.1016/j.jascer.2014.06.005.

[250] S. Divya, and S. Das, "Eco-friendly $Li_3InB_2O_6$ based red pigments for various IR blocking cool coating applications," *Opt. Mater. (Amst).*, vol. 109, p. 110410, 2020, http://doi.org/10.1016/j.optmat.2020.110410.

[251] G. Sukmarani *et al.*, "Synthesis of manganese ferrite from manganese ore prepared by mechanical milling and its application as an inorganic heat-resistant pigment," *J. Mater. Res. Technol.*, vol. 9, pp. 8497–8506, 2020, http://doi.org/10.1016/j.jmrt.2020.05.122.

[252] L. Frolova, and A. Pivovarov, "Obtaining of brown pigments from concentrated wastewater containing nickel," *Chem. Chem. Technol.*, vol. 10, no. 2, pp. 209–211, 2016, http://doi.org/10.23939/chcht10.02.209.

[253] D. Melo *et al.*, "Lanthanum cobaltite black pigments with perovskite structure," *Dye. Pigment.*, vol. 98, pp. 459–463, 2013, http://doi.org/10.1016/j.dyepig.2013.03.012.

[254] L. Verger *et al.*, "Spectroscopic properties of Cr^{3+} in the spinel solid solution $ZnAl_{2-x}Cr_xO_4$," *Phys. Chem. Miner.*, vol. 43, no. 1, pp. 33–42, 2016, http://doi.org/10.1007/s00269-015-0771-8.

[255] Y. Youn *et al.*, "Effects of Metal Dopings on $CuCr_2O_4$ Pigment for Use in Concentrated Solar Power Solar Selective Coatings," *ACS Appl. Energy Mater.*, vol. 2, pp. 882–888, 2019, http://doi.org/10.1021/acsaem.8b01976.

[256] M. Dondi *et al.*, "Ni-free, black ceramic pigments based on Co-Cr-Fe-Mn spinels: A reappraisal of crystal structure, colour and technological behaviour," *Ceram. Int.*, vol. 39, no. 8, pp. 9533–9547, 2013, http://doi.org/10.1016/j.ceramint.2013.05.072.

[257] R. J. H. Clark, "Pigment identification by spectroscopic means: an arts/science interface," *Comptes Rendus Chim.*, vol. 5, no. 1, pp. 7–20, 2002, http://doi.org/10.1016/s1631-0748(02)01341-3.

[258] G. L. Qing-Fen Geng, Xin Zhao, and Xiang-Hu Gao, "Sol-Gel Combustion-Derived CoCuMnO spinels as pigment for Spectrally Selective Paints," *J. Am. Ceram. Soc.*, vol. 94, pp. 827–832, 2011, http://doi.org/10.1111/j.1551-2916.2010.04182.x.

[259] E. Pakzad, Z. Ranjbar, and M. Ghahari, "Synthesized of octahedral copper chromite spinel for spectrally selective absorber (SSA) coatings," *Prog. Org. Coatings*, vol. 132, no. January, pp. 21–28, 2019, http://doi.org/10.1016/j.porgcoat.2019.03.027.

[260] T. Sofia Nirmala et al., "Effect of Cu^{2+} ions on structural, morphological, optical and magnetic behaviours of $ZnAl_2O_4$ spinel," *Mater. Res. Express*, vol. 7, no. 4, 2020, http://doi.org/10.1088/2053-1591/ab7a7a.

[261] V. Jeseentharani et al., "Synthesis of metal ferrite (MFe_2O_4, M = Co, Cu, Mg, Ni, Zn) nanoparticles as humidity sensor materials," *J. Exp. Nanosci.*, vol. 8, no. August 2014, pp. 358–370, 2014, http://doi.org/10.1080/174580.2012.690893.

[262] S. Li, X. Jia, and Y. Qi, "Synthesis of Nano-crystalline Magnesium Chromate Spinel by Citrate Sol-Gel Method," *Adv. Mater. Res.*, vol. 286, pp. 730–733, 2011, http://doi.org/10.4028/www.scientific.net/AMR.284-286.730.

[263] M. Saeed *et al.*, "Synthesis and Fabrication of $Co_{1-x}Ni_xCr_2O_4$ Chromate Nanoparticles and the Effect of Ni Concentration on Their Bandgap, Structure, and Optical Properties," *J. Compos. Sci.*, vol. 5, pp. 1–9, 2021.

[264] M. A. S. A. Hassanzadeh-Tabrizi, "Polyacrylamide gel synthesis, characterization, and optical properties of $Co_{1-x}Ni_xCr_2O_4$ spinel nano pigments," *J. Sol-Gel Sci. Technol.*, vol. 99, pp. 534–545, 2021, http://doi.org/10.1007/s10971-021-05590-2.

[265] I. Matulkova *et al.*, "On preparation of nanocrystalline chromites by co-precipitation and auto combustion methods," *Mater. Sci. Eng. B Solid-State Mater. Adv. Technol.*, vol. 195, pp. 66–73, 2015, http://doi.org/10.1016/j.mseb.2015.01.011.

[266] B. Paul *et al.*, "Facile synthesis of spinel $CuCr_2O_4$ nanoparticles and studies of their photocatalytic activity in degradation of some selected organic dyes," *J. Alloys Compd.*, vol. 648, pp. 629–635, 2015, http://doi.org/10.1016/j.jallcom.2015.07.012.

[267] Z. Hu *et al.*, "Preparation And Photoelectric Properties Of $CuCr_2O_4$ Nanopowders," *Adv. Mater. Res.*, vol. 286, pp. 974–979, 2011, http://doi.org/10.4028/www.scientific.net/AMR.284-286.974.

[268] M. J. Akhtar, and M. Younas, "Structural and transport properties of nanocrystalline $MnFe_2O_4$ synthesized by co-precipitation method," *Solid State Sci.*, vol. 14, no. 10, pp. 1536–1542, 2012, http://doi.org/10.1016/j.solidstatesciences.2012.08.026.

[269] S. S. Acharyya, S. Ghosh, and R. Bal, "Surfactant Promoted Synthesis of $CuCr_2O_4$ Spinel Nanoparticles : A Recyclable Catalyst for One-Pot Synthesis of Acetophenone from Ethylbenzene," *Ind. Eng. Chem. Res.*, p. A-H, 2014.

[270] S. Ali, I. Ahmad, and M. Islam, "Study of magnetic and dielectric properties of $ZnFe_2O_4/CoCr_2O_4$ nanocomposites produced using sol-gel and hydrothermal processes," *J. Alloys Compd.*, vol. 865, p. 158953, 2021, http://doi.org/10.1016/j.jallcom.2021.158953.

[271] J. Gilabert et al., "Characteristics reproducibility of (Fe, Co)(Cr, Al)$_2$O$_4$ pigments obtained by solution combustion synthesis," *Ceram. Int.*, pp. 1–8, 2016, http://doi.org/10.1016/j.ceramint.2016.05.054.

[272] Q. Geng, X. Zhao, and X. Gao, "Low-temperature combustion synthesis of $CuCr_2O_4$ spinel powder for spectrally selective paints," *J. Sol-Gel Sci. Technol.*, vol. 61, pp. 281–288, 2012, http://doi.org/10.1007/s10971-011-2625-2.

[273] M. Comstock, "Complex Inorganic Colored Pigments : Comparison of," pp. 9–30, 2017.

[274] A. V. Nikam, B. L. V. Prasad, and A. A. Kulkarni, "Wet chemical synthesis of metal oxide nanoparticles: A review," *R. Soc. Chem.*, vol. 20, no. 35, pp. 5091–5107, 2018, http://doi.org/10.1039/C8CE00487K.

[275] A. P. Geo Georgescu, "Analysis of thickness influence on refractive index and absorption coefficient of zinc selenide thin films," *Opt. Express*, vol. 27, no. 24, pp. 34803–34823, 2019.

[276] A. R. Robertson, "The CIE 1976 Color-Difference Formulae," *Color Res. Appl.*, vol. 2, no. 1, pp. 7–11, 1977, http://doi.org/10.1002/j.1520-6378.1977.tb00104.x

[277] P. Chartrand, A. Barnab, and L. Cassayre, "Thermodynamic and Structural Properties of $CuCrO_2$ and $CuCr_2O_4$: Experimental Investigation and Phase Equilibria Modeling of the Cu−Cr− O System," *A J. Am. Chem. Soc. Phys. Chem. C*, vol. 125, pp. 12069–15084, 2021, http://doi.org/10.1021/acs.jpcc.1c04179.

[278] S. Lan *et al.*, "Synthesis and characterization of Mn-doped C@$ZrSiO_4$ black pigment via a non-hydrolytic sol-gel method," *Adv. Powder Technol.*, vol. 32, no. 8, pp. 2940–2949, 2021, http://doi.org/10.1016/j.apt.2021.06.007.

[279] R. D. Shannon, and C. T. Prewitt, "Effective ionic radii in oxides and fluorides," *Acta Crystallogr. Sect. B Struct. Crystallogr. Cryst. Chem.*, vol. 25, no. 5, pp. 925–946, 1969, http://doi.org/10.1107/s0567740869003220.

[280] P. Monisha et al., "Influence of Mn dopant on the crystallite size, optical and magnetic behaviour of $CoFe_2O_4$ magnetic nanoparticles," *J. Phys. Chem. Solids*, vol. 148, p. 109654, 2021, http://doi.org/10.1016/j.jpcs.2020.109654.

[281] "Pigments," *https//www.pslc.ws/macrog/mpm/coatings/pigments/pigments.htm Pigment.*, vol. c, 2022.

[282] O. Ruiz, F. Sanmiguel, and A. Tolosa, “Determination of the Refractive Index of Ceramic Materials,” *CASTELLÓN (SPAIN)*, no. 1, pp. 1–14, 2012.

[283] B. J. Reddy, and R. L. Frost, “Spectroscopic characterization of chromite from the Moa-Baracoa Ophiolitic Massif, Cuba,” *Spectrochim. Acta - Part A Mol. Biomol. Spectrosc.*, vol. 61, no. 8, pp. 1721–1728, 2005, http://doi.org/10.1016/j.saa.2004.07.002.

[284] B. He *et al.*, “Synthesis of Ceramic Pigments with Chromium Content from Leather Waste,” *Trans. Indian Ceram. Soc.*, vol. 80, no. 2, pp. 103–109, 2021, http://doi.org/10.1080/0371750X.2021.1887766.

[285] B. Tanisan, and S. Turan, “Black ceramic pigments for porcelain tile bodies produced with chromite ores and iron oxide waste,” *J. Ceram. Process. Res.*, vol. 12, no. 4, pp. 462–467, 2011.

[286] S. G. Matthias Krause *et al.*, “Formation, structure, and optical properties of copper chromite thin films for high-temperature solar absorbers,” *Materialia*, 2021, http://doi.org/10.1016/j.mtla.2021.101156.

[287] J. Carneiro *et al.*, “Synthesis of ceramic pigments from industrial wastes: Red mud and electroplating sludge,” *Waste Manag.*, vol. 80, pp. 371–378, 2018, http://doi.org/10.1016/j.wasman.2018.09.032.

[288] J. Korhonen, A. Honkasalo, and J. Seppälä, “Circular Economy: The Concept and its Limitations,” *Ecol. Econ.*, vol. 143, pp. 37–46, 2018, http://doi.org/10.1016/j.ecolecon.2017.06.041.

[289] K. Shen, L. Li, and J. Wang, “Circular Economy Model For Recycling Waste Resources Under Government Participation: A Case Study In Industrial Waste Water Circulation In China,” *Technol. Econ. Dev. Econ.*, vol. 26, no. 1, pp. 21–47, 2020.

[290] M. S. Andersen, “An introductory note on the environmental economics of the circular economy,” *Sustain. Sci.*, pp. 133–140, 2007, http://doi.org/10.1007/s11625-006-0013-6.

[291] A. Krysztafkiewicz, B. Klapiszewska, and T. Jesionowski, “Precipitated green pigments: Products of chromate post-galvanic waste utilization,” *Environ. Sci. Technol.*, vol. 42, no. 19, pp. 7482–7488, 2008, http://doi.org/10.1021/es800416e.

[292] D. Esteves *et al.*, “Use of industrial wastes in the formulation of olivine green pigments,” *J. Eur. Ceram. Soc.*, vol. 30, pp. 3079–3085, 2010, http://doi.org/10.1016/j.jeurceramsoc.2010.07.006.

[293] E. Ozel et al., “Production of brown and black pigments by using flotation waste from copper slag,” *Waste Manag. Res.*, vol. 24, pp. 125–133, 2006, http://doi.org/10.1177/0734242X06062690.

[294] R. Zhu *et al.*, “Ceramic tiles with black pigment made from stainless steel plant dust: Physical properties and long-term leaching behaviour of heavy metals,” *J. Air Waste Manag. Assoc.*, vol. 66, no. 4, pp. 402–411, 2016, http://doi.org/10.1080/10962247.2016.1140096.

[295] L. Matovi, “Designing of technological scheme for the conversion of Cr-rich electroplating sludge into the black ceramic pigments of consistent composition, following the principles of circular economy,” *J. Environ. Chem. Eng.*, vol. 9, pp. 1–10, 2021, http://doi.org/10.1016/j.jece.2021.105038.

[296] C. Gargori *et al.*, “Recycling of Cr/Ni/Cu Plating wastes as black ceramic pigments,” *Mater. Lett.*, vol. 218, pp. 341–345, 2018, http://doi.org/10.1016/j.matlet.2018.02.047.

[297] J. Carneiro *et al.*, “Waste-based pigments for application in ceramic glazes and stoneware bodies,” *Materials (Basel).*, vol. 12, pp. 1–13, 2019, http://doi.org/10.3390/ma12203396.

[298] D. M. Sherman, “The electronic structures of Fe^{3+} coordination sites in iron oxides: Applications to spectra, bonding, and magnetism,” *Phys. Chem. Miner.*, vol. 12, no. 3, pp. 161–175, 1985, http://doi.org/10.1007/BF00308210.

[299] K. Z. Yufei Tang *et al.*, “Synthesis and luminescence properties of Er-doped and Er/Yb-codoped $CoAl_2O_4$ pigments,” *Ceram. Int.*, 2018, http://doi.org/10.1016/j.ceramint.2018.04.102.

[300] A. B. Kadam *et al.*, “Influence of gadolinium (Gd^{3+}) ion substitution on structural, magnetic and electrical properties of cobalt ferrites,” *J. Alloys Compd.*, vol. 840, p. 155669, 2020, http://doi.org/10.1016/j.jallcom.2020.155669.

[301] A. Monshi, M. R. Foroughi, and M. R. Monshi, “Modified Scherrer Equation to Estimate More Accurately Nano-Crystallite Size Using XRD,” *World J. Nano Sci. Eng.*, vol. 2012, no. September, pp. 154–160, 2012.

[302] S. Ikram *et al.*, “Role of Nature of Rare Earth Ion Dopants on Structural, Spectral, and Magnetic Properties in Spinel Ferrites,” *J. Supercond. Nov. Magn.*, 2020, http://doi.org/http://doi.org/10.1007/s10948-020-05723-8.

[303] P. Prcro *et al.*, "Effect of bismuth doping on optical properties of polycrystalline $PrCrO_3$ Effect of Bismuth Doping on Optical Properties of," *AIP Conf. Proc.*, vol. 040017, pp. 0–4, 2020, https://doi.org/10.1063/5.0002651.

[304] F. Lin *et al.*, "Magnetic, electrical and optical properties of p-type Fe-doped $CuCrO_2$ semiconductor thin films," *J. Alloys Compd.*, vol. 581, pp. 502–507, 2013, http://doi.org/10.1016/j.jallcom.2013.07.160.

[305] B. Tanisan, and S. Turan, "Synthesis of Fe-Mn black pigments by using hematite waste and manganese ore mixtures," *Trans. Indian Ceram. Soc.*, vol. 71, pp. 17–20, 2012, http://doi.org/10.1080/0371750X.2012.689506.

[306] L. Ou, M. R. Luo, and A. Wright, "A Study of Colour Emotion and Colour Preference. Part I : Colour Emotions for Single Colours," pp. 232–240, 2003, http://doi.org/10.1002/col.20010.

[307] L. Ou, M. R. Luo, and A. Wright, "A Study of Colour Emotion and Colour Preference. Part II : Colour Emotions for Two-Colour Combinations," pp. 292–298, 2003, http://doi.org/10.1002/col.20024.

[308] H. Yurdakul, S. Turan, and E. Ozel, "The mechanism for the colour change of iron-chromium black pigments in glazes through transmission electron microscopy techniques," *Dye. Pigment.*, vol. 91, no. 2, pp. 126–133, 2011, http://doi.org/10.1016/j.dyepig.2011.03.014.

OUTCOMES OF THE RESEARCH

PUBLICATIONS, ONGOING RESEARCH OUTPUTS

1. Effect of Annealing Temperature of Brownish-Red Pigment Based on Iron Oxide Extracted by Hydrothermal Route from Mill-Scale Steel Slag, (Published on Journal of Sustainable Metallurgy, Springer)
2. Effects of Doping Iron Oxide on the Coloring Properties of Copper Chromite Pigment (Submitted to Bulletin of Materials Science)
3. Effect of doping Extracted Iron Oxide on the Coloring Property of Copper Chromate; A Comparative Study. (writing the manuscript)

FUTURE WORKS RELATED TO THIS RESEARCH

2. Corrosion Protection Property of the Extracted iron Oxide (ongoing)
3. Extraction of Chromium Oxide from Leather Industrial Waste for Pigment application (Future work)
4. The Coloring Property of $Fe_xCu_{1-x}Cr_2O_4$ when the synthetic Chromium oxide is replaced by the extracted one. (Future work).
5. Extraction of Copper from e-waste and cost-benefit analysis (ongoing)

PUBLICATIONS OUT OF THE DISSERTATION

[1] Dye-Sensitized Solar Cell Using Natural Dye Extracted From Damakase (Ocimum Lamiifolium) And Dambursa (New Plant). (Published On Advances In Materials Chemistry).

[2] Corrosion Behavior Of Low Carbonsteel Sheet Metals in Selected Acidic Medium (IJIRAE)

CONTRIBUTED TO ACADEMIC CONFERENCES

[1] Oral presentation at the Second National Science Research Conference (SNSRC), held From May 21-22/2021, at Hawassa University, Main campus. (Have a certificate)

[2] Oral Presentation at the 6th Annual Research Conference on “Science Technology and Innovation for Industries” held at Addis Ababa Science and Technology University (organized by AASTU) on May 9. and 10/2022. (Have a Certificate)

[3] Oral Presentation at the 1st National Conference on Challenges & Untapped Opportunities of Chemical & Bioengineering Researches For National Dev’t, at Diredawa University, on June 11/2022. (Have a certificate)

INTERNATIONAL AND NATIONAL WORKSHOPS, TRAINING, AND CONFERENCES

[1] Participated in the training program on science skill development, R and D, Science and Technology school clubs, and the use of science kits. [Have a certificate]

[2] Participated in the teaching science and mathematics education, organized by Ethiopian Teachers Association in collaboration with initiative Africa and SIDA. [Have a certificate]

[3] Participated in the training on Environmental reporting organized by Forum for Environment. [Have a certificate]

[4] Attend training on Foundation of Project Management-Hybride organized by Maryland Global University(School of Management) and Ministry of Innovation and Technology. [Have a certificate]

[5] Participated in training on Solar Technologies and applications organized by Indian Technical and Economic Co-operation (ITEC) at Gurugram, Hariyana, India. [Have a certificate]

[6] Participated in the 1st national workshop as an organizing committee, entitled Promoting Materials Science and Nanotechnology for the Advancement of Science and Technology in Ethiopia, Organized by Ethiopian Biotechnology and Adama Science and Technology University.

[7] Participated in the 2nd national workshop as an organizing committee, entitled Opportunity and Challenges of Nanotechnology and Advanced Materials for Sustainable Development and Economic Transformation for the Advancement of Science and Technology in Ethiopia, Organized by Ethiopian Biotechnology.

[8] Participated in integrating universities and Industries as a start-up business incubation program, Organized by Tallinn University of Technology and The University's Hackathon program (Mekatory) in Tallinn, Estonia.

[9] Participated national workshop as an organizing committee entitled "Agro and Industrial Chemicals and E-wastes in Ethiopia: Current Status, their Challenges, and Mitigation Strategy", organized by Ethiopian Biotechnology(The current Bio and Emerging Technology Institute), Public procurement, and Property Administration Authority, and Ministry of Finance and Economic Development.

COMMUNITY SERVICE

[1] As a co-founder and Volunteer service on the SNNRP Association of the Blind.

[2] As a founder and chairperson of the Ethiopian Space Science Society, Hawassa Branch

[3] Coordinating the Urban agriculture done at Addis Ababa Kirkos sub-city, Wereda 11.

ACADEMIC CONTRIBUTION

[1] Advised one M.Sc student in Ceramic Engineering at Materials Science and Engineering Faculty, Jimma Institute of Technology (As Co-Advisor)

ANNEX

Zekarias Gebreyes Eticha earned his Bachelor's degree in Physics from Alemaya University (The current Haromay) and MSc in Materials Science from Hawassa University, Ethiopia. Currently, he is a PhD candidate in Materials Science and Engineering (Metallurgical Engineering) under the supervision of Prof. Dr Ing. Esayas Alemayehu at Jimma Institute of Technology, Jimma University, Ethiopia, and Co-advised by Femi Emanuel Olu (PhD) at Jimma Institute of Technology and Abubeker Yimam (PhD) from AAiT, Addis Ababa University. Moreover, he got the opportunity to conduct his PhD research abroad (Tallinn University of Technology, Tallinn, Estonia, with a scholarship opportunity from the European Development Fund and Internationalization, DoRa Plus, and National Metallurgical Laboratory, Jamshedpur, India with the opportunity of Indian National Science Academy (INSA) and TATA Fellowship program). His research interests include extracting valuable metals from industrial and electronic wastes for different applications, Corrosion and protection mechanisms, and the production of various construction materials from locally available materials.

EXAMINATION BOARD DISSERTATION APPROVAL FORM

JIMMA UNIVERSITY SCHOOL OF GRADUATE STUDIES

Individual: PhD. Dissertation Defence Evaluation Form

Name of the Candidate: **Zekarias Gebreyes Eticha**

Title of the PhD. Dissertation**: Effects of Doping Extracted Iron Oxide Powder from Steel Rolling Industry Waste on Copper Chromate Pigment**

Date of Defence: _____

Evaluation Criteria

S/N	Item	%	Score Obtained	Remark
1	Problem Formulation/Gap Analysis	20%		
2	Research Methodology	20%		
3	Data Presentation and Interpretation	20%		
4	Relevance of Literatures Cited and Coverage	10%		
5	Overall Organization	10%		
6	Thesis Presentation	10%		
7	Response to Questions	10%		
Total				

Total Points _____ Letter grade: _____

Name of Examiner: _____ Signature _____ Date: _____

Grading system:

Excellent >= 85%; Very good = 75-84.9%; Good = 65-74.9%; Satisfactory = 50-64.9%; Fail <50%

SUMMARY
PHD. DISSERTATION DEFENCE EVALUATION FORM

Name of the Candidate: Zekarias Gebreyes Eticha

Title of the PhD dissertation:

Effects of Doping Extracted Iron Oxide Powder from Steel Rolling Industry Waste on Copper Chromate Pigment

Defence Date: _____

Evaluation Criteria

S/N	Item	%	Score Obtained	Remark
1	Problem Formulation/Gap Analysis	20%		
2	Research Methodology	20%		
3	Data Presentation and Interpretation	20%		
4	Relevance of Literatures Cited and Coverage	10%		
5	Overall Organization	10%		
6	Thesis Presentation	10%		
7	Response to Questions	10%		
Total				

Total Ponts _____ Letter grade_____

Examiners

Name of Examiner 1. _____ Signature _____ Date _____

Name of Examiner 2. _____ Signature _____ Date _____

Name of Examiner 3. _____ Signature _____ Date _____

Grading system:

Excellent >= 85%; Very good = 75-84.9%; Good = 65-74.9%; Satisfactory = 50-64.9%; Fail <50%